Altered stereostructures of the DNA-binding domains in the mutant mating proteins of *Ophiocordyceps sinensis* and the *Cordyceps sinensis* insect–fungal complex

Xiu-Zhang Li, Yu-Ling Li, Jia-Shi Zhu*

State Key Laboratory of Plateau Ecology and Agriculture, Qinghai Academy of Animal and Veterinary Sciences, Qinghai University, Xining, Qinghai, China

* Corresponding author

E-mail: zhujosh@163.com (JSZ)

Abstract

The MATα_HMGbox and HMG-box_ROX1-like domains of the MAT1-1-1 and MAT1-2-1 proteins, respectively, play essential roles in DNA binding and the downstream regulation of gene transcription that controls sexual reproduction in *Ophiocordyceps sinensis*. Alternative splicing, differential occurrence and transcription of the *MAT1-1-1* and *MAT1-2-1* genes have been revealed in *Hirsutella sinensis* (Genotype #1 of the 17 *O. sinensis* genotypes), suggesting the occurrence of self-sterility under heterothallic or hybrid outcrossing. This study demonstrates that the MATα_HMGbox domains of MAT1-1-1 proteins in wild-type *Cordyceps sinensis* isolates cluster into 5 clades with or without branches in the Bayesian clustering tree and belong to diverse 3D structural morphs under 19 AlphaFold codes. The HMG-box_ROX1-like domains of MAT1-2-1 proteins cluster into 2 clades with branches in the Bayesian clustering tree and belong to diverse 3D structural morphs under 25 AlphaFold codes. Correlation analysis reveals that 1–3 amino acid substitutions at various sites in the DNA-binding domains of the mutant mating proteins result in alterations in the hydrophobicity and the secondary and tertiary structures of the DNA-binding domains of the proteins. Fungal origin analysis reveals heterospecific fungal sources or genome-independent, genotypic sources of the mating proteins with stereostructure variations in the wild-type *C. sinensis* isolates that represent the changed functionalities of the proteins in regulating and ensuring the accuracy and genetic diversity of the heterothallic and hybrid sexual reproductive processes of *O. sinensis* during the lifecycle of the *C. sinensis* insect–fungi complex.

Keywords: MATα_HMGbox domain of MAT1-1-1 protein; HMG-box_ROX1-like domain of MAT1-2-1 protein; heteromorphic primary, secondary, and tertiary structures of proteins; Bayesian clustering; wild-type *Cordyceps sinensis* isolates; reproduction of *O. sinensis*; sexual life of the *Cordyceps sinensis* insect–fungal complex

I. Introduction

Natural *Cordyceps sinensis* is one of most expensive therapeutic agents in traditional Chinese medicine and has a rich history of clinical use for several centuries for health maintenance, disease amelioration, post-illness and postoperative recovery, and antiaging therapy [Zhu *et al*. 1998a, 1998b, 2011]. This prestige natural therapeutic agent consists of the *Ophiocordyceps sinensis* fruiting body and the remains of a *Hepialidae* moth larva containing an intact, thick larval body wall with numerous bristles, an intact larval intestine, head tissues, and fragments of other larval tissues [Ren *et al*. 2013; Zhang *et al*. 2014; Lu *et al*. 2016; Zhu & Li 2017; Li *et al*. 2022, 2023a, 2023d, 2023e]. Studies of natural *C. sinensis* have demonstrated its multicellular heterokaryotic structures and genetic heterogeneity; the latter includes 17 genomically independent genotypes of *O. sinensis* fungi, >90 other fungal species spanning at least 37 fungal genera, and larval genes [Li 1988; Dai *et al*. 1989; Kinjo & Zang 2001; Jiang & Yao 2003; Stensrud *et al*. 2005, 2007; Leung *et al*. 2006; Zhu *et al*. 2007, 2010; Yang *et al*. 2008, 2021; Zhang *et al*. 2010, 2018; Li *et al*. 2013, 2016b, 2020b, 2022, 2023e; Ren *et al*. 2013; Meng *et al*. 2015; Xia *et al*. 2015; Guo *et al*. 2017; Zhu & Li 2017; Zhong *et al*. 2018; Kang *et al*. 2024]. Thus, the Chinese Pharmacopoeia defines natural *C. sinensis* as an insect–fungal complex classified as a LEVEL-II endangered natural species [China Ministry of Agriculture and Rural Affairs 2021]. Among the numerous heterogeneous fungal species [Jiang & Yao 2003; Zhang *et al*. 2010; Xia *et al*. 2015], *Hirsutella sinensis* has been postulated to be the sole anamorph of *O. sinensis* by Wei *et al*. [2006]. However, ten years later in an artificial cultivation study conducted in an industrial product-oriented setting, Wei *et al*. [2016] reported a species contradiction between anamorphic inoculates of GC-biased Genotype #1 *H. sinensis* on *Hepialidae* moth larvae and the sole teleomorph (the genomically independent AT-biased Genotype #4 of *O. sinensis*) in the fruiting body of cultivated *C. sinensis*. Notably, the Latin name *Cordyceps sinensis* has been indiscriminately used since the 1840s to refer to both the teleomorph/holomorph of the fungus *C. sinensis* and the wild insect–fungal complex; the fungus was renamed *O. sinensis* in 2007 with use of the *H. sinensis* strain EFCC 7287 as the nomenclature reference [Sung *et al*. 2007; Zhang *et al*. 2012; Ren *et al*. 2013; Zhu & Li 2017; Wang *et al*. 2018; Li *et al*. 2022]. Although Zhang *et al*. [2013] proposed improper implementation of the "One Fungus=One Name" nomenclature rule set by the International Mycological Association [Hawksworth *et al*. 2011], disregarded the presence of multiple genomically independent genotypes of *O. sinensis* fungi and inappropriately replaced the anamorphic name *H. sinensis* with the teleomorphic name *O. sinensis*, in this paper, we continue to use the anamorphic name *H. sinensis* for GC-biased Genotype #1 of the 17 *O. sinensis* genotypes that may share the same evolutionary ancestor [Stensrud *et al*. 2007] and refer to the genomically independent Genotypes #2–17 fungi as *O. sinensis* following the taxonomic descriptions that are used in several public depository databases, such as the GenBank and AlphaFold databases, before the systematic

positions of these evolutionarily related genotypes are individually determined and differentiated, regardless of whether they are GC- or AT-biased genetically. In this study, we continue the customary use of the name *C. sinensis* to refer to the wild or cultivated insect–fungal complex because the renaming of *C. sinensis* to *O. sinensis* in 2007 using the *H. sinensis* strain EFCC 7287 as the nomenclature reference did not involve the indiscriminately used Latin name for the natural insect–fungal complex [Sung *et al*. 2007; Yao & Zhu 2016; Zhu & Li 2017; Li *et al*. 2022]. However, this practice will likely be revised in the future by the differential use of proprietary and exclusive Latin names for the multiple genome–independent *O. sinensis* genotypic fungi and the insect–fungal complex.

The sexual reproductive behavior of ascomycetes is strictly regulated by transcription factors encoded at the mating-type (*MAT*) locus. These transcription factors constitute the core mechanism that determines mating compatibility, regulates mating type recognition, and controls the development of fruiting bodies, reproductive structure ascocarps and ascospores [Turgeon & Yoder 2006; Debuchy *et al*. 2006; Jones & Bennett 2011; Zheng & Wang 2013; Wilson *et al*. 2015; Sun *et al*. 2019; Ramšak *et al*. 2020, 2021; Ramšak & Kück 2022]. Like other fungi in Ascomycota, the reproductive behavior of *O. sinensis* relies on the synergistic interaction of 2 mating proteins, the *MAT1-1* and *MAT1-2* idiomorphs. These proteins contain 2 types of critical domains that specifically regulate gene expression related to sexual reproduction: (1) the mating-type alpha high mobility group box (MATα_HMGbox) domain in the MAT1-1-1 protein and (2) the high mobility group box ROX1-like (HMG-box_ROX1-like) domain in the MAT1-2-1 protein [Metin *et al*. 2010; Bushley *et al*. 2013; Hu *et al*. 2013; Zheng & Wang 2013; Li *et al*. 2025]. However, alternative splicing, differential occurrence, and differential transcription of mating-type and pheromone receptor genes and heteromorphic stereostructures of the entire MAT1-1-1 and MAT1-2-1 proteins in *H. sinensis* strains and wild-type *C. sinensis* isolates have been demonstrated, invalidating the self-fertilization hypothesis under homothallism and pseudohomothallism for *H. sinensis*, which was postulated as the sole anamorph of *O. sinensis* and instead suggesting that self-sterility under heterothallism or hybridization requires sexual partners to accomplish sexual reproduction within the lifecycle of natural *C. sinensis* insect–fungi complex [Wei *et al*. 2006; Zhou *et al*. 2013; Zhang & Zhang 2015; Li *et al*. 2019, 2023c, 2024b, 2025].

Mutations of the 2 critical DNA-binding domains of mating proteins that result in a few amino acid substitutions may cause conformational changes in the core stereostructures of the domains, thereby affecting the synergistic interaction of the proteins, probably through regulation of the expression of complementary downstream genes of the 2 idiomorphic mating proteins. Continuing our previous study [Li *et al*. 2025], which demonstrated the variations in the 3D structures of complete mating proteins, this study focuses on amino acid substitutions within the MATα_HMGbox domain and the HMG-box_ROX1-like

105 domain of the full-length MAT1-1-1 and MAT1-2-1 proteins, respectively, and correlates the variable
106 primary structures of these domains with changes in the hydrophobic properties and the secondary and
107 tertiary structures of the DNA-binding domains in wild-type *C. sinensis* isolates. Correlations between
108 changes in hydrophobicity and the primary and secondary structures of the DNA-binding domains of mating
109 proteins encoded by the genome, transcriptome and metatranscriptome assemblies of *H. sinensis* and C.
110 *sinensis* insect–fungal complexes were also analyzed.

111 II. Materials and methods

112 II-1 The MAT1-1-1 and MAT1-2-1 protein sequences of the wild-type *C. sinensis* 113 isolates

114 The AlphaFold database lists the AlphaFold-predicted 3D structures for 138 MAT1-1-1 proteins and
115 74 MAT1-2-1 proteins [Li *et al*. 2025]. Of these proteins, 118 MAT1-1-1 proteins and 69 MAT1-2-1 proteins
116 are full-length proteins, as shown in Tables S1–S2. Three full-length MAT1-1-1 proteins (ALH24945,
117 AGW27560, and EQK97643) and 2 full-length MAT1-2-1 proteins (AEH27625 and EQL04085) are
118 derived from *H. sinensis* strains. All other full-length mating proteins are from wild-type *C. sinensis* isolates
119 that were collected from various production areas on the Qinghai–Tibet Plateau [Zhang *et al*. 2009, 2011,
120 2012, 2013, 2014; Hu *et al*. 2013; Zhang & Zhang 2015; Tunyasuvunakool *et al*. 2021; Li *et al*. 2025]. The
121 internal transcribed spacer (ITS) genotypic information is available in the GenBank database for the mutant
122 full-length MAT1-1-1 and MAT1-2-1 proteins that are derived from 34 wild-type *C. sinensis* isolates and
123 aligned with the reference ITS sequences of the 17 genotypes of *O. sinensis* (*cf*. Table S3).

124 The remaining 20 MAT1-1-1 proteins (AGW27517–AGW27536) and 5 MAT1-2-1 proteins
125 (AGW27543, AGW27548, AGW27552, AGW27554, and AGW27555) are truncated and will be analyzed
126 elsewhere [Bushley *et al*. 2013; Li *et al*. 2013].

127 II-2 Genome, transcriptome, and metatranscriptome assemblies of *H. sinensis* strains 128 and *C. sinensis* insect–fungal complexes

129 The GenBank database lists 5 genome assemblies, LKHE00000000, NGJJ00000000, ANOV00000000,
130 JAAVMX000000000, and LWBQ00000000, of the *H. sinensis* strains 1229, CC1406-20395, Co18, IOZ07,
131 and ZJB12195, respectively, and a transcriptome assembly, GCQL00000000, of the *H. sinensis* strain
132 L0106 [Hu *et al*. 2013; Liu *et al*. 2015, 2020; Li *et al*. 2016a; Jin *et al*. 2020; Shu *et al*. 2020].

133 The metatranscriptome assembly GAGW00000000 for the *C. sinensis* insect–fungal samples
134 (unknown maturation stages) collected from Kangding County, Sichuan Province, China [Xiang *et al*. 2014]
135 is available in the GenBank database.

136 Another metatranscriptome assembly was derived from mature *C. sinensis* samples collected from

137 Deqin, Yunnan Province, China, and was uploaded to a repository database,
138 www.plantkingdomgdb.com/Ophiocordyceps_sinensis/data/cds/Ophiocordyceps_sinensis_CDS.fas [Xia
139 *et al*. 2017]. Although this database is currently inaccessible, it was accessed from 18 May 2017 to 18
140 January 2018, and a cDNA file was downloaded.

141 The genome, transcriptome, and metatranscriptome assemblies were used to analyze the
142 MATα_HMGbox and HMG-box_ROX1-like domains of the MAT1-1-1 and MAT1-2-1 proteins,
143 respectively.

144 II-3 Alignment of the DNA-binding domain sequences of the mating proteins

145 The amino acid sequences of the MATα_HMGbox domains of the MAT1-1-1 proteins and the HMG-
146 box_ROX1-like domains of the MAT1-2-1 proteins of the wild-type *C. sinensis* isolates and *C. sinensis*
147 insect–fungal complexes were aligned using the GenBank Blastp program (https://blast.ncbi.nlm.nih.gov/
148 (Bethesda, MD, USA), accessed from 18 October 2024 to 10 July 2025).

149 II-4 Bayesian clustering analysis of the DNA-binding domains of the mating proteins

150 Multiple sequence alignment of the DNA-binding domains of the mating proteins of the wild-type *C.*
151 *sinensis* isolates and *C. sinensis* insect–fungal complexes was performed via the auto mode of MAFFT
152 (v7.427; Osaka, Japan). The intron regions were removed using trimAl (v1.4. rev15; Barcelona, Spain).
153 Under the Bayesian information criterion, ProtTest v3.4.2 (University of Vigo and University of A Coruña,
154 Spain) was used to find the optimal amino acid substitution model. Bayesian clustering trees of the DNA
155 binding domain sequences of the MAT1-1-1 and MAT1-2-1 proteins were then inferred using MrBayes
156 v3.2.7 software (Markov chain Monte Carlo [MCMC] algorithm; Uppsala, Sweden) at a sampling
157 frequency of 100 iterations after discarding the initial 25% of the samples from a total of 1 million iterations.
158 This yielded final majority rule consensus trees for the MATα_HMGbox domains of the full-length MAT1-
159 1-1 proteins and the HMG-box_ROX1-like domains of the full-length MAT1-2-1 proteins [Huelsenbeck &
160 Ronquist 2001; Ronquist *et al*. 2012; Li *et al*. 2022, 2023c, 2024b, 2025]. Clustering analysis was conducted
161 at Nanjing Genepioneer Biotechnologies Co. (Nanjing, China).

162 II-5 Amino acid properties and scale analysis

163 The amino acid sequences of the DNA-binding domains of the mating proteins were scaled on the
164 basis of the general chemical characteristics of their side chains (Table S4) as reported at
165 https://web.expasy.org/protscale/ (Basel, Switzerland), accessed from 18 October 2024 to 20 May 2025
166 [Kyte & Doolittle 1982; Deleage & Roux 1987; Gasteiger *et al*. 2005; Peters & Elofsson 2014; Simm *et al*.
167 2016; Li *et al*. 2024b, 2025]. The MATα_HMGbox domain of MAT1-1 proteins (amino acids 51→225 of
168 the reference sequence AGW27560 derived from the *H. sinensis* strain CS68-2-1229 [Bushley *et al*. 2013])
169 and the HMG-box_ROX1-like domain of MAT1-2-1 proteins (amino acids 127→197 of the reference

170 sequence AEH27625 derived from the *H. sinensis* strain CS2 [Zhang *et al*. 2009]), with additional 9 amino
171 acid residues extending upstream and downstream of the domains, were plotted sequentially with a window
172 size of 9 amino acid residues using the linear weight variation model of the ExPASy ProtScale algorithms
173 [Kyte & Doolittle 1982; Deleage & Roux 1987; Gasteiger *et al*. 2005; Li *et al*. 2024b, 2025] to generate
174 ExPASy ProtScale plots to display and compare the topology and waveform changes in hydrophobicity and
175 the 2D structures for α-helices, β-sheets, β-turns, and coils of the DNA-binding domains of the mating
176 proteins.

177 II-6 AlphaFold-based prediction of the 3D structures of the mating proteins

178 For heteromorphic stereostructure analysis in this study, the 3D structures of the MAT1-1-1 and MAT1-
179 2-1 proteins of the wild-type *C. sinensis* isolates were computationally predicted from their amino acid
180 sequences using the artificial intelligence (AI)-based machine learning technology AlphaFold
181 (https://alphafold.com/, Cambridgeshire, UK), downloaded from the AlphaFold database (accessed from 18
182 October 2024 to 10 May 2025) [Jumper *et al*. 2021; David *et al*. 2022; Monzon *et al*. 2022; Rettie *et al*.
183 2023; Xu *et al*. 2023; Abramson *et al*. 2024; Varadi *et al*. 2024; Wroblewski & Kmiecik 2024; Li *et al*.
184 2025].

185 The AlphaFold database provides per-residue model confidence, predicts scores between 0 and 100 on
186 the local distance difference test (pLDDT) and provides a per-residue score that is assigned to each
187 individual residue [Jumper *et al*. 2021; David *et al*. 2022; Monzon *et al*. 2022; Xu *et al*. 2023; Abramson *et*
188 *al*. 2024; Varadi *et al*. 2024]. The model confidence bands are used to color-code the residues in the 3D
189 structures: residues with very high confidence (pLDDT>90) are shown in dark blue, those with high
190 confidence (90>pLDDT>70) appear in light blue, residues with low confidence (70>pLDDT>50) are shown
191 in yellow, and residues with very low confidence (pLDDT<50) are shown in orange [Mariani *et al*. 2013;
192 Wroblewski & Kmiecik 2024; Li *et al*. 2025]. The AlphaFold database provides an average pLDDT score
193 for each of the AI-predicted 3D structural models.

194 II-7 Correlation of the primary, secondary, and tertiary structures of the DNA-
195 binding domains of the MAT1-1-1 and MAT1-2-1 proteins

196 The AlphaFold-predicted 3D structures of the MATα_HMGbox domains of the MAT1-1-1 proteins
197 and the HMG-box_ROX1-like domains of the MAT1-2-1 proteins were amplified at the sites of amino acid
198 substitutions. The locally magnified 3D structures at the mutation sites were correlated with the amino acid
199 substitutions to obtain the primary structures and the changes in topology and waveform using ExPASy
200 ProtScale plotting showing the hydropathy, α-helices, β-sheets, β-turns, and coils for altered hydrophobicity
201 and the 2D structures of the DNA binding domains of the MAT1-1-1 and MAT1-2-1 proteins.

III. Results

III-1 Primary structures of the MATα_HMGbox domains of the full-length MAT1-1-1 proteins

Of the 138 MAT1-1-1 proteins in the AlphaFold database, 118 (85.5%) are full length. Each of these proteins contains 372 amino acid residues. These proteins contribute to 15 heteromorphic 3D structure morphs belonging to 5 Bayesian clusters (Table S1) [Li *et al*. 2025]. Twenty-nine (24.6%) of the 118 full-length MAT1-1-1 proteins derived from wild-type *C. sinensis* isolates contain variable amino acid substitutions.

The MAT1-1-1 proteins contain a MATα_HMGbox domain that locates at amino acids 51→225 (shown in blue and underlined in Figure S1), as represented by the reference MAT1-1-1 protein AGW27560 derived from the *H. sinensis* strain CS68-2-1229 [Bushley *et al*. 2013]. Other MAT1-1-1 proteins derived from wild-type *C. sinensis* isolates or encoded by the genome assemblies of the *H. sinensis* strains and the metatranscriptome assemblies of *C. sinensis* insect–fungal complexes contain various amino acid substitutions, as shown in red in Figure S1. The MATα_HMGbox domains of 10 (34.5%) of the 29 mutant proteins are 100% identical to that of the query protein AGW27560. Each of the remaining 19 proteins (65.5%) contains 1 or 2 substitutions in the amino acid residues at various sites within the MATα_HMGbox domains.

Figure S1 also shows the MATα_HMGbox domains of the MAT1-1-1 proteins encoded by the genome assemblies ANOV01017390 (794←1129 & 1280←1396), LKHE01001116 (4183←4620 & 4667←4759), and JAAVMX010000001 (6,699,061→6,699,153 & 6,699,203→6,699.637) of the *H. sinensis* strains Co18, 1229, and IOZ07, respectively [Hu *et al*. 2013; Li *et al*. 2016a; Shu *et al*. 2020]. (Note: the arrows "→" and "←" indicate sequences in the sense and antisense strands of the genomes, respectively; "&" refers to the removed intron portion.) These genome-encoded MAT1-1-1 proteins are truncated at their C-termini; the truncation segments are located far downstream of the MATα_HMGbox domains.

The genome assemblies LWBQ00000000 and NGJJ00000000 and the transcriptome assembly GCQL00000000 of the *H. sinensis* strains ZJB12195, CC1406-20395, and L0106, respectively, do not contain the genes or transcripts that encode the MAT1-1-1 proteins [Jin *et al*. 2020; Liu *et al*. 2015, 2020].

The metatranscriptome assemblies GAGW01008880 (300←1127) and OSIN7648 (1→1065) of natural *C. sinensis* insect–fungal complexes encode the MAT1-1-1 proteins (*cf*. Figure S1) [Xiang *et al*. 2014; Xia *et al*. 2017]. The MAT1-1-1 protein OSIN7648 is truncated in midsequence by 18 amino acid residues (SMQREYQAPRFFYDYSVS) between residues 863 and 864; the truncation segment is located downstream of the MATα_HMGbox domain (151→675). The N-terminus of the MATα_HMGbox domain (741←1127) of the MAT1-1-1 protein encoded by GAGW01008880 is truncated by 46 amino acid residues

235 (AAASRATRQTKEASCDRAKRPLNAFMAFRSYYLKLFPDVQQKTASG).

236 III-2 Primary structures of the HMG-box_ROX1-like domains of the full-length 237 MAT1-2-1 proteins

238 Of the 74 MAT1-2-1 proteins listed in the AlphaFold database, 69 (93.2%) are full-length proteins,
239 each of which contains 249 amino acid residues; these proteins contribute to 17 heteromorphic AlphaFold
240 tertiary structure morphs belonging to 5 Bayesian clusters (Table S2) [Li *et al*. 2025]. Of the 69 full-length
241 proteins, 39 (56.5%) are 100% identical to the representative MAT1-2-1 protein AEH27625, which was
242 derived from the *H. sinensis* strain CS2 [Zhang *et al*. 2009]. The remaining 30 full-length proteins (43.5%)
243 contain amino acid substitutions at various sites, as shown in red in Figure S2. The HMG-box_ROX1-like
244 domains of the MAT1-2-1 proteins are located at amino acid residues 127→197, as shown in blue and
245 underlined in Figure S2; whereas the 9 external amino acid residues upstream and downstream of the
246 domain are shown blue but not underlined. The HMG-box_ROX1-like domain sequences of 3 of the 30
247 variable AMT1-2-1 proteins are 100% identical to the domain sequence of the query protein AEH27625,
248 whereas the domains of the remaining 27 proteins contain 1–3 amino acid substitutions, as shown in red in
249 Figure S2.

250 Figure S2 also shows the MAT1-2-1 proteins encoded by the genome assemblies ANOV01000063,
251 LKHE01001605, LWBQ01000021, and NGJJ01000619 of the *H. sinensis* strains Co18, 1229, ZJB12195,
252 and CC1406-20395, respectively [Hu *et al*. 2013; Li *et al*. 2016a; Jin *et al*. 2020; Liu *et al*. 2020]. An S-to-
253 A substitution occurred in each of the HMG-box_ROX1-like domains of the genome-encoded MAT1-2-1
254 proteins ANOV01000063 (9759→9851 & 9907→10,026), LKHE01001605 (14,016←14,135 &
255 14,191←14,283), LWBQ01000021 (239,029←239,148 & 239,204←239,269), and NGJJ01000619
256 (23,186←23,305 & 23,361←23,453). An additional Y-to-H substitution occurred in the HMG-box_ROX1-
257 like domains of LKHE01001605, LWBQ01000021 and NGJJ01000619 but not in the HMG-box_ROX1-
258 like domain of ANOV01000063, resulting in 97.2–98.6% similarity to the sequence of the HMG-
259 box_ROX1-like domain of the query protein AEH27625 [Zhang *et al*. 2009].

260 The genome assembly JAAVMX000000000 of the *H. sinensis* strain IOZ07 and the metatranscriptome
261 assembly GAGW00000000 of the *C. sinensis* insect–fungi complex do not contain genes or transcripts
262 encoding MAT1-2-1 proteins [Xiang *et al*. 2014; Shu *et al*. 2020].

263 Figure S2 also shows the protein sequences encoded by the MAT1-2-1 transcripts of the transcriptome
264 assembly GCQL01020543 (397←1143) of the *H. sinensis* strain L0106 and the metatranscriptome
265 assembly OSIN7649 (1→747) of the mature *C. sinensis* insect–fungal complex [Liu *et al*. 2015; Xia *et al*.
266 2017]. The HMG-box_ROX1-like domains (553←765 of GCQL01020543 and 379→591 of OSIN7649)
267 of these proteins contain Y-to-H substitutions, resulting in 98.6% similarity to the sequence of that domain

in the query protein AEH27625 [Zhang *et al*. 2013].

III-3 Bayesian analysis of the MATα_HMGbox domains of the full-length MAT1-1-1 proteins

The sequences of the MATα_HMGbox domains of 19 full-length MAT1-1-1 proteins that display various amino acid substitutions were subjected to Bayesian clustering analysis and compared with the sequences of 6 authentic MAT1-1-1 proteins as the references (Figure 1).

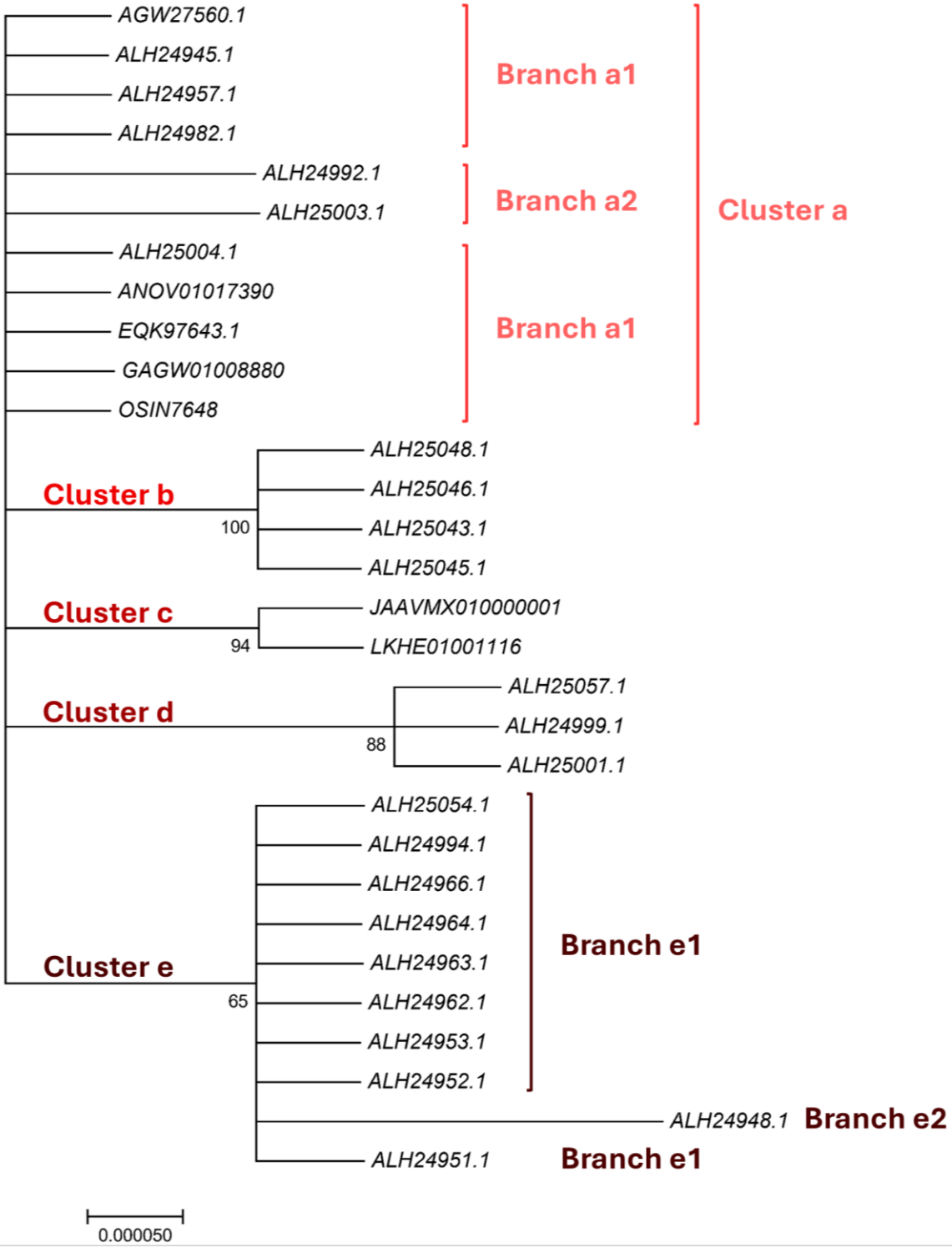

Figure 1. A Bayesian majority rule consensus clustering tree for the MATα_HMGbox domain sequences of the 25 MAT1-1-1 proteins of the wild-type *C. sinensis* isolates and the corresponding domain sequences encoded by the genome and metatranscriptome assemblies of the *H. sinensis* strains and *C. sinensis* insect–fungal complexes was obtained by MrBayes v3.2.7 software.

The MATα_HMGbox domains of the full-length MAT1-1-1 proteins were clustered into 5 Bayesian clusters (Figure 1), among which Clusters a and d were branched. The domains of the 19 proteins with various amino acid substitutions were clustered into Clusters/Branches a2, b, d, and e1−e2 in the Bayesian clustering tree. Cluster d has a longer clustering distance than some of the other clusters do, and Branch e2 has the longest clustering distance. The MATα_HMGbox domains encoded by the genome assemblies JAAVMX010000001 (6,699,061→6,699,153 & 6,699,203→6,699.637) and LKHE01001116 (4183←4620 & 4667←4759) of the *H. sinensis* strains 1229 and IOZ07 contain Y-to-M substitutions [Li *et al*. 2016; Shu *et al*. 2020]. The domains encoded by the genome assembly ANOV01017390 (794←1129 & 1280←1396) of *H. sinensis* strain Co18 and the metatranscriptome assembly OSIN7648 (151→675) of the *C. sinensis* insect–fungal complex contain no changed amino acid residues [Hu *et al*. 2013; Xia *et al*. 2017]. The domain encoded by the metatranscriptome assembly GAGW01008880 (714←1127) of the *C. sinensis* insect–fungal complex is truncated at the N-terminus (Figure S1) [Xiang *et al*. 2014]. The MATα_HMGbox domains encoded by the genome assembly ANOV01017390 and metatranscriptome assemblies OSIN7648 and GAGW01008880 cluster into Branch a1 in the Bayesian clustering tree, together with the 6 authentic MAT1-1-1 proteins (Figure 1).

Tables S5−S6 summarize the Bayesian clustering results and show the amino acid substitutions and deletions in the MATα_HMGbox domains of the MAT1-1-1 proteins derived from wild-type *C. sinensis* isolates and those encoded by the genome and metatranscriptome assemblies of *H. sinensis* strains and natural *C. sinensis* insect–fungal complexes, respectively.

III-4 Bayesian analysis of the HMG-box_ROX1-like domains of the full-length MAT1-2-1 protein sequences

Thirty full-length MAT1-2-1 proteins that are present in wild-type *C. sinensis* isolates or encoded by the genome and transcriptome assemblies of *H. sinensis* strains and by the metatranscriptome assembly of the *C. sinensis* insect–fungal complex and that have various amino acid substitutions in their HMG-box_ROX1-like domains were subjected to Bayesian clustering analysis and compared with the HMG-box_ROX1-like domains of 6 authentic MAT1-2-1 proteins as the references. Figure 2 shows 2 branched clusters (a and b). Branches b2−b3 have longer clustering distances than do some of the other branches, and Branch b2β has the longest clustering distance.

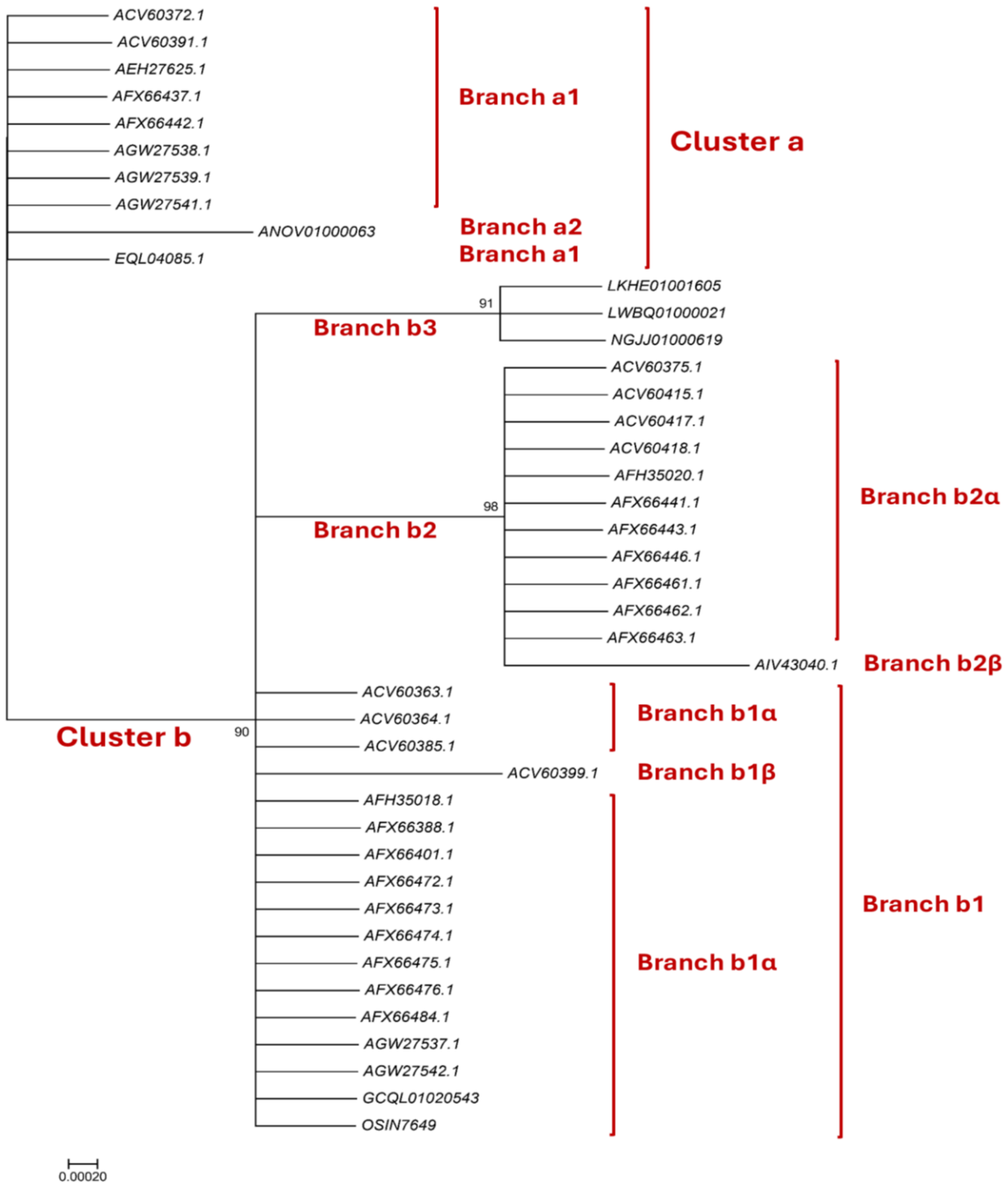

Figure 2. Bayesian majority rule consensus clustering tree inferred via MrBayes v3.2.7 software for the HMG-box_ROX1-like domain sequences of 35 full-length MAT1-2-1 proteins of the wild-type *C. sinensis* isolates and the corresponding domain segments of the translated genome, transcriptome, and metatranscriptome assemblies of the *H. sinensis* strains and *C. sinensis* insect–fungal complexes.

The HMG-box_ROX1-like domain encoded by the genome assembly ANOV01000063 (9759→9851 & 9907→10,026) of *H. sinensis* strain Co18 contains an S-to-A substitution and is clustered into Branch a2 with a slightly longer clustering distance (Figures 2 and S2) [Hu *et al*. 2013]. The domains encoded by other genome assemblies [LKHE01001605 (14,016←14,135 & 14,191←14,135 & 14,191←14,283),

316 LWBQ01000021 (239,029←239,148 & 239,204←239,269), and NGJJ01000619 (23,186←23,305 &
317 23,361←23,453) of the *H. sinensis* strains 1229, ZJB12195, and CC1406-20395, respectively] [Li *et al*.
318 2016; Jin *et al*. 2020; Liu *et al*. 2020] contain Y-to-H and S-to-A substitutions and are clustered into Branch
319 b3 in the Bayesian clustering tree (Figures 2 and S2).

320 The HMG-box_ROX1-like domain of the MAT1-2-1 protein encoded by the transcriptome assembly
321 GCQL01020543 (553←765) of the *H. sinensis* strain L0106 contains a Y-to-H substitution [Liu *et al*. 2015].
322 The domain of the MAT1-2-1 protein encoded by the metatranscriptome assembly OSIN7649 (379→591)
323 of the *C. sinensis* insect–fungi complex is 100% identical to the reference MAT1-2-1 protein AEH27625
324 [Zhang *et al*. 2009; Xia *et al*. 2017]. The domains of the MAT1-2-1 proteins encoded by the transcriptome
325 and metatranscriptome assemblies were clustered into Branch b1α in the Bayesian clustering tree (Figures
326 2 and S2).

327 Tables S7–S8 summarize the Bayesian clustering results that reflect the amino acid substitutions and
328 deletions in the HMG-box_ROX1-like domains of MAT1-2-1 proteins derived from wild-type *C. sinensis*
329 isolates or encoded by the genome, transcriptome and metatranscriptome assemblies of *H. sinensis* strains
330 and natural *C. sinensis* insect–fungal complexes, respectively.

331 III-5 Heteromorphic stereostructures of the MATα_HMGbox domains of full-length 332 MAT1-1-1 proteins derived from wild-type *C. sinensis* isolates

333 Section III-5 presents analyses of the correlations between the changes in the structure and
334 hydrophobicity of the MATα_HMGbox domains of full-length MAT1-1-1 proteins (under 7 AlphaFold 3D
335 structure codes; *cf*. Table S5) derived from wild-type *C. sinensis* isolates, compared to the reference MAT1-
336 1-1 proteins represented by AGW27560 (under the AlphaFold code U3N942) derived from the *H. sinensis*
337 strain CS68-2-1229 (*cf*. Table S1) [Bushley *et al*. 2013]. The MATα_HMGbox domain sequences (amino
338 acid residues 51→225) were extended by 9 amino acid residues both upstream and downstream of the
339 domains because of the setting of the sequential ExPASy ProtScale plotting for hydropathy, α-helices, β-
340 sheets, β-turns, and coils at a window size of 9 amino acid residues (*cf*. Section II-5 of Materials and
341 methods).

342 Figure 3 compares the hydrophobicities and the structures of the MATα_HMGbox domain of the
343 mutant MAT1-1-1 protein ALH24992 (under the AlphaFold code A0A0N9R5B3) derived from the wild-
344 type *C. sinensis* isolate SC09_65 (*cf*. Tables S1 and S5) [Zhang & Zhang 2015] with those of the
345 MATα_HMGbox domain of the reference protein AGW27560 (under the AlphaFold code U3N942) derived
346 from the *H. sinensis* strain CS68-2-1229 [Bushley *et al*. 2013]. Panel A shows an A-to-T substitution
347 (aliphatic alanine to threonine with polar side chains; hydropathy indices changed from 1.8 to -0.7). This
348 substitution causes reduced hydrophobicity (the larger the hydropathy value is the stronger the

hydrophobicity, whereas negative values indicate hydrophilicity [Kyte & Doolittle 1982]), as illustrated by the changes in topology and waveform in the hydropathy plot shown in Panel B. These changes result in an altered secondary structure of the protein in the area surrounding the mutation site in the MATα_HMGbox domain of the mutant MAT1-1-1 protein ALH24992, as illustrated by the changes in topology and waveform in the ExPASy ProtScale plots for α-helices, β-sheets, β-turns, and coils shown in Panels C–F, respectively.

Panel A: Alignment of amino acid sequences

```
AGW27560 42  ADVLTPVSTAAASRATRQTKEASCDRAKRPLNAFMAFRSYYLKLFPDVQQKTASGFLTTL 101
ALH24992 42  ---------T------------------------------------------------- 101

AGW27560 102 WHKDPFRNKWALIAKVYSFVRDQIGKDKVSLSYFMSLACPTMTIIEPAAYLNALGWCVQD 161
ALH24992 102 ------------------------------------------------------------ 161

AGW27560 162 DDAGSQKLFQDESSANLDQSSLLSAEYPSTEIELLSALVNIGYFPDHGADLVERMGSSHS 221
ALH24992 162 ------------------------------------------------------------ 221

AGW27560 222 GIMAPRAANCTPP                                                234
ALH24992 222 -------------                                                234
```

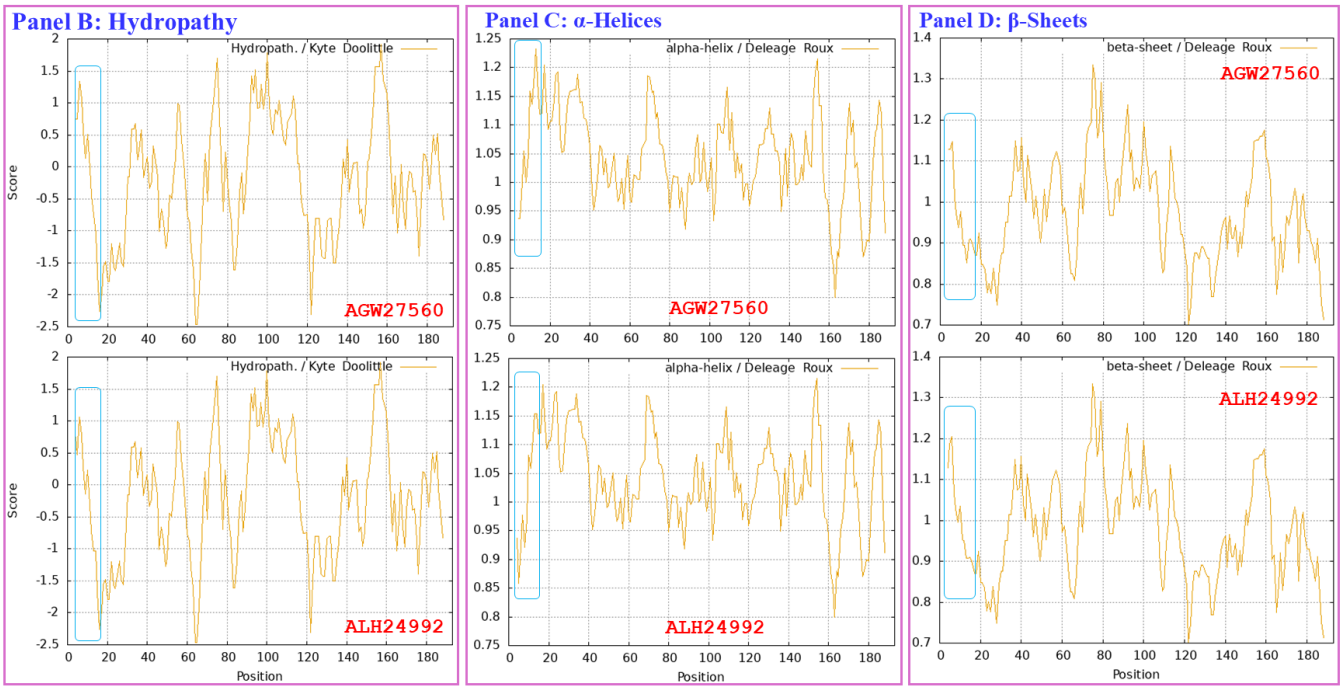

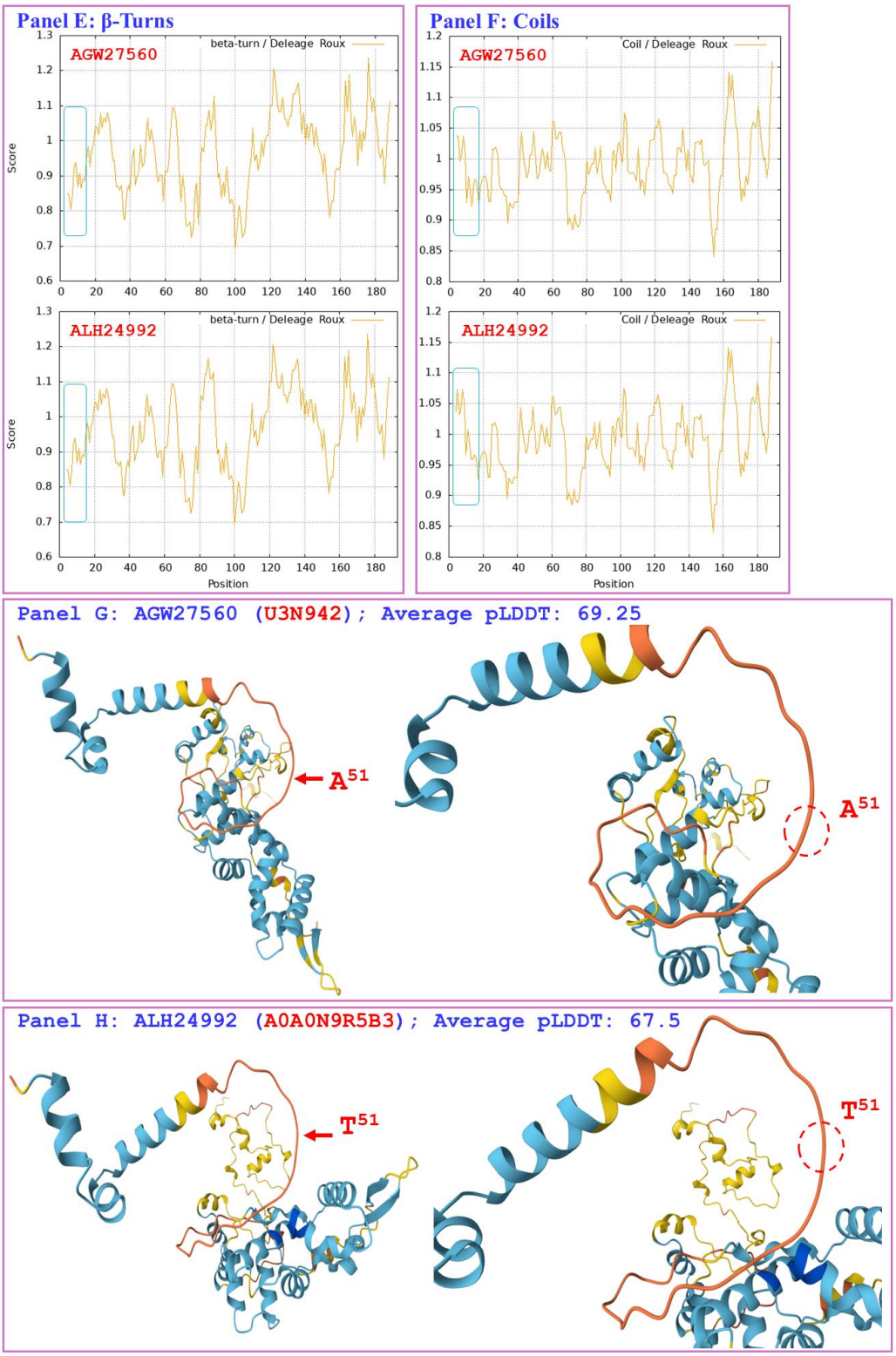

Figure 3. Correlation of the changes in the hydrophobicity and the primary, secondary, and tertiary structures of the MATα_HMGbox domains of MAT1-1-1 proteins: the reference protein AGW27560 (under the AlphaFold code U3N942) derived from the *H. sinensis* strain CS68-2-1229 and the mutant protein ALH24992 (under the AlphaFold code A0A0N9R5B3) derived from the wild-type *C. sinensis* isolate SC09_65. Panel A shows an alignment of the amino acid sequences of the MATα_HMGbox domains of the MAT1-1-1 proteins; the amino acid substitution is shown in red, whereas the hyphens indicate identical amino acid residues. The ExPASy ProtScale plots show the changes in hydrophobicity (Panel B) and in the 2D structure (Panels C–F for α-helices, β-sheets, β-turns, and coils, respectively) of the protein; the open rectangles in blue outline the changes in topology and waveform of the ExPASy plots. Panels G–H show the 3D structures of the full-length proteins on the left and the locally amplified structures

surrounding the mutation site on the right. The model confidence for the AlphaFold-predicted 3D structures is indicated: ■ very high (pLDDT>90); ■ high (90>pLDDT>70); ■ low (70>pLDDT>50); ■ very low (pLDDT<50).

As shown in Panels G–H of Figure 3, which illustrate the 3D structures of the proteins, the substitution is located upstream of the core structure of 3 α-helices and may not directly participate in stabilizing the hydrophobic core structure of the DNA-binding domain [Baxevanis *et al*. 1995; Thapar 2015]. However, replacement of alanine with a threonine residue with reduced hydrophobicity caused altered stereostructure of the MATα_HMGbox domain of the MAT1-1-1 protein ALH24992 under the AlphaFold code A0A0N9R5B3, perhaps through long-range spatial interactions. The mutant MATα_HMGbox domain clustered into Branch a2 in the Bayesian clustering tree (*cf*. Figure 1, Table S5).

Figure 4 compares the hydrophobicities and the structure of the MATα_HMGbox domain of the MAT1-1-1 protein ALH24948 (under the AlphaFold code A0A0N9QUF3) derived from the wild-type *C. sinensis* isolate GS09_143 (*cf*. Table S1) [Zhang & Zhang 2015] with those of the MATα_HMGbox domain of the reference protein AGW27560 (under the AlphaFold code U3N942) derived from the *H. sinensis* strain CS68-2-1229 [Bushley *et al*. 2013]. Panel A shows substitutions of two adjacent residues: Q-to-S (glutamine to serine, both of which have polar side chains; hydropathy indices changed from -3.5 to -0.8 [Kyte & Doolittle 1982]) and I-to-F (aliphatic isoleucine to aromatic phenylalanine; hydropathy indices changed from 4.5 to 2.8), causing altered hydrophobicity as illustrated by the changes in topology and waveform in the hydropathy plot in Panel B. These changes alter the secondary structure surrounding the mutation sites in the MATα_HMGbox domain, as illustrated by the changes in topology and waveform in the ExPASy ProtScale plots for α-helices, β-sheets, β-turns, and coils shown in Panels C–F. As shown in Panels G–H for the diagrams of 3D structure, the adjacent amino acid substitutions are located at the end of one of the 3 α-helices that form the hydrophobic core stereostructure [Baxevanis *et al*. 1995; Thapar 2015], and they cause the altered tertiary structure of the MATα_HMGbox domain of the mutant protein ALH24948 under the AlphaFold code A0A0N9QUF3. The mutant MATα_HMGbox domain clustered into Branch e2 in the Bayesian clustering tree (*cf*. Figure 1, Table S5).

Panel A: Amino acid sequence alignment

```
AGW27560 42  ADVLTPVSTAAASRATRQTKEASCDRAKRPLNAFMAFRSYYLKLFPDVQQKTASGFLTTL 101
ALH24948 42  ------------------------------------------------------------ 101

AGW27560 102 WHKDPFRNKWALIAKVYSFVRDQIGKDKVSLSYFMSLACPTMTIIEPAAYLNALGWCVQD 161
ALH24948 102 ----------------------SF------------------------------------ 161

AGW27560 162 DDAGSQKLFQDESSANLDQSSLLSAEYPSTEIELLSALVNIGYFPDHGADLVERMGSSHS 221
ALH24948 162 ------------------------------------------------------------ 221

AGW27560 222 GIMAPRAANCTPP                                                234
ALH24948 222 -------------                                                234
```

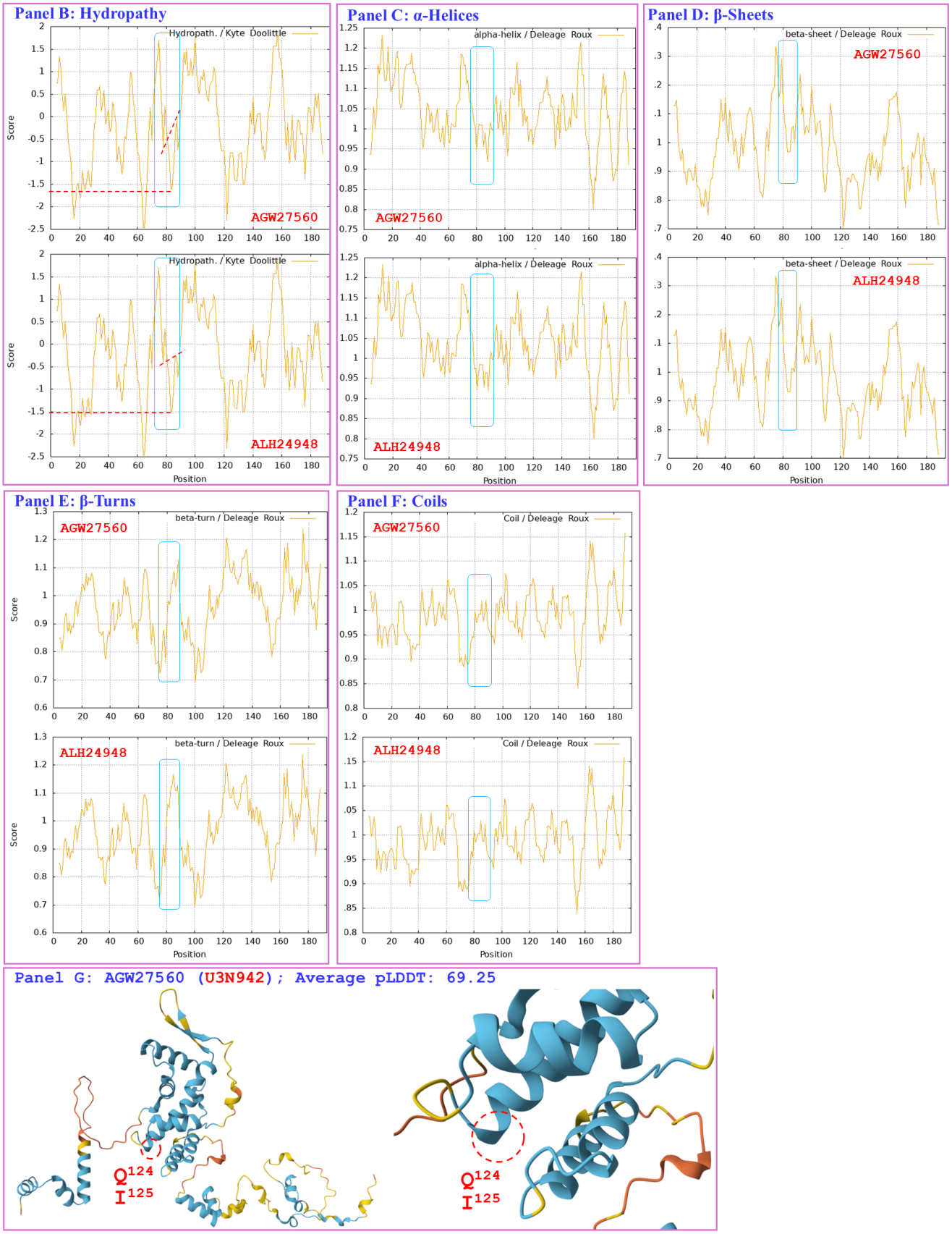
Panel B: Hydropathy
Hydropath. / Kyte Doolittle
AGW27560
ALH24948
Score
Position
Panel C: α-Helices
alpha-helix / Deleage Roux
AGW27560
ALH24948
Position
Panel D: β-Sheets
beta-sheet / Deleage Roux
AGW27560
ALH24948
Position
Panel E: β-Turns
beta-turn / Deleage Roux
AGW27560
ALH24948
Score
Position
Panel F: Coils
Coil / Deleage Roux
AGW27560
ALH24948
Position
Panel G: AGW27560 (U3N942); Average pLDDT: 69.25
Q124
I125
Q124
I125

393

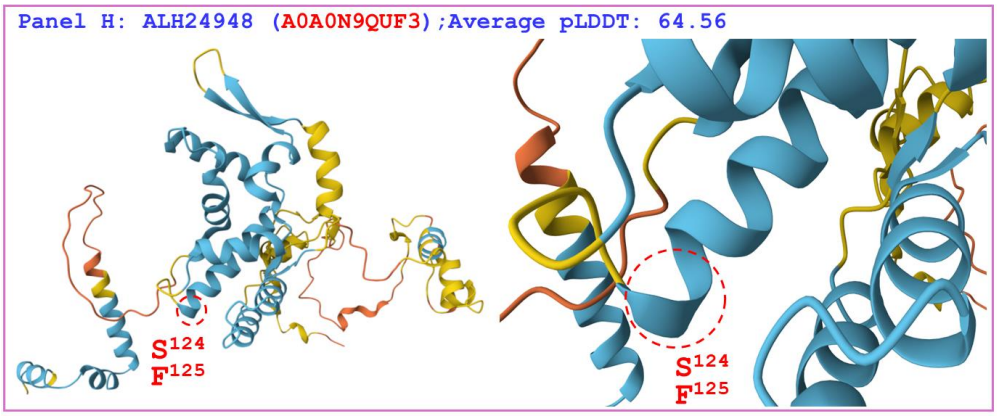

Figure 4. Correlations among the changes in the primary, secondary, and tertiary structures of the MATα_HMGbox domains of MAT1-1-1 proteins: the reference protein AGW27560 (under the AlphaFold code U3N942) derived from the *H. sinensis* strain CS68-2-1229 and the mutant MAT1-1-1 protein ALH24948 (under the AlphaFold code A0A0N9QUF3) derived from the wild-type *C. sinensis* isolate GS09_143. Panel A shows an alignment of the MATα_HMGbox domain sequences of the MAT1-1-1 proteins; amino acid substitutions are shown in red, whereas the hyphens indicate identical amino acid residues. The ExPASy ProtScale plots show the changes in hydrophobicity (Panel B) and in the 2D structure (Panels C–F for α-helices, β-sheets, β-turns, and coils, respectively) of the protein; the open rectangles in blue outline the changes in topology and waveform shown in the ExPASy plots. Panels G–H show the 3D structures of the full-length proteins on the left and the locally amplified structures at the sites of substitutions on the right. The model confidence for the AlphaFold-predicted 3D structures is indicated as follows: very high (pLDDT>90); high (90>pLDDT>70); low (70>pLDDT>50); very low (pLDDT<50).

Figure 5 compares the hydrophobicities and the structures of the MATα_HMGbox domains of the MAT1-1-1 proteins ALH25043, ALH25045, ALH25046, and ALH25048 (under the AlphaFold code A0A0N9QMS9) derived from the wild-type *C. sinensis* isolates YN09_22, YN09_51, YN09_6, and YN09_64, respectively, (*cf*. Table S1) [Zhang & Zhang 2015] with those of the MATα_HMGbox domain of the reference protein AGW27560 (under the AlphaFold code U3N942) derived from the *H. sinensis* strain CS68-2-1229 [Bushley *et al*. 2013]. Panel A shows substitutions of R-to-I (basic arginine to aliphatic isoleucine; hydropathy indices changed from -4.5 to 4.5 [Kyte & Doolittle 1982]) and P-to-T (proline to threonine, both of which possess polar neutral side chains; hydropathy indices changed from -1.6 to -0.7). These substitutions result in increased hydrophobicity, as illustrated by the changes in topology and waveform that are apparent in the hydropathy plot in Panel B. They also result in altered secondary structure surrounding the mutation sites in the MATα_HMGbox domains of the MAT1-1-1 proteins ALH25043, ALH25045, ALH25046, and ALH25048, as illustrated by the changes in topology and waveform shown in the ExPASy ProtScale plots for α-helices, β-sheets, β-turns, and coils in Panels C–F. As shown in the diagrams of 3D structure in Panels G–H, the sites of the R-to-I and P-to-T substitutions are inside and outside, respectively, the hydrophobic core formed by the 3 α-helices, and the substantial increases in hydrophobicity alter the tertiary structures of the MATα_HMGbox domains of MAT1-1-1 proteins under the AlphaFold code A0A0N9QMS9. The mutant MATα_HMGbox domain clustered into Cluster 2 in the Bayesian clustering tree (*cf*. Figure 1, Table S5).

Panel A: Amino acid sequence alignment

```
AGW27560 42  ADVLTPVSTAAASRATRQTKEASCDRAKRPLNAFMAFRSYYLKLFPDVQQKTASGFLTTL 101
ALH25043 42  ------------------------------------------------------------ 101
ALH25045 42  ------------------------------------------------------------ 101
ALH25046 42  ------------------------------------------------------------ 101
ALH25048 42  ------------------------------------------------------------ 101

AGW27560 102 WHKDPFRNKWALIAKVYSFVRDQIGKDKVSLSYFMSLACPTMTIIEPAAYLNALGWCVQD 161
ALH25043 102 ------------------------------------------------------------ 161
ALH25045 102 ------------------------------------------------------------ 161
ALH25046 102 ------------------------------------------------------------ 161
ALH25048 102 ------------------------------------------------------------ 161

AGW27560 162 DDAGSQKLFQDESSANLDQSSLLSAEYPSTEIELLSALVNIGYFPDHGADLVERMGSSHS 221
ALH25043 162 ----------------------------------------------------I------- 221
ALH25045 162 ----------------------------------------------------I------- 221
ALH25046 162 ----------------------------------------------------I------- 221
ALH25048 162 ----------------------------------------------------I------- 221

AGW27560 222 GIMAPRAANCTPP                                               234
ALH25043 222 ----T--------                                               234
ALH25045 222 ----T--------                                               234
ALH25046 222 ----T--------                                               234
ALH25048 222 ----T--------                                               234
```

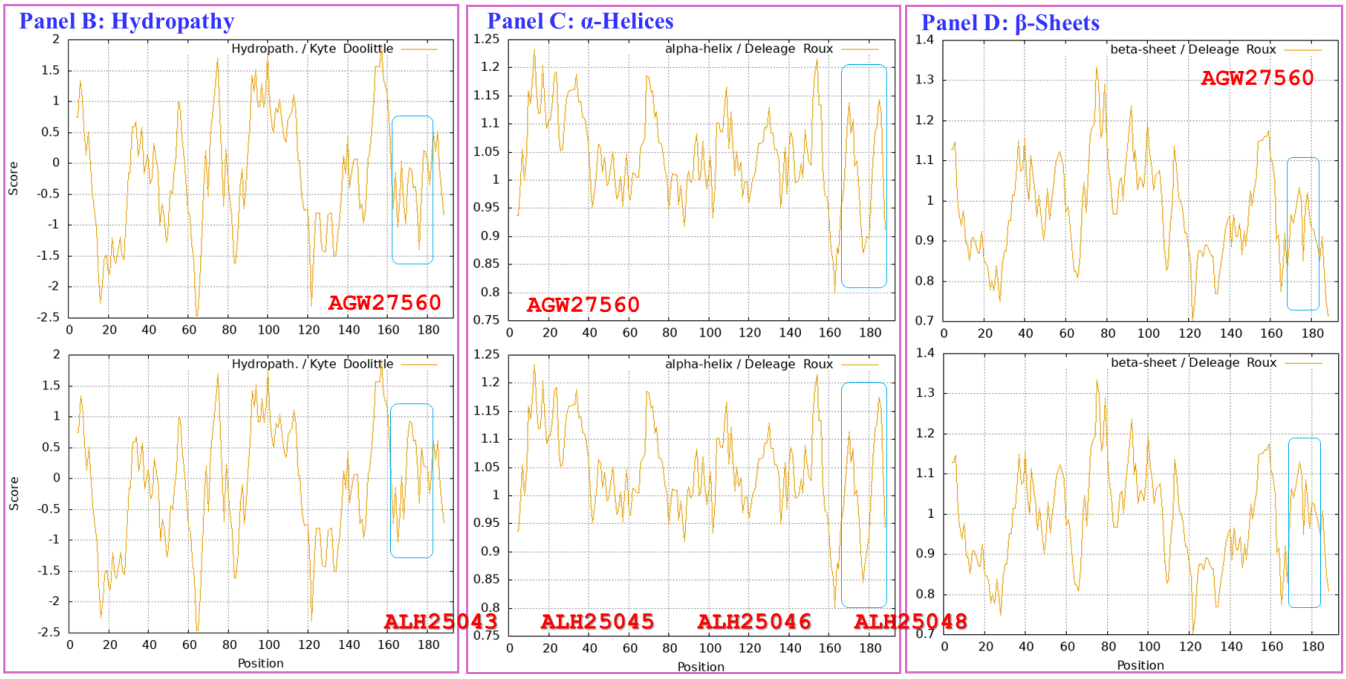

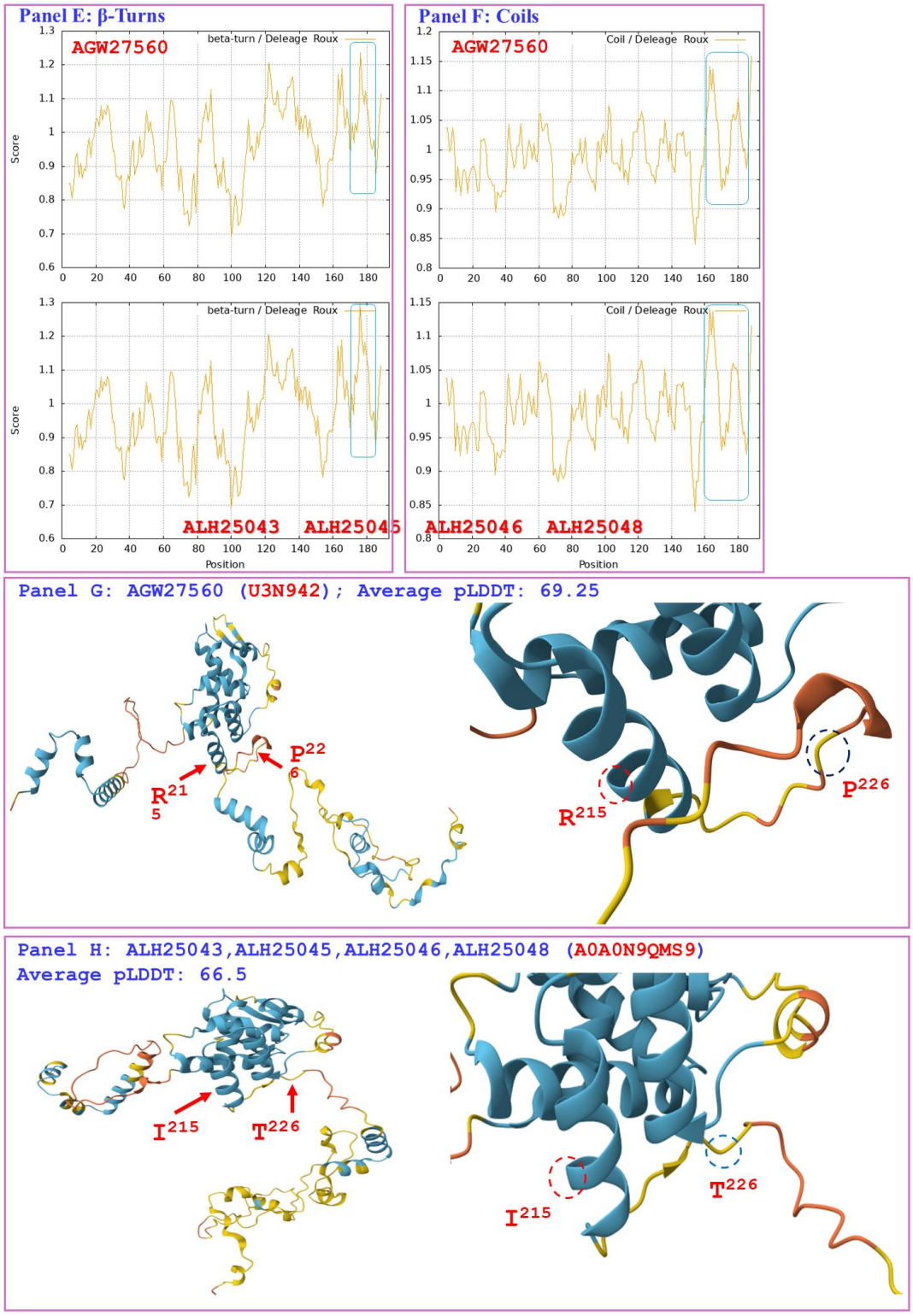

Figure 5. Correlation of changes in the primary, secondary, and tertiary structures of the MATα_HMGbox domains of the MAT1-1-1 proteins: the reference protein AGW27560 (under the AlphaFold code U3N942) is derived from the *H. sinensis* strain CS68-2-1229 and the mutant MAT1-1-1 proteins ALH25043, ALH25045, ALH25046, and ALH25048 (under the AlphaFold code A0A0N9QMS9) are derived from the wild-type *C. sinensis* isolates YN09_22, YN09_51, YN09_6, and YN09_64, respectively. Panel A shows an alignment of the amino acid sequences of the MATα_HMGbox domains of the MAT1-1-1 proteins; amino acid substitutions are shown in red, whereas the hyphens indicate identical amino acid residues. The ExPASy ProtScale plots show the changes in hydrophobicity (Panel B) and in the 2D structure (Panels C–F for α-helices, β-sheets, β-turns, and coils, respectively) of the proteins; the open rectangles in blue outline the changes in topology and waveform of the plots. Panels G–H show the 3D structures of

the full-length proteins on the left and the locally amplified structures at the sites of substitutions on the right. The model confidence for the AlphaFold-predicted 3D structures is indicated as follows: ■ very high (pLDDT>90); ■ high (90>pLDDT>70); ■ low (70>pLDDT>50); ■ very low (pLDDT<50).

Figure 6 compares the hydrophobicities and structures of the MATα_HMGbox domains of the MAT1-1-1 proteins ALH25054, ALH24951, ALH24952, ALH24953, ALH24962, ALH24963, ALH24964, ALH24966, and ALH24994 (under the AlphaFold code A0A0N7G845) derived from the wild-type *C. sinensis* isolates GS09_311, GS09_229, GS09_281, GS10_1, QH09_164, QH09_173, QH09_201, QH09_210, and SC09_87, respectively (*cf.* Table S1) [Zhang & Zhang 2015] with those of the reference protein AGW27560 (under the AlphaFold code U3N942) derived from the *H. sinensis* strain CS68-2-1229 [Bushley *et al.* 2013]. Panel A shows I-to-L substitutions (aliphatic isoleucine to aliphatic leucine, hydropathy indices changed from 4.5 to 3.8 [Kyte & Doolittle 1982]); these substitutions resulted in reduced hydrophobicity, as illustrated by the changes in topology and waveform shown in Panel B for the hydropathy plot.

Panel A: Amino acid sequence alignment

```
AGW27560 42  ADVLTPVSTAAASRATRQTKEASCDRAKRPLNAFMAFRSYYLKLFPDVQQKTASGFLTTL 101
ALH25054 42  ------------------------------------------------------------ 101
ALH24951 42  ------------------------------------------------------------ 101
ALH24952 42  ------------------------------------------------------------ 101
ALH24953 42  ------------------------------------------------------------ 101
ALH24962 42  ------------------------------------------------------------ 101
ALH24963 42  ------------------------------------------------------------ 101
ALH24964 42  ------------------------------------------------------------ 101
ALH24966 42  ------------------------------------------------------------ 101
ALH24994 42  ------------------------------------------------------------ 101

AGW27560 102 WHKDPFRNKWALIAKVYSFVRDQIGKDKVSLSYFMSLACPTMTIIEPAAYLNALGWCVQD 161
ALH25054 102 -----------------------L------------------------------------ 161
ALH24951 102 -----------------------L------------------------------------ 161
ALH24952 102 -----------------------L------------------------------------ 161
ALH24953 102 -----------------------L------------------------------------ 161
ALH24962 102 -----------------------L------------------------------------ 161
ALH24963 102 -----------------------L------------------------------------ 161
ALH24964 102 -----------------------L------------------------------------ 161
ALH24966 102 -----------------------L------------------------------------ 161
ALH24994 102 -----------------------L------------------------------------ 161

AGW27560 162 DDAGSQKLFQDESSANLDQSSLLSAEYPSTEIELLSALVNIGYFPDHGADLVERMGSSHS 221
ALH25054 162 ------------------------------------------------------------ 221
ALH24951 162 ------------------------------------------------------------ 221
ALH24952 162 ------------------------------------------------------------ 221
ALH24953 162 ------------------------------------------------------------ 221
ALH24962 162 ------------------------------------------------------------ 221
ALH24963 162 ------------------------------------------------------------ 221
ALH24964 162 ------------------------------------------------------------ 221
ALH24966 162 ------------------------------------------------------------ 221
ALH24994 162 ------------------------------------------------------------ 221

AGW27560 222 GIMAPRAANCTPP                                               234
ALH25054 222 -------------                                               234
ALH24951 222 -------------                                               234
ALH24952 222 -------------                                               234
ALH24953 222 -------------                                               234
ALH24962 222 -------------                                               234
ALH24963 222 -------------                                               234
ALH24964 222 -------------                                               234
ALH24966 222 -------------                                               234
ALH24994 222 -------------                                               234
```

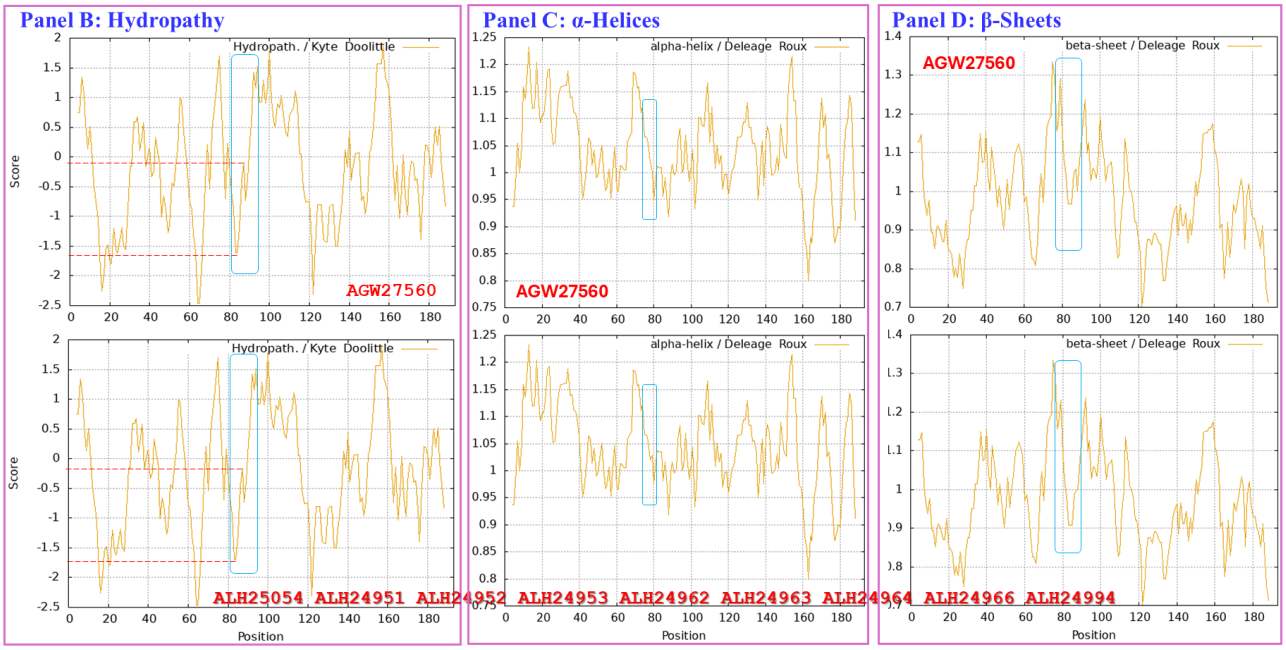
Panel B: Hydropathy
Hydropath. / Kyte Doolittle
Score
AGW27560
ALH25054 ALH24951 ALH24952
Position
Panel C: α-Helices
alpha-helix / Deleage Roux
AGW27560
ALH24953 ALH24962 ALH24963 ALH24964
Position
Panel D: β-Sheets
beta-sheet / Deleage Roux
AGW27560
ALH24966 ALH24994
Position

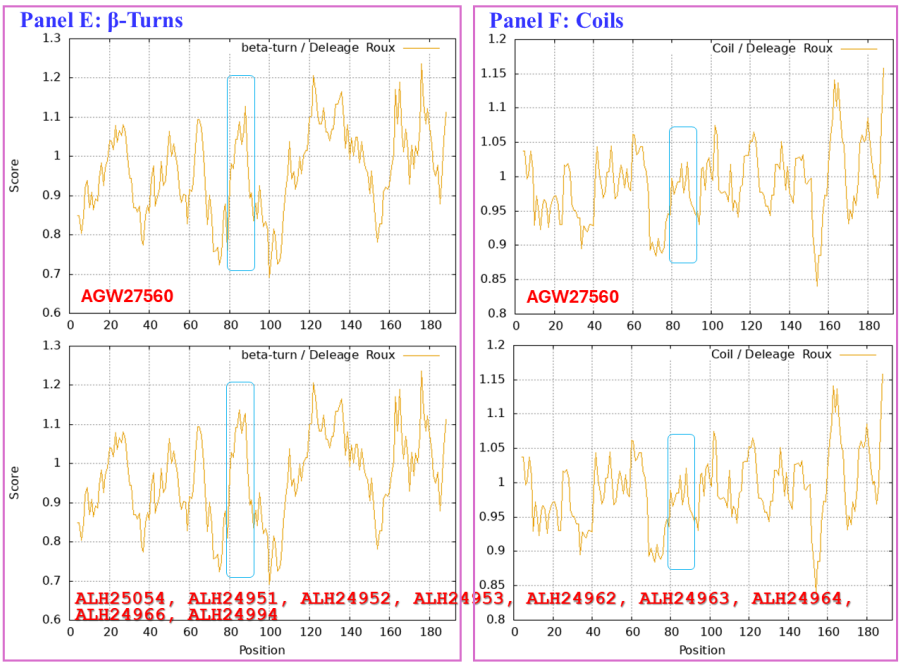
Panel E: β-Turns
beta-turn / Deleage Roux
Score
AGW27560
ALH25054, ALH24951, ALH24952, ALH24953,
ALH24966, ALH24994
Position
Panel F: Coils
Coil / Deleage Roux
AGW27560
ALH24962, ALH24963, ALH24964,
Position

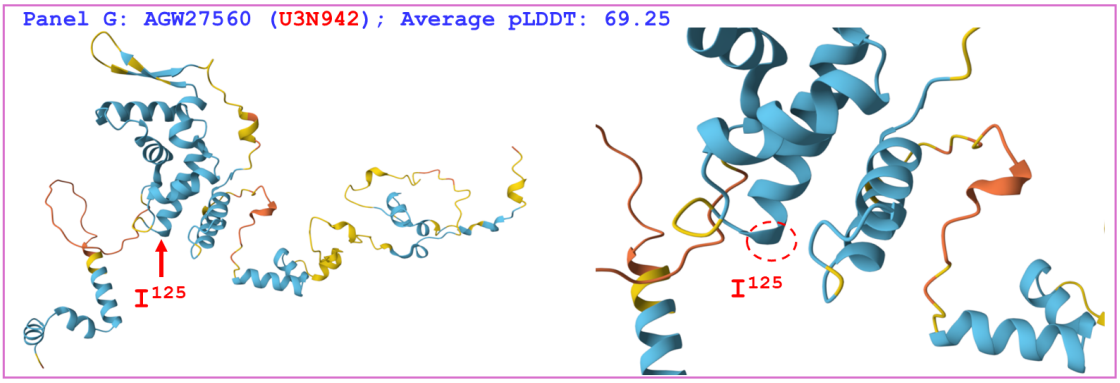
Panel G: AGW27560 (U3N942); Average pLDDT: 69.25
I125
I125

450

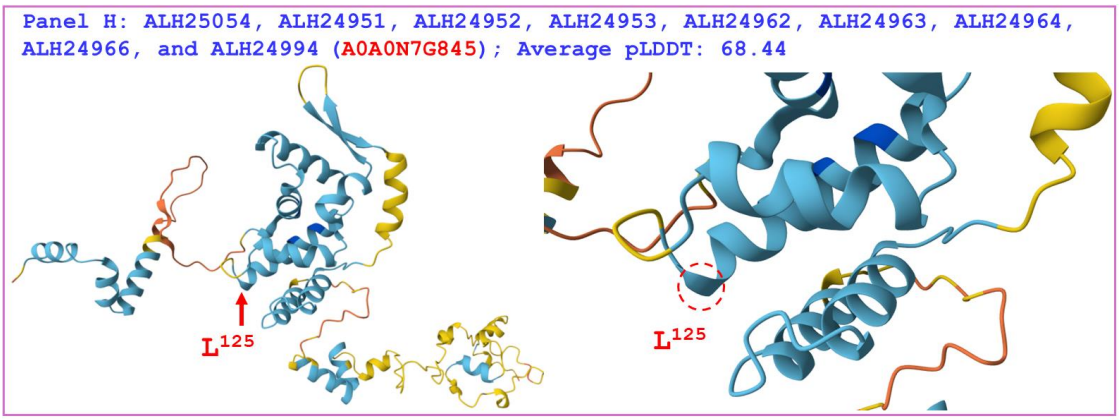

Figure 6. Correlation of changes in the primary, secondary, and tertiary structures of the MATα_HMGbox domains in the MAT1-1-1 proteins. The reference protein AGW27560 (under the AlphaFold code U3N942) is derived from the *H. sinensis* strain CS68-2-1229, and the mutant MAT1-1-1 proteins ALH25054, ALH24951, ALH24952, ALH24953, ALH24962, ALH24963, ALH24964, ALH24966, and ALH24994 (under the AlphaFold code A0A0N7G845) are derived from the wild-type *C. sinensis* isolates GS09_311, GS09_229, GS09_281, GS10_1, QH09_164, QH09_173, QH09_201, QH09_210, and SC09_87, respectively. Panel A shows an alignment of the amino acid sequences of the MATα_HMGbox domains of the MAT1-1-1 proteins; amino acid substitutions are shown in red, whereas the hyphens indicate identical amino acid residues. The ExPASy ProtScale plots show the changes in hydrophobicity (Panel B) and in the 2D structure (Panels C–F for α-helices, β-sheets, β-turns, and coils, respectively) of the proteins; the open rectangles in blue outline the changes in topology and waveform shown in the plots. Panels G–H show the 3D structures of the full-length proteins on the left and the locally amplified structures at the site of substitution on the right. The model confidence for the AlphaFold-predicted 3D structures is indicated as follows: ■ very high (pLDDT>90); ■ high (90>pLDDT>70); ■ low (70>pLDDT>50); ■ very low (pLDDT<50).

As shown in Panels C–F of Figure 6, the secondary structure of the proteins near the mutation sites in the MATα_HMGbox domains of the MAT1-1-1 proteins ALH25054, ALH24951, ALH24952, ALH24953, ALH24962, ALH24963, ALH24964, ALH24966, and ALH24994 (*cf.* Table S1) was altered, as illustrated by the changes in topology and waveform in the ExPASy ProtScale plots for α-helices, β-sheets, β-turns, and coils, respectively. As shown in the representations of the 3D structures presented in Panels G–H, the substituted amino acid residues are located within the core structures of the α-helices, and they destabilize the hydrophobic core of the protein [Baxevanis *et al.* 1995; Thapar 2015]; this alters the tertiary structures of the MATα_HMGbox domains of the MAT1-1-1 proteins under the AlphaFold code A0A0N7G845, which clustered into Branch e1 in the Bayesian clustering tree (*cf.* Figure 1, Table S5).

Figure 7 shows the hydrophobicities and structures of the MATα_HMGbox domains of the MAT1-1-1 proteins ALH24999 and ALH25057 (under the AlphaFold code A0A0N9QMT4) and the MAT1-1-1 protein ALH25001 (under the AlphaFold code A0A0N9R4Q4) derived from the wild-type *C. sinensis* isolates XZ07_H2, XZ12_16, and XZ05_2, respectively, (*cf.* Table S1) [Zhang & Zhang 2015], compared with the reference protein AGW27560 (under the AlphaFold code U3N942) derived from the *H. sinensis* strain CS68-2-1229 [Bushley *et al.* 2013]. Panel A shows substitutions of A-to-V (aliphatic alanine to aliphatic valine; hydropathy indices changed from 1.8 to 4.2 [Kyte & Doolittle 1982]) and A-to-T (aliphatic isoleucine to threonine, an amino acid that contains polar neutral side chains; hydropathy indices changed from 1.8 to -0.7). These substitutions altered the hydrophobicity of the protein, as illustrated by the changes

in topology and waveform shown in the hydropathy plot in Panel B. These changes altered the secondary structure surrounding the mutation sites in the MATα_HMGbox domain of the MAT1-1-1 proteins ALH24999, ALH25057, and ALH25001, as illustrated by the changes in topology and waveform in the ExPASy ProtScale plots for α-helices, β-sheets, β-turns, and coils shown in Panels C–F, respectively. As shown in the 3D structures represented in Panels G–H, the mutation sites are located upstream of the hydrophobic core structure of 3 α-helices in the MATα_HMGbox domains, and mutations at these sites alter the tertiary structures of the MATα_HMGbox domains of MAT1-1-1 proteins under the AlphaFold codes A0A0N9QMT4 and A0A0N9R4Q4, which clustered into Cluster d in the Bayesian clustering tree (*cf.* Figure 1, Table S5).

Panel A: Amino acid sequence alignment

```
AGW27560 42  ADVLTPVSTAAASRATRQTKEASCDRAKRPLNAFMAFRSYYLKLFPDVQQKTASGFLTTL 101
ALH24999 42  ---------V----T---------------------------------------------- 101
ALH25057 42  ---------V----T---------------------------------------------- 101
ALH25001 42  ---------V----T---------------------------------------------- 101

AGW27560 102 WHKDPFRNKWALIAKVYSFVRDQIGKDKVSLSYFMSLACPTMTIIEPAAYLNALGWCVQD 161
ALH24999 102 ------------------------------------------------------------ 161
ALH25057 102 ------------------------------------------------------------ 161
ALH25001 102 ------------------------------------------------------------ 161

AGW27560 162 DDAGSQKLFQDESSANLDQSSLLSAEYPSTEIELLSALVNIGYFPDHGADLVERMGSSHS 221
ALH24999 162 ------------------------------------------------------------ 221
ALH25057 162 ------------------------------------------------------------ 221
ALH25001 162 ------------------------------------------------------------ 221

AGW27560 222 GIMAPRAANCTPP                                                234
ALH24999 222 -------------                                                234
ALH25057 222 -------------                                                234
ALH25001 222 -------------                                                234
```

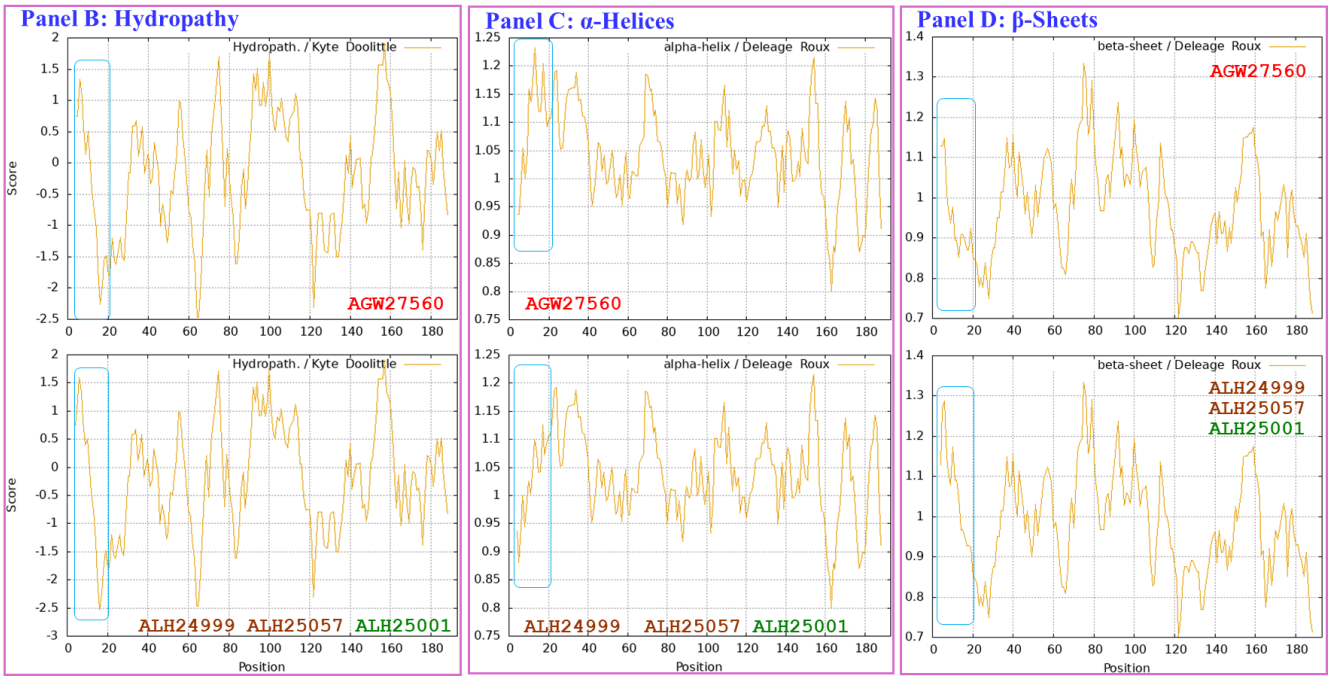

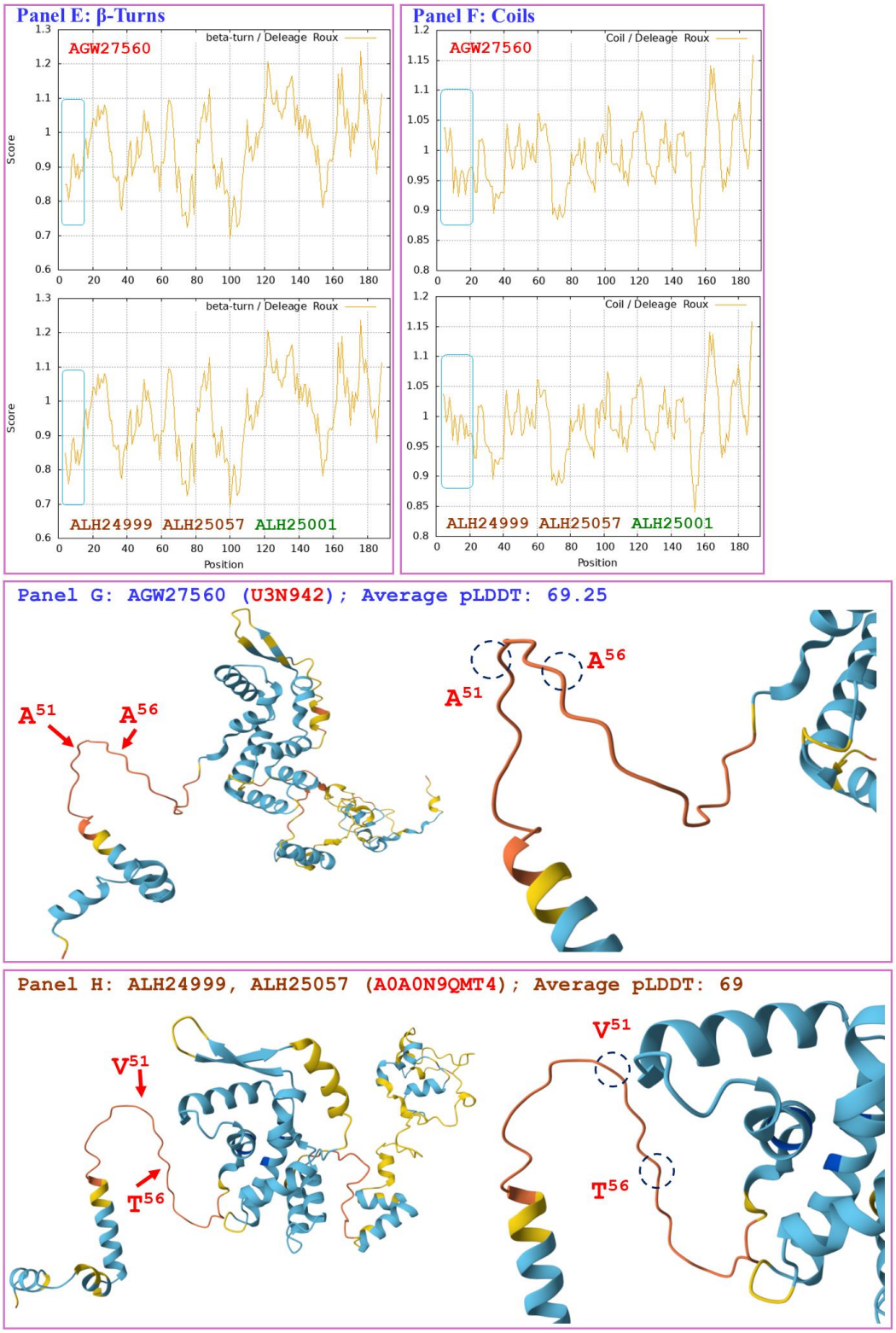
Panel E: β-Turns
AGW27560
beta-turn / Deleage Roux
Score
ALH24999 ALH25057 ALH25001
Position
Panel F: Coils
AGW27560
Coil / Deleage Roux
Score
ALH24999 ALH25057 ALH25001
Position
Panel G: AGW27560 (U3N942); Average pLDDT: 69.25
A51
A56
A51
A56
Panel H: ALH24999, ALH25057 (A0A0N9QMT4); Average pLDDT: 69
V51
T56
V51
T56

494

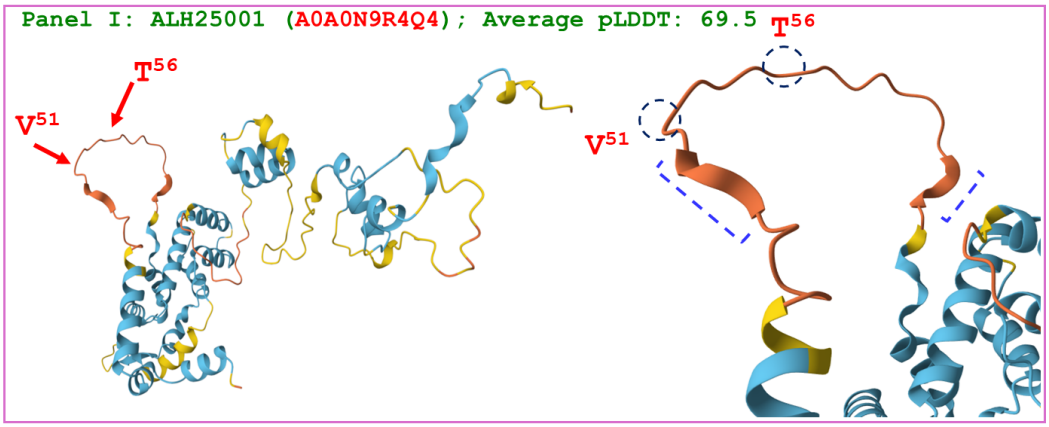

Figure 7. Correlation of the changes in the primary, secondary, and tertiary structure of the MATα_HMGbox domains in the MAT1-1-1 proteins: the reference protein AGW27560 (under the AlphaFold code U3N942) is derived from the *H. sinensis* strain CS68-2-1229, and the mutant MAT1-1-1 proteins ALH24999 and ALH25057 (under the AlphaFold code A0A0N9QMT4) and the protein ALH25001 (under the AlphaFold code A0A0N9R4Q4) are derived from the wild-type *C. sinensis* isolates XZ07_H2, XZ12_16, and XZ05_2, respectively. Panel A shows an alignment of the amino acid sequences of the MATα_HMGbox domains of the MAT1-1-1 proteins; amino acid substitutions are shown in red; the sequences displayed in brown and green represent the MAT1-1-1 proteins under the AlphaFold codes A0A0N9QMT4 and A0A0N9R4Q4, respectively, and the hyphens indicate identical amino acid residues. The ExPASy ProtScale plots show the changes in hydrophobicity (Panel B) and in the 2D structure (Panels C–F, which display the α-helices, β-sheets, β-turns, and coils, respectively) of the proteins. The open rectangles in blue outline the changes in topology and waveform shown in the plots. Panels G–H show the 3D structures of the full-length proteins on the left and the locally amplified structures at the substitution sites on the right. The model confidence for the AlphaFold-predicted 3D structures is indicated as follows: very high (pLDDT>90); high (90>pLDDT>70); low (70>pLDDT>50); very low (pLDDT<50).

Although Panels A of Figure 7 shows the same substitutions of A-to-V and A-to-T in the MATα_HMGbox domains of the mutant proteins ALH24999, ALH25057, and ALH25001 (under the AlphaFold codes A0A0N9QMT4 and A0A0N9R4Q4) [Zhang & Zhang 2015], Panels H and I show different tertiary structures for the MATα_HMGbox domains of the mutant MAT1-1-1 proteins under the 2 AlphaFold codes. Specifically, the protein ALH25001 contains 2 extra short β-sheet structures upstream and downstream of the mutation sites in the MATα_HMGbox domain shown in Panel I; these are marked with dashed half brackets in blue. In contrast, the distinct tertiary structures for the mutant proteins ALH24999 and ALH25057 without the β-sheet structures are shown in Panel H.

Figure 8 compares the hydrophobicities and structures of the MATα_HMGbox domain of the MAT1-1-1 protein ALH25003 (under the AlphaFold code A0A0N7G850) derived from the wild-type *C. sinensis* isolate XZ05_6 (*cf.* Table S1) [Zhang & Zhang 2015] with those of the reference protein AGW27560 (under the AlphaFold code U3N942) derived from the *H. sinensis* strain CS68-2-1229 [Bushley *et al*. 2013]. Panel A shows an S-to-G substitution (serine, which has polar neutral side chains, is replaced by the unique amino acid glycine; hydropathy indices changed from -0.8 to -0.4 [Kyte & Doolittle 1982]). This substitution resulted in a slight increase in hydrophobicity, as illustrated by the changes in topology and waveform shown in the hydropathy plot in Panel B. These changes altered the secondary structure of the mutant MAT1-1-1 protein ALH25003 in the region surrounding the mutation site in the MATα_HMGbox domain,

as illustrated by the changes in topology and waveform in the ExPASy ProtScale plots for α-helices, β-sheets, β-turns, and coils shown in Panels C–F. As shown in the representations of the protein's 3D structure in Panels G–H, the amino acid residue (serine), which is located at the end of one of the 3 α-helices that form the hydrophobic core structure of the MATα_HMGbox domain [Baxevanis *et al*. 1995; Thapar 2015], was substituted by glycine, which became the first residue after the α-helix in the domain. This single-residue substitution plus additional E-to-K and Y-to-H substitutions downstream of the MATα_HMGbox domain (*cf*. Figure S1) significantly altered the tertiary structure of the protein ALH25003 under the unique AlphaFold code A0A0N7G850. The mutant MATα_HMGbox domain clustered into Branch a2 in the Bayesian clustering tree (*cf*. Figure 1, Table S5).

Panel A: Amino acid sequence alignment

```
AGW27560 42  ADVLTPVSTAAASRATRQTKEASCDRAKRPLNAFMAFRSYYLKLFPDVQQKTASGFLTTL 101
ALH25003 42  ------------------------------------------------------------ 101

AGW27560 102 WHKDPFRNKWALIAKVYSFVRDQIGKDKVSLSYFMSLACPTMTIIEPAAYLNALGWCVQD 161
ALH25003 102 ------------------------------------------------------------ 161

AGW27560 162 DDAGSQKLFQDESSANLDQSSLLSAEYPSTEIELLSALVNIGYFPDHGADLVERMGSSHS 221
ALH25003 162 ------------------------------------------------------------G-- 221

AGW27560 222 GIMAPRAANCTPP                                                234
ALH25003 222 -------------                                                234
```

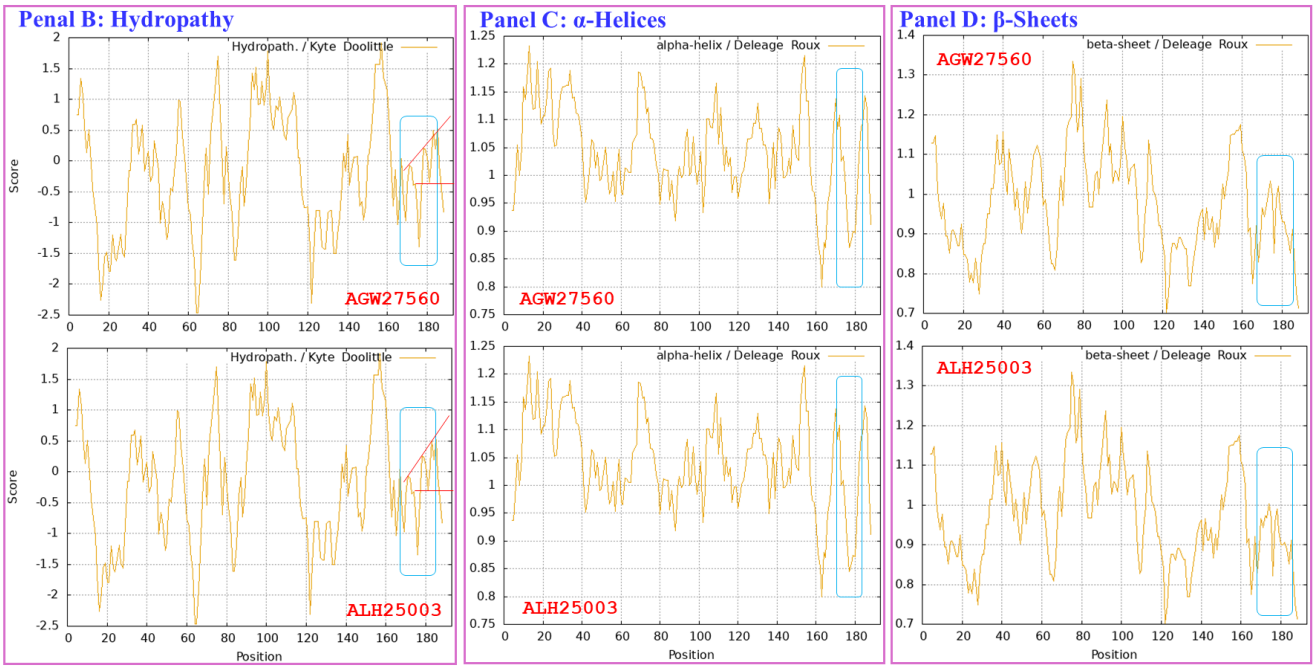

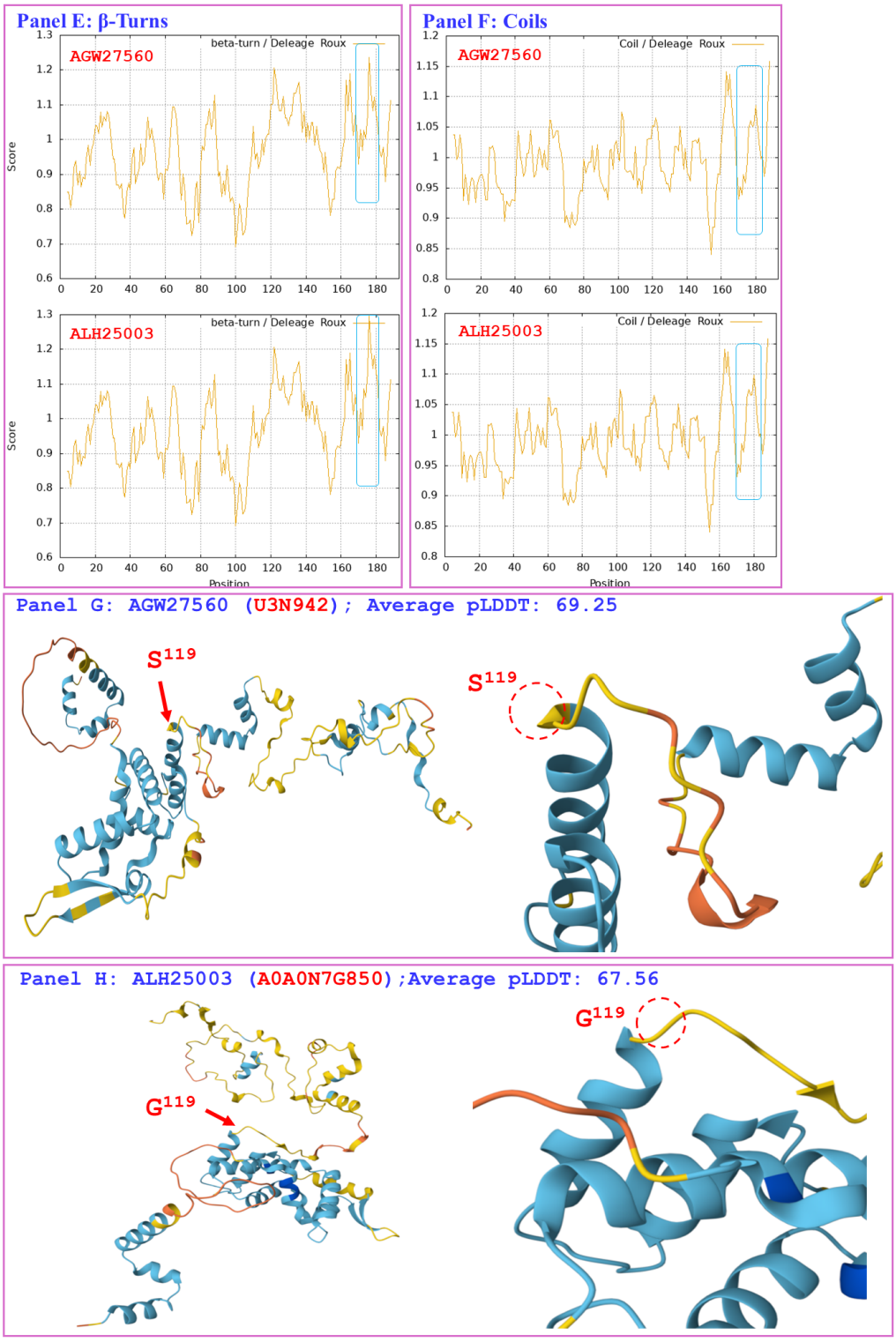

Figure 8. Correlation of the changes in the primary, secondary, and tertiary structures of the MATα_HMGbox domains of the MAT1-1-1 proteins: the reference protein AGW27560 (under the AlphaFold code U3N942) is derived from the *H. sinensis* strain CS68-2-1229, and the mutant MAT1-1-1 protein ALH25003 (under the AlphaFold code A0A0N7G850) is derived from the wild-type *C. sinensis* isolate XZ05_6. Panel A shows an alignment of the amino acid sequences of the MATα_HMGbox domains of the MAT1-1-1 proteins; the amino acid substitution is shown in red, whereas the hyphens indicate identical amino acid residues. The ExPASy ProtScale plots show the changes in the hydrophobicity (Panel B) and in the 2D structure of the protein (Panels C–F for the α-helices, β-sheets, β-turns, and coils, respectively) of the protein, and the open rectangles in blue outline the changes in topology and waveform shown in the plots. Panels G–H show the 3D structures of the full-length proteins on the left and the locally amplified structures at the sites of substitutions on the right. The model confidence for the AlphaFold-predicted 3D structures

is indicated as follows: very high (pLDDT>90); high (90>pLDDT>70); low (70>pLDDT>50); very low (pLDDT<50).

Aggregating the data presented in Section III-5, Panels A of Figures 3–8 demonstrate the 1–2 amino acid substitutions in the MATα_HMGbox domains of MAT1-1-1 proteins under various AlphaFold 3D structure codes derived from wild-type *C. sinensis* isolates compared with the reference MAT1-1-1 protein AGW27560 under the AlphaFold code U3N942 [Bushley *et al*. 2013]. The substitutions within the MATα_HMGbox domains caused changes in the topologies and waveforms shown in the ExPASy ProtScale plots in Panels B–F of Figures 3–8. These changes indicate the changes in the hydrophobicity and secondary structure (α-helices, β-sheets, β-turns, and coils) of the mutant full-length proteins. The changes in hydrophobicity and in the primary and secondary structures of the MATα_HMGbox domains altered the AlphaFold 3D structures of the domains of the proteins under various AlphaFold codes (*cf*. Panels H of Figures 3–8 and Panel I of Figure 7). The mutant domain sequences containing 1 or 2 amino acid substitutions were clustered into different clades in the Bayesian clustering tree (*cf*. Figure 1, Table S5), and the altered 3D structures of the proteins ultimately changed the DNA binding affinities, and the functionalities of gene transcriptional regulation related to the sexual reproduction of *O. sinensis*.

III-6 Diverse primary and secondary structures of the MATα_HMGbox domains of MAT1-1-1 proteins encoded by the genome and metatranscriptome assemblies of *H. sinensis* and *C. sinensis* insect–fungal complexes

Figure 9 compares the hydrophobicities and secondary structures (α-helices, β-sheets, β-turns, and coils) of the MATα_HMGbox domains of the MAT1-1-1 proteins encoded by the genome assemblies JAAVMX010000001 (6,699,061→6,699,153 & 6,699,206→6,699,637) and LKHE01001116 (4183←4620 & 4667←4759) of the *H. sinensis* strains IOZ07 and 1229 [Li *et al*. 2016a; Shu *et al*. 2020] with those of the reference MAT1-1-1 protein AGW27560 derived from the *H. sinensis* strain CS68-2-1229 [Bushley *et al*. 2013]. Panel A shows a Y-to-M substitution (aromatic tyrosine to methionine, an amino acid that has polar neutral side chains; hydropathy indices changed from -1.3 to 1.9 [Kyte & Doolittle 1982]). This substitution caused increased hydrophobicity in the MATα_HMGbox domains of the MAT1-1-1 proteins encoded by the genome assemblies JAAVMX010000001 and LKHE01001116 [Li *et al*. 2016a; Shu *et al*. 2020], as illustrated by the changes in topology and waveform in the hydropathy plot shown in Panel B. These changes resulted in altered secondary structures surrounding the mutation sites in the MATα_HMGbox domains of the MAT1-1-1 proteins, as illustrated in the ExPASy ProtScale plots for α-helices, β-sheets, β-turns, and coils in Panels C–F, respectively. The MATα_HMGbox domains of the MAT1-1-1 proteins were clustered into Branch c in the Bayesian clustering tree (*cf*. Figure 1, Table S6).

Panel A: Amino acid sequence alignment

```
AGW27560         42        ADVLTPVSTAAASRATRQTKEASCDRAKRPLNAFMAFRSYYLKLFPDVQQKTASGFLTTL 101
JAAVMX010000001  6,699,034 ----------------------------------------M-------------------- 6,699,213
LKHE01001116     4786      ----------------------------------------M-------------------- 4555

AGW27560         85        WHKDPFRNKWALIAKVYSFVRDQIGKDKVSLSYFMSLACPTMTIIEPAAYLNALGWCVQD 161
JAAVMX010000001  6,699,214 ------------------------------------------------------------ 6,699,393
LKHE01001116     4554      ------------------------------------------------------------ 4375

AGW27560         145       DDAGSQKLFQDESSANLDQSSLLSAEYPSTEIELLSALVNIGYFPDHGADLVERMGSSHS 221
JAAVMX010000001  6,699,214 ------------------------------------------------------------ 6,699,573
LKHE01001116     4374      ------------------------------------------------------------ 4195

AGW27560         205       GIMAPRAANCTPP                                                234
JAAVMX010000001  6,699,574 -------------                                                6,699,664
LKHE01001116     4194      -------------                                                4156
```

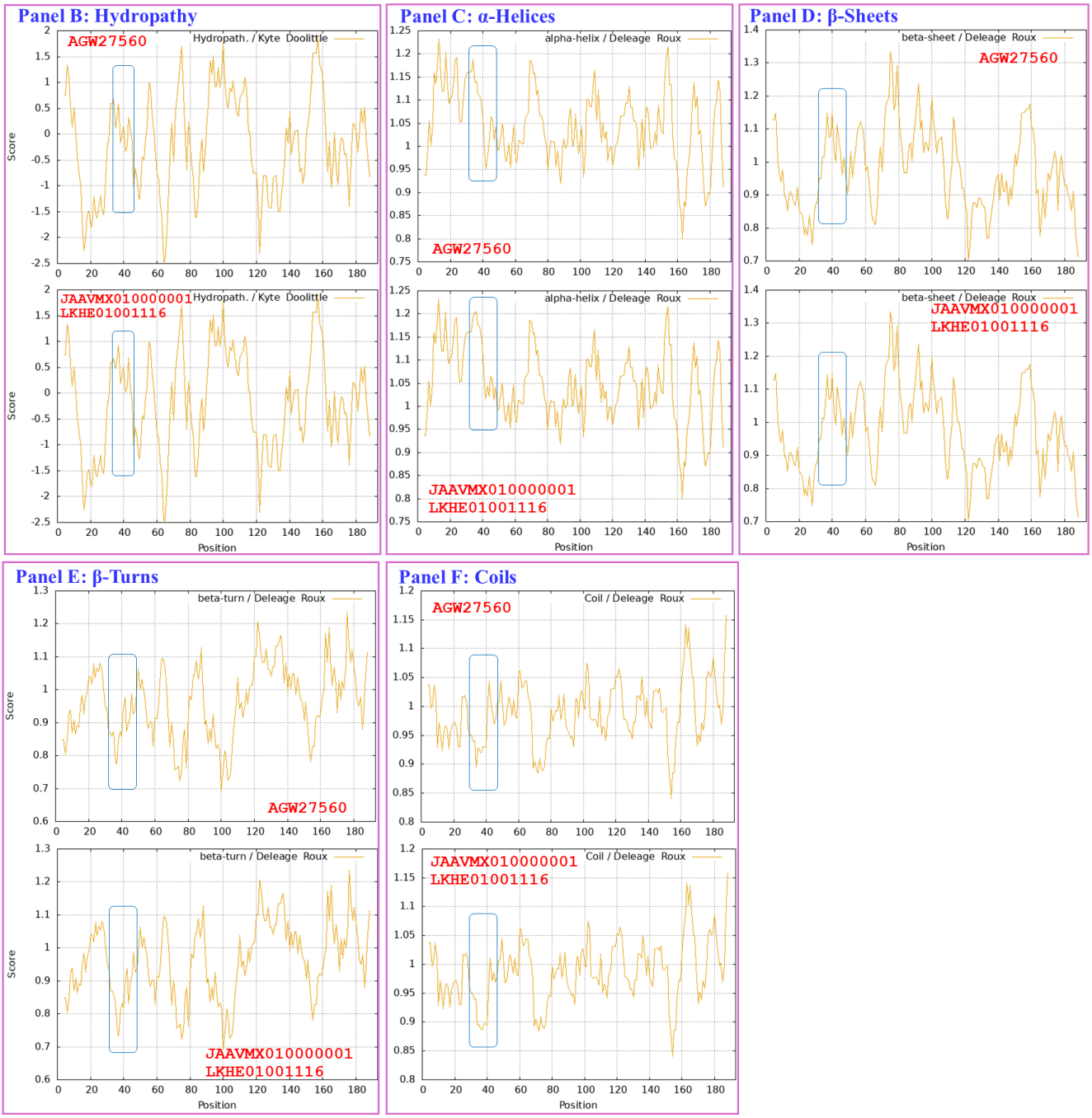

Figure 9. Correlation of the changes in the primary and secondary structures of the MATα_HMGbox domains of the MAT1-1-1 proteins: the reference protein AGW27560 is derived from the *H. sinensis* strain CS68-2-1229, and the

585 truncated MAT1-1-1 proteins are encoded by the genome assemblies JAAVMX010000001 and LKHE01001116 of
586 the *H. sinensis* strains IOZ07 and 1229, respectively. Panel A shows an alignment of the amino acid sequences in the
587 MATα_HMGbox domains of the MAT1-1-1 proteins; amino acid substitutions are shown in red, whereas the hyphens
588 indicate identical amino acid residues. The ExPASy ProtScale plots show the changes in hydrophobicity (Panel B)
589 and in the 2D structures (Panels C–F show the α-helices, β-sheets, β-turns, and coils, respectively) of the proteins;
590 the open rectangles in blue outline the changes in topology and waveform shown in the plots.

591 Compared with the reference MAT1-1-1-1 protein AGW27560 (*cf*. Figure S1, Table S6), no changes
592 were detected in the amino acid sequences, hydrophobicities, or secondary structures (α-helices, β-sheets,
593 β-turns, and coils) of the MATα_HMGbox domains of the MAT1-1-1 proteins encoded by the genome
594 assembly ANOV01017390 (794←1228 & 1280←1369) of the *H. sinensis* strain Co18 or the
595 metatranscriptome assembly OSIN7648 (151→675) of the *C. sinensis* insect–fungal complex collected
596 from Deqin, Yunnan, China [Kyte & Doolittle 1982; Bushley *et al*. 2013; Hu *et al*. 2013; Liu *et al*. 2015].
597 The MATα_HMGbox domains of the genome- and metatranscriptome-encoded MAT1-1-1 proteins
598 clustered into Branch a1 in the Bayesian clustering tree (*cf*. Figure 1, Table S6).

599 The MATα_HMGbox domain of the MAT1-1-1 protein encoded by the metatranscriptome assembly
600 GAGW01008880 (714←1127) of the *C. sinensis* insect–fungi complex is truncated at its N-terminus, as
601 shown in Figure S1 and in Panel A of Figure S3 [Xiang *et al*. 2014]. The remaining portion of the
602 MATα_HMGbox domain of this protein is 100% identical to the query protein AGW27560 (under the
603 AlphaFold code U3N942) derived from the *H. sinensis* strain CS68-2-1229 [Bushley *et al*. 2013], and it
604 showed no apparent changes in hydrophobicity or secondary structure, as illustrated by the identical
605 topology and waveform that can be observed in the ExPASy ProtScale plots for hydropathy, α-helices, β-
606 sheets, β-turns, and coils shown in Panels B–F, respectively, of Figure S3. Although the MATα_HMGbox
607 domain of the metatranscriptome-encoded protein clustered into Branch a1 in the Bayesian clustering tree
608 together with the 6 reference authentic MAT1-1-1 proteins (*cf*. Figure 1, Table S6), the truncated
609 MATα_HMGbox domain, which lacks 50 and 48 amino acid residues encoded by exons I and II of the
610 *MAT1-1-1* gene, respectively, may not be able to form the core stereostructure containing 3 critical α-helices
611 that supports high-affinity DNA binding and full functionality in the regulation of gene transcription related
612 to the sexual reproduction of *O. sinensis* [Baxevanis *et al*. 1995; Thapar 2015; Li *et al*. 2025].

613 The genome assemblies LWBQ00000000 and NGJJ00000000 and the transcriptome assembly
614 GCQL00000000 of the *H. sinensis* strains ZJB12195, CC1406-20395, and L0106, respectively, do not
615 contain genes or transcripts that encode MAT1-1-1 proteins [Liu *et al*. 2015, 2020; Jin *et al*. 2020].

616 III-7 Heteromorphic stereostructures of the HMG-box_ROX1-like domains of the 617 MAT1-2-1 proteins derived from wild-type *C. sinensis* isolates

618 Section III-7 presents analyses of the correlation between the changes in the hydrophobicity and
619 structure of the HMG-box_ROX1-like domains of full-length MAT1-2-1 proteins (under 12 AlphaFold

codes, *cf*. Table S7) derived from wild-type *C. sinensis* isolates, compared to the reference MAT1-2-1 proteins represented by AEH27625 (under the AlphaFold code D7F2E9) derived from the *H. sinensis* strain CS2 (*cf*. Table S2) [Zhang *et al*. 2009]. The HMG-box_ROX1-like domain sequences (amino acid residues 127→197) were extended both upstream and downstream by 9 external amino acid residues because the sequential ExPASy ProtScale plotting for hydropathy, α-helices, β-sheets, β-turns, and coils was set up at a window size of 9 amino acids (*cf*. Section II-5 of Materials and Methods).

Figure 10 compares the hydrophobicities and structures of the HMG-box_ROX1-like domain of the MAT1-2-1 protein AIV43040 (under the AlphaFold code A0A0A0RCF5) derived from the *C. sinensis* isolate XZ12_16 (*cf*. Table S2) [Zhang *et al*. 2014] with those of the reference protein AEH27625 (under the AlphaFold code D7F2E9) derived from the *H. sinensis* strain CS2 [Zhang *et al*. 2009]. Panel A shows 3 amino acid substitutions: Y-to-H (aromatic tyrosine to basic histidine; hydropathy indices changed from -1.3 to -3.2 [Kyte & Doolittle 1982]), M-to-I (methionine, which possesses polar neutral side chains, to aliphatic isoleucine; hydropathy indices changed from 1.9 to 4.5) and Q-to-R (glutamine, which has polar neutral side chains, to basic arginine; hydropathy indices changed from -3.5 to -4.5). Individually, these substitutions caused decreased or increased hydrophobicity, as illustrated by the changes in topology and waveform in the hydropathy plot shown in Panel B. These changes resulted in altered secondary structures surrounding the mutation sites in the HMG-box_ROX1-like domain of the MAT1-2-1 protein AIV43040, as illustrated by the changes in topology and waveform in the ExPASy ProtScale plots for α-helices, β-sheets, β-turns, and coils shown in Panels C–F, respectively. As shown in the representations of 3D structures in Panels G–H, the replaced residues are located in each of the 3 core α-helices, and they alter the stability of the hydrophobic core of the HMG-box_ROX1-like domain [Baxevanis *et al*. 1995; Thapar 2015] as well as the stereostructure of the domain of the MAT1-2-1 protein AIV43040 under the AlphaFold code A0A0A0RCF5. The mutant HMG-box_ROX1-like domain clustered into Branch b2β, which displays the longest clustering distance in the Bayesian clustering tree (*cf*. Figure 2, Table S7).

Panel A: Amino acid sequence alignment

```
AEH27625 118 APPSPKDIKIPRPPNAYILYRKERHHYVKDANPGITNNEISQILGKAWNMESNDVRQKYK 177
AIV43040 118 --------------------------H----------------------I---------- 177

AEH27625 178 DMSQQVKQALLEKHPDYQYKPRRPCERRR                                206
AIV43040 178 ----R------------------------                                206
```

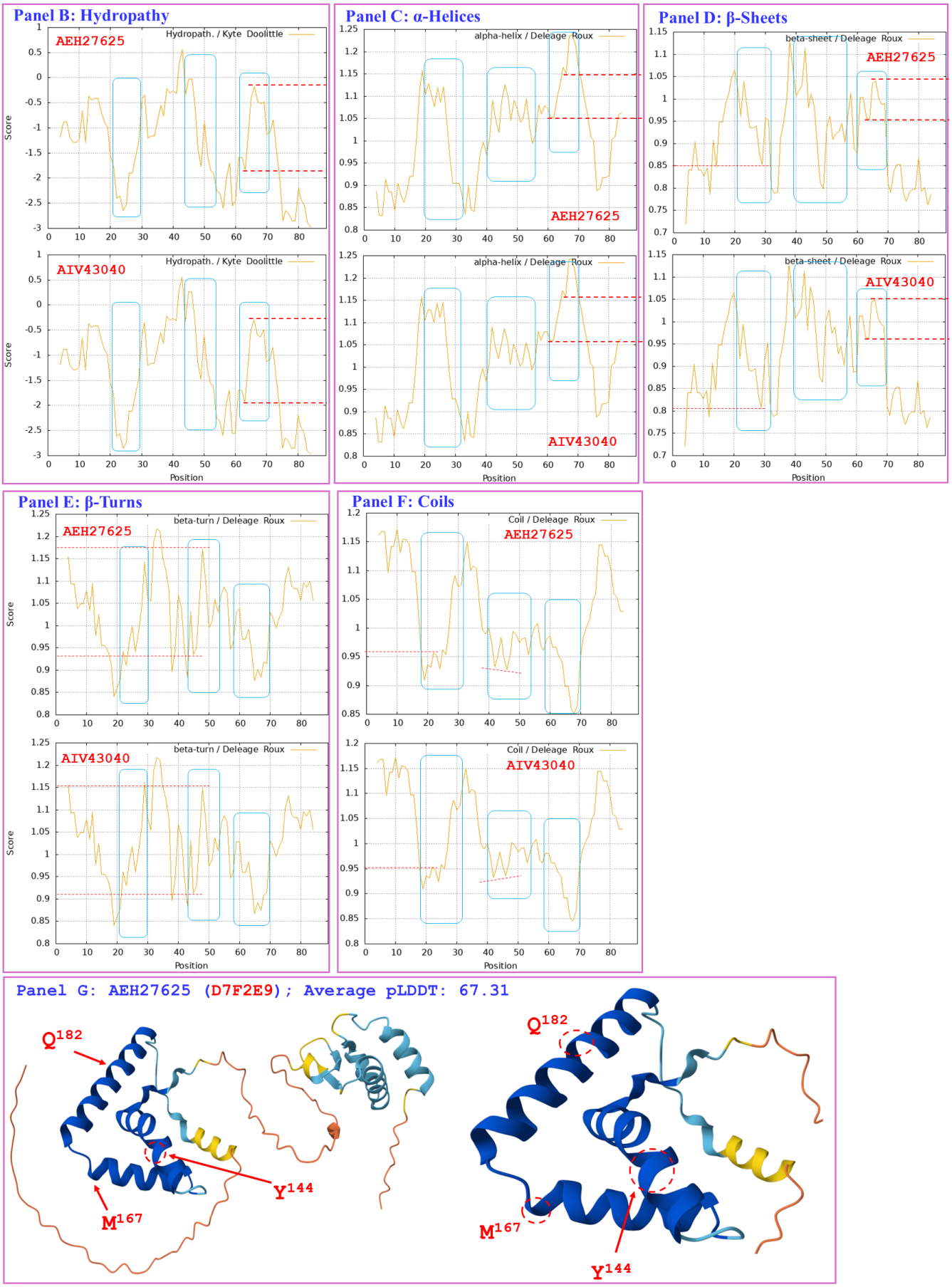
Panel B: Hydropathy
Hydropath. / Kyte Doolittle
AEH27625
AIV43040
Score
Position
Panel C: α-Helices
alpha-helix / Deleage Roux
AEH27625
AIV43040
Position
Panel D: β-Sheets
beta-sheet / Deleage Roux
AEH27625
AIV43040
Position
Panel E: β-Turns
beta-turn / Deleage Roux
AEH27625
AIV43040
Score
Position
Panel F: Coils
Coil / Deleage Roux
AEH27625
AIV43040
Position
Panel G: AEH27625 (D7F2E9); Average pLDDT: 67.31
Q182
Y144
M167
Q182
M167
Y144

645

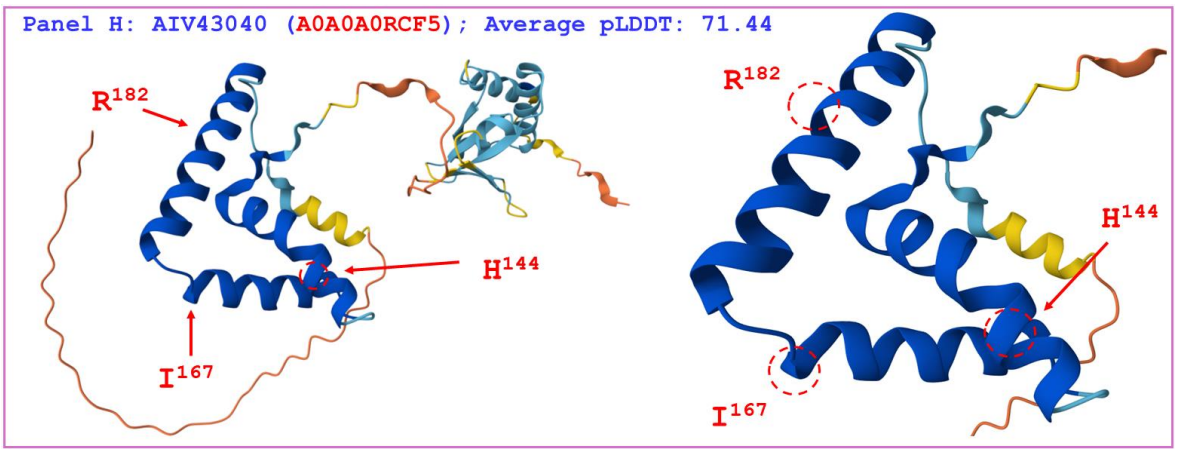

Figure 10. Correlation of the changes in the primary, secondary, and tertiary structures of the HMG-box_ROX1-like domains of MAT1-2-1 proteins. The reference protein AEH27625 (under the AlphaFold code D7F2E9) is derived from the *H. sinensis* strain CS2, and the mutant MAT1-2-1 protein AIV43040 (under the AlphaFold code A0A0A0RCF5) is derived from the wild-type *C. sinensis* isolate XZ12_16. Panel A shows an alignment of the amino acid sequences of the HMG-box_ROX1-like domains of the MAT1-2-1 proteins; amino acid substitutions are shown in red, whereas the hyphens indicate identical amino acid residues. The ExPASy ProtScale plots show the changes in hydrophobicity (Panel B) and in the 2D structure (Panels C–F show the α-helices, β-sheets, β-turns, and coils, respectively) of the protein; the open rectangles in blue outline the changes in topology and waveform seen in the plots. Panels G–H show representations of the 3D structures of the full-length proteins on the left; the locally amplified structures at the sites of substitutions are shown on the right. The model confidence for the AlphaFold-predicted 3D structures is indicated as follows: ▯ very high (pLDDT>90); ▯ high (90>pLDDT>70); ▯ low (70>pLDDT>50); ▯ very low (pLDDT<50).

Figure 11 compares the hydrophobicities and structures of the HMG-box_ROX1-like domains of the MAT1-2-1 proteins under the AlphaFold code D7F2J7 (ACV60417, ACV60418, AFH35020, and AFX66443 shown in brown in Figure 11, derived from the wild-type *C. sinensis* isolates XZ-LZ07-H1, XZ-LZ07-H2, XZ06-124, and XZ05_8, respectively), and the hydrophobicities and structures of the proteins under the AlphaFold code D7F2F5 (ACV60375, ACV60415, AFX66441, AFX66446, and AFX66461 shown in green in Figure 11, derived from the wild-type *C. sinensis* isolates XZ-SN-44, XZ-LZ05-6, XZ05_2, XZ06_260, and XZ09_80, respectively) (*cf.* Table S2) [Zhang *et al*. 2009, 2012, 2014] with those of the reference protein AEH27625 (under the AlphaFold code D7F2E9) derived from the *H. sinensis* strain CS2 [Zhang *et al*. 2009]. Panel A shows substitutions of Y-to-H (aromatic tyrosine to basic histidine; hydropathy indices changed from -1.3 to -3.2 [Kyte & Doolittle 1982]) and M-to-I (methionine, which contains polar neutral side chains, to aliphatic isoleucine; hydropathy indices changed from 1.9 to 4.5). These substitutions caused changes in hydrophobicity, as illustrated by the changes in topology and waveform shown in the hydropathy plot in Panel B. They also resulted in altered secondary structures surrounding the mutation sites in the HMG-box_ROX1-like domains of the mutant MAT1-2-1 proteins ACV60417, ACV60418, AFH35020, and AFX66443 (under the AlphaFold code D7F2J7) and in those regions in the proteins ACV60375, ACV60415, AFX66441, AFX66446, and AFX66461 (under the AlphaFold code D7F2F5), as illustrated by the changes in topology and waveform shown in Panels C–F,

which display the ExPASy ProtScale plots for α-helices, β-sheets, β-turns, and coils. As shown in the 3D structures presented in Panels G–I of Figure 11, the substituted residues are located within two of the 3 core α-helices, and they differentially alter the stability of the core structure of the HMG-box_ROX1-like domain [Baxevanis *et al.* 1995; Thapar 2015] and the tertiary structure of this domain in the MAT1-2-1 proteins under the AlphaFold 3D structural codes D7F2J7 and D7F2F5. The sequences of HMG-box_ROX1-like domain of the mutant proteins ACV60417, ACV60418, AFH35020, AFX66443, ACV60375, ACV60415, AFX66441, AFX66446, and AFX66461 clustered into Branch b2α in the Bayesian clustering tree (*cf.* Figure 2, Table S7).

Panel A: Amino acid sequence alignment

```
AEH27625 118 APPSPKDIKIPRPPNAYILYRKERHHYVKDANPGITNNEISQILGKAWNMESNDVRQKYK 177
ACV60417 118 --------------------------H----------------------I---------- 177
ACV60418 118 --------------------------H----------------------I---------- 177
AFH35020 118 --------------------------H----------------------I---------- 177
AFX66443 118 --------------------------H----------------------I---------- 177
ACV60375 118 --------------------------H----------------------I---------- 177
ACV60415 118 --------------------------H----------------------I---------- 177
AFX66441 118 --------------------------H----------------------I---------- 177
AFX66446 118 --------------------------H----------------------I---------- 177
AFX66461 118 --------------------------H----------------------I---------- 177

AEH27625 178 DMSQQVKQALLEKHPDYQYKPRRPCERRR                                206
ACV60417 178 ------------------------------                                206
ACV60418 178 ------------------------------                                206
AFH35020 178 ------------------------------                                206
AFX66443 178 ------------------------------                                206
ACV60375 178 ------------------------------                                206
ACV60415 178 ------------------------------                                206
AFX66441 178 ------------------------------                                206
AFX66446 178 ------------------------------                                206
AFX66461 178 ------------------------------                                206
```

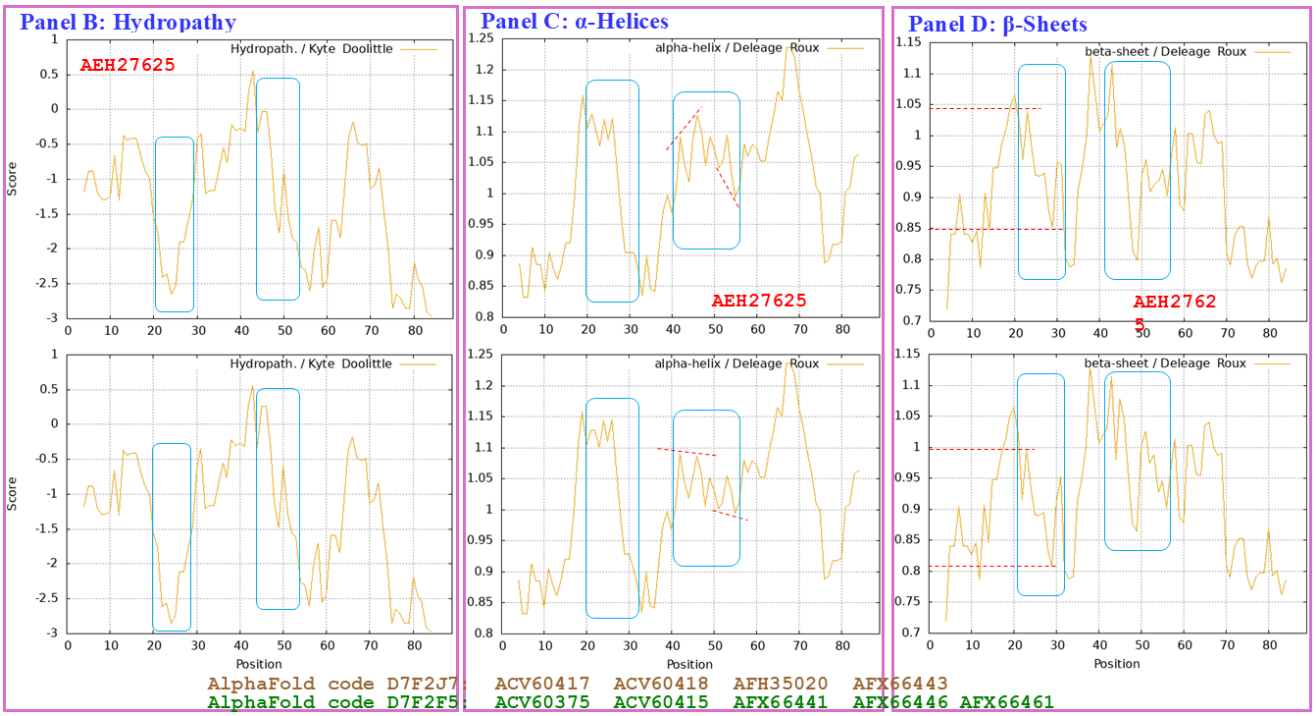

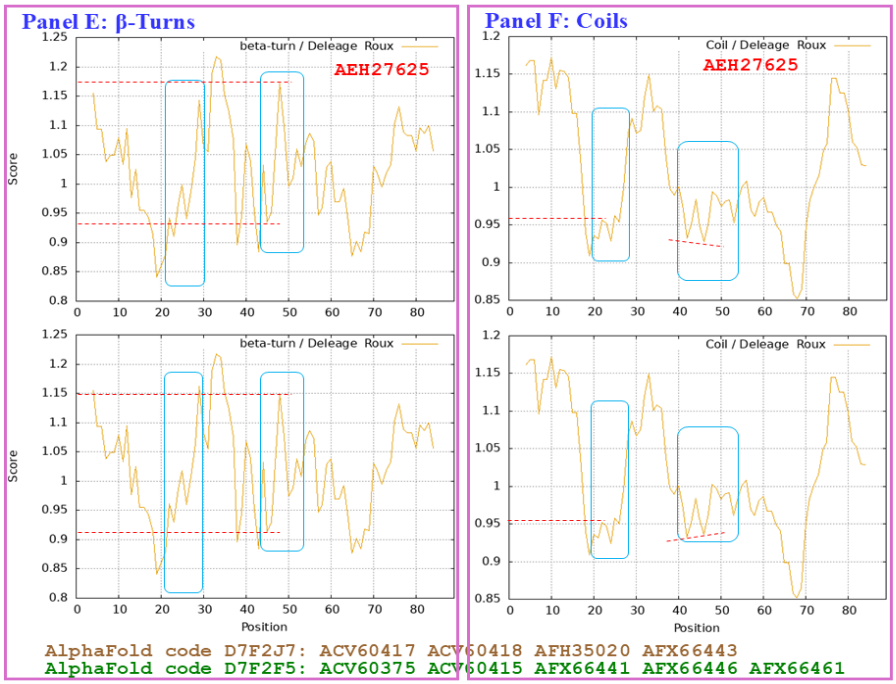
Panel E: β-Turns
beta-turn / Deleage Roux
AEH27625
Score
Position
Panel F: Coils
Coil / Deleage Roux
AEH27625
AlphaFold code D7F2J7: ACV60417 ACV60418 AFH35020 AFX66443
AlphaFold code D7F2F5: ACV60375 ACV60415 AFX66441 AFX66446 AFX66461

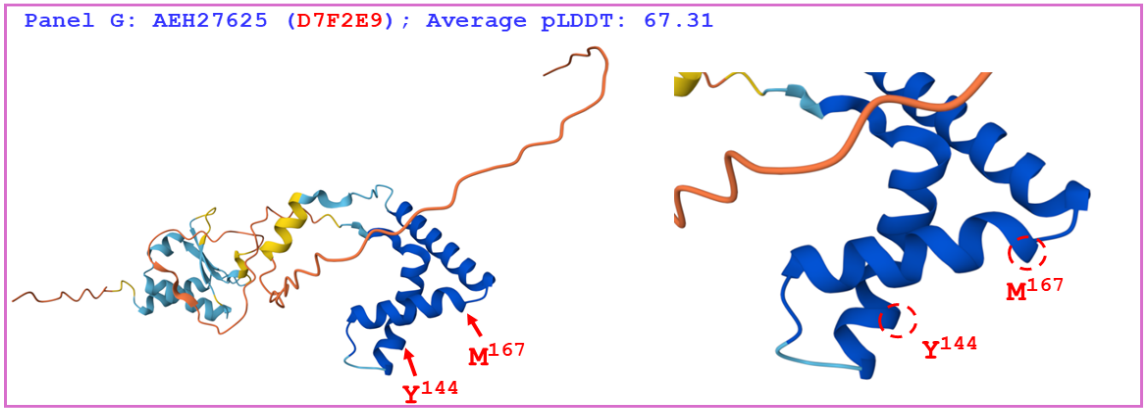
Panel G: AEH27625 (D7F2E9); Average pLDDT: 67.31
M167
Y144

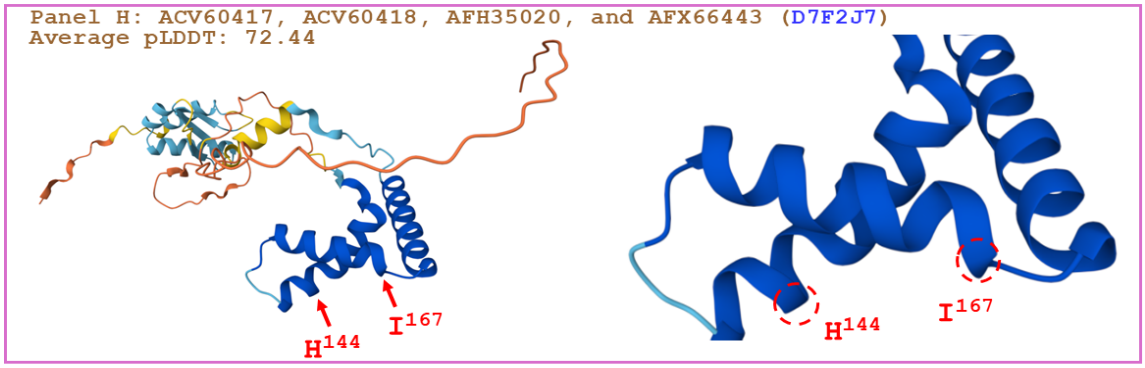
Panel H: ACV60417, ACV60418, AFH35020, and AFX66443 (D7F2J7)
Average pLDDT: 72.44
H144
I167

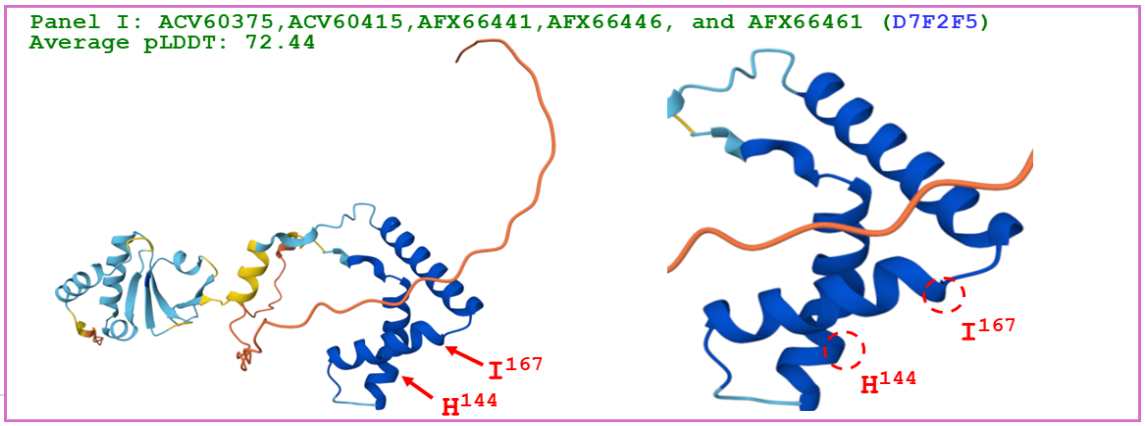
Panel I: ACV60375,ACV60415,AFX66441,AFX66446, and AFX66461 (D7F2F5)
Average pLDDT: 72.44
I167
H144

Figure 11. Correlation of the changes in the primary, secondary, and tertiary structures of the HMG-box_ROX1-like domains of MAT1-2-1 proteins. The reference protein AEH27625 (under the AlphaFold code D7F2E9) is derived from the *H. sinensis* strain CS2; the mutant MAT1-2-1 proteins under the AlphaFold code D7F2J7 (ACV60417, ACV60418, AFH35020, and AFX66443 shown in brown are derived from the wild-type *C. sinensis* isolate XZ-LZ07-H1, XZ-LZ07-H2, XZ06-124, and XZ05_8), and the mutant proteins under the AlphaFold code D7F2F5 (ACV60375, ACV60415, AFX66441, AFX66446, and AFX66461 shown in green are derived from the wild-type *C. sinensis* isolates XZ-SN-44, XZ-LZ05-6, XZ05_2, XZ06_260, and XZ09_80). Panel A shows an alignment of the amino acid sequences of the HMG-box_ROX1-like domains of the MAT1-2-1 proteins; amino acid substitutions are shown in red; the sequences displayed in brown and green represent the MAT1-2-1 proteins under the AlphaFold codes D7F2J7 and D7F2F5, respectively, and the hyphens indicate identical amino acid residues. The ExPASy ProtScale plots show the changes in hydrophobicity (Panel B) and in the 2D structures (Panels C–F for α-helices, β-sheets, β-turns, and coils, respectively) of the HMG-box_ROX1-like domains of the proteins; the open rectangles in blue outline the changes in topology and waveform seen in the plots. Panels G–H show representations of the 3D structures of the full-length proteins on the left and of the locally amplified structures at the sites of substitutions on the right. The model confidence for the AlphaFold-predicted 3D structures is indicated as follows: ■ very high (pLDDT>90); ■ high (90>pLDDT>70); ■ low (70>pLDDT>50); ■ very low (pLDDT<50).

Figure 12 compares the hydrophobicities and structures of the HMG-box_ROX1-like domains of the MAT1-2-1 proteins under the AlphaFold codes **D7F2E3** (ACV60363, ACV60364, AFX66388, AFH35018, and AGW27542), **D7F2G5** (ACV60385), **V9LW71** (AFX66401), **V9LVS8** (AFX66472, AFX66473, and AFX66474), **V9LVU8** (AFX66475), **V9LWC9** (AFX66476), **V9LWG5** (AFX66484), and **U3N6V5** (AGW27537) derived from the wild-type *C. sinensis* isolates YN09_64, YN09_6, YN09_22, YN09_51, XZ-NQ-154, XZ-NQ-155, GS09_111, QH09-93, CS560-961, QH-YS-199, QH09_11, ID10_1, and CS6-251, respectively (*cf.* Table S2) [Zhang *et al*. 2009, 2012, 2014; Bushley *et al*. 2013], with the hydrophobicity and structure of the reference protein AEH27625 (under the AlphaFold code D7F2E9) derived from the *H. sinensis* strain CS2 [Zhang *et al*. 2009]. Panel A shows Y-to-H substitutions (aromatic tyrosine to basic histidine; hydropathy indices changed from -1.3 to -3.2 [Kyte & Doolittle 1982]) in the HMG-box_ROX1-like domains of all the mutant MAT1-2-1 proteins mentioned above; these substitutions caused reduced hydrophobicity, as illustrated by the changes in topology and waveform shown in the hydropathy plots in Panel B. The substitutions resulted in alteration of the secondary structure surrounding the mutation sites in the HMG-box_ROX1-like domains of the MAT1-2-1 proteins, as illustrated by the changes in topology and waveform in the ExPASy ProtScale plots for α-helices, β-sheets, β-turns, and coils that can be seen in Panels C–F, respectively.

Panel A: Amino acid sequence alignment

```
AEH27625 118 APPSPKDIKIPRPPNAYILYRKERHHYVKDANPGITNNEISQILGKAWNMESNDVRQKYK 177
ACV60363 118 ---------------------------H---------------------------------- 177
ACV60364 118 ---------------------------H---------------------------------- 177
AFX66388 118 ---------------------------H---------------------------------- 177
AFH35018 118 ---------------------------H---------------------------------- 177
AGW27542 118 ---------------------------H---------------------------------- 177
ACV60385 118 ---------------------------H---------------------------------- 177
AFX66401 118 ---------------------------H---------------------------------- 177
AFX66472 118 ---------------------------H---------------------------------- 177
AFX66473 118 ---------------------------H---------------------------------- 177
AFX66474 118 ---------------------------H---------------------------------- 177
AFX66475 118 ---------------------------H---------------------------------- 177
AFX66476 118 ---------------------------H---------------------------------- 177
AFX66484 118 ---------------------------H---------------------------------- 177
AGW27537 118 ---------------------------H---------------------------------- 177

AEH27625 178 DMSQQVKQALLEKHPDYQYKPRRPCERRR                                 206
ACV60363 178 ------------------------------                                 206
ACV60364 178 ------------------------------                                 206
AFX66388 178 ------------------------------                                 206
AFH35018 178 ------------------------------                                 206
AGW27542 178 ------------------------------                                 206
ACV60385 178 ------------------------------                                 206
AFX66401 178 ------------------------------                                 206
AFX66472 178 ------------------------------                                 206
AFX66473 178 ------------------------------                                 206
AFX66474 178 ------------------------------                                 206
AFX66475 178 ------------------------------                                 206
AFX66476 178 ------------------------------                                 206
AFX66484 178 ------------------------------                                 206
AGW27537 178 ------------------------------                                 206
```

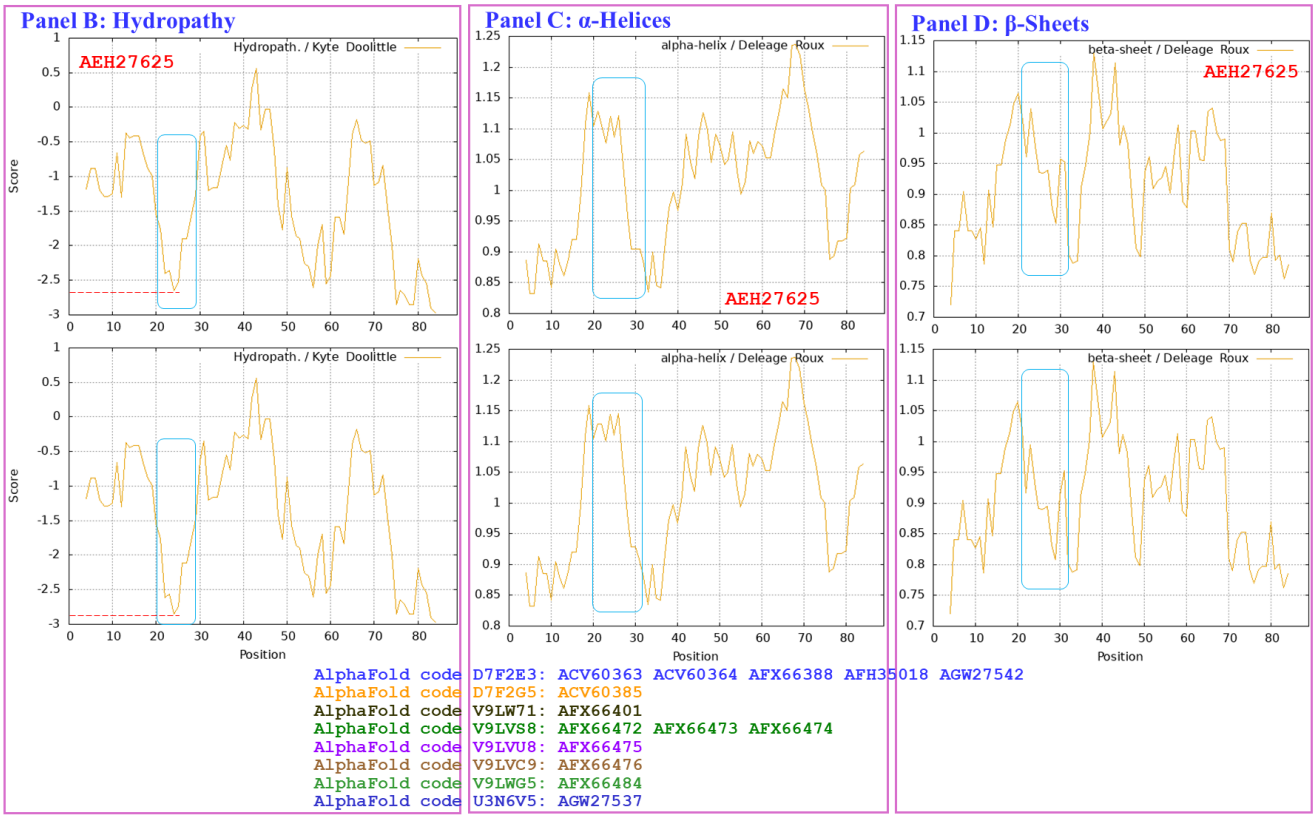

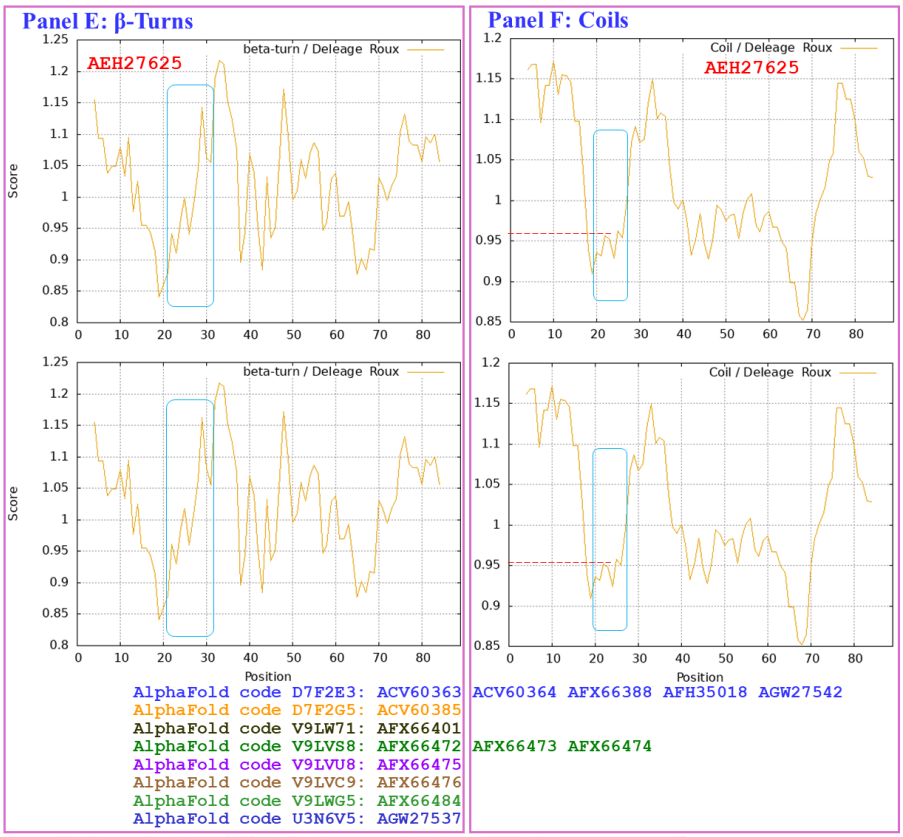
Panel E: β-Turns
beta-turn / Deleage Roux
AEH27625
Score
Position
Panel F: Coils
Coil / Deleage Roux
AEH27625
Score
Position
AlphaFold code D7F2E3: ACV60363 ACV60364 AFX66388 AFH35018 AGW27542
AlphaFold code D7F2G5: ACV60385
AlphaFold code V9LW71: AFX66401
AlphaFold code V9LVS8: AFX66472 AFX66473 AFX66474
AlphaFold code V9LVU8: AFX66475
AlphaFold code V9LVC9: AFX66476
AlphaFold code V9LWG5: AFX66484
AlphaFold code U3N6V5: AGW27537

721

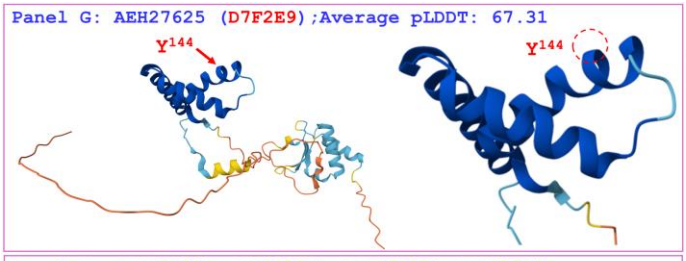
Panel G: AEH27625 (D7F2E9);Average pLDDT: 67.31
Y144
Y144

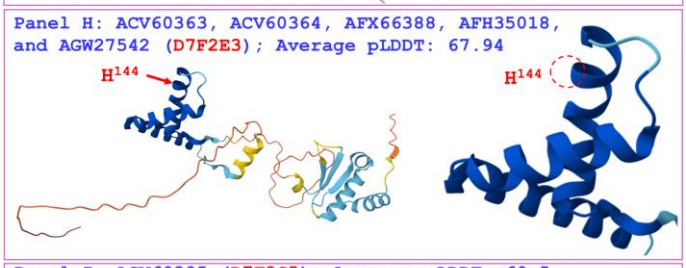
Panel H: ACV60363, ACV60364, AFX66388, AFH35018,
and AGW27542 (D7F2E3); Average pLDDT: 67.94
H144
H144

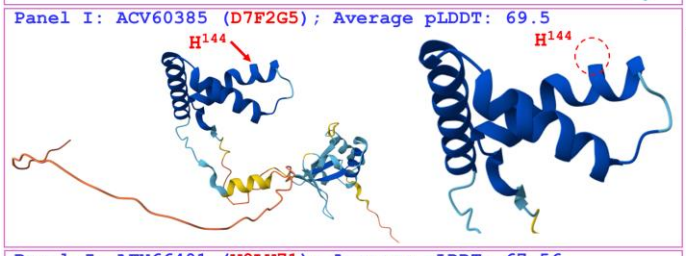
Panel I: ACV60385 (D7F2G5); Average pLDDT: 69.5
H144
H144

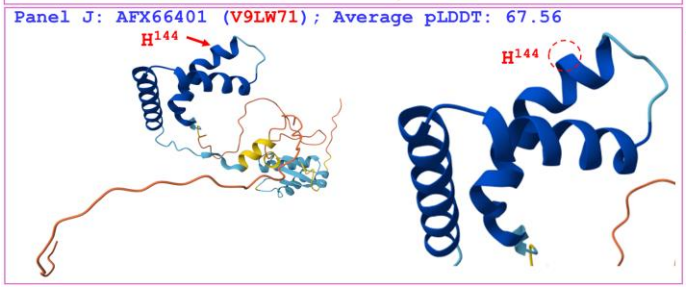
Panel J: AFX66401 (V9LW71); Average pLDDT: 67.56
H144
H144

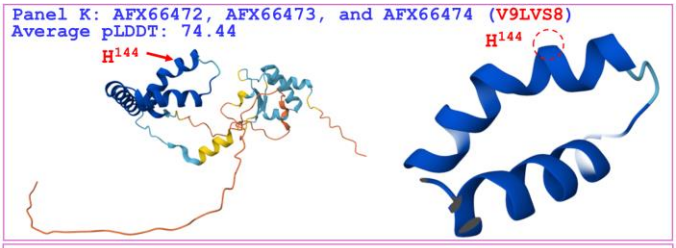
Panel K: AFX66472, AFX66473, and AFX66474 (V9LVS8)
Average pLDDT: 74.44
H144
H144

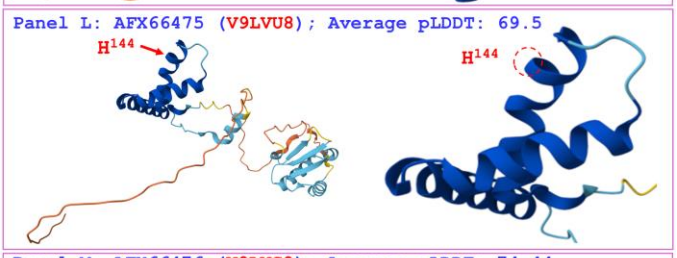
Panel L: AFX66475 (V9LVU8); Average pLDDT: 69.5
H144
H144

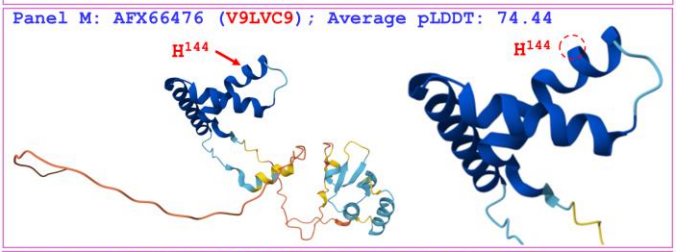
Panel M: AFX66476 (V9LVC9); Average pLDDT: 74.44
H144
H144

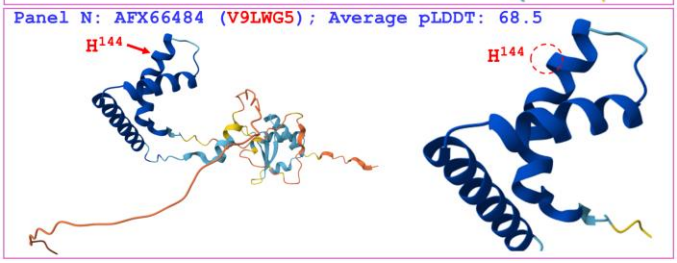
Panel N: AFX66484 (V9LWG5); Average pLDDT: 68.5
H144
H144

722

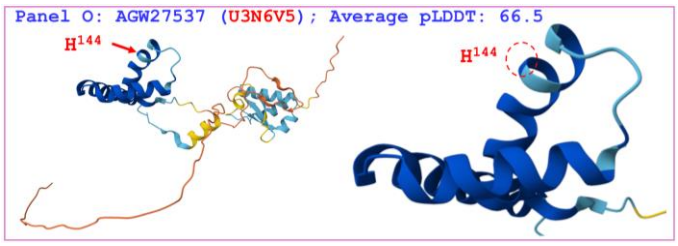

Figure 12. Correlation of the changes in the hydrophobicities and the primary, secondary, and tertiary structures of the HMG-box_ROX1-like domains of MAT1-2-1 proteins: the reference protein AEH27625 (under the AlphaFold code D7F2E9) is derived from the *H. sinensis* strain CS2, and the mutant MAT1-2-1 proteins under the AlphaFold codes **D7F2E3** (ACV60363, ACV60364, AFX66388, AFH35018, and AGW27542), **D7F2G5** (ACV60385), **V9LW71** (AFX66401), **V9LVS8** (AFX66472, AFX66473, and AFX66474), **V9LVU8** (AFX66475), **V9LWC9** (AFX66476), **V9LWG5** (AFX66484), and **U3N6V5** (AGW27537) are derived from the wild-type *C. sinensis* isolates YN09_64, YN09_6, YN09_22, YN09_51, XZ-NQ-154, XZ-NQ-155, GS09_111, QH09-93, CS560-961, QH-YS-199, QH09_11, ID10_1, and CS6-251, respectively. Panel A shows an alignment of the amino acid sequences of the HMG-box_ROX1-like domains of the MAT1-2-1 proteins; amino acid substitutions are shown in red, and the sequences depicted in various colors represent the MAT1-2-1 proteins under the AlphaFold codes V9LWC9, V9LVS8, D7F2E3, V9LVU8, D7F2G5, V9LW71, V9LWG5, and U3N6V5; the hyphens indicate identical amino acid residues. The ExPASy ProtScale plots show the changes in hydrophobicity (Panel B) and in the 2D structures (Panels C–F for α-helices, β-sheets, β-turns, and coils, respectively) of the proteins. The open rectangles in blue outline the changes in topology and waveform shown in the plots. Panels G–O show representations of the 3D structures of the full-length proteins on the left and the locally amplified structures at the mutation site on the right. The model confidence for the AlphaFold-predicted 3D structures is indicated as follows: very high (pLDDT>90); high (90>pLDDT>70); low (70>pLDDT>50); very low (pLDDT<50).

As shown in the representations of the tertiary structures presented in Panels G–O of Figure 12, the substituted residues with reduced hydrophobicity are located within the core α-helices in the HMG-box_ROX1-like domains, and they destabilize the hydrophobic core and alter the hydrophobic stereostructures of the domains [Baxevanis *et al*. 1995; Thapar 2015]. Although Panel A of Figure 12 shows the same Y-to-H substitution that caused the changes in hydrophobicity and second-order structure (shown in the ExPASy ProtScale plots in Panels B–F) in the HMG-box_ROX1-like domains of the MAT1-2-1 proteins ACV60363–ACV60364, ACV60385, AFH35018, AFX66388, AFX66472–AFX66476, AFX66401, AFX66484, AGW27537, and AGW27542, additional amino acid substitutions outside the HMG-box_ROX1-like domains (*cf*. Figure S2) might play synergistic roles in altering the tertiary structures of the proteins through long-range spatial interactions with the mutations within the domains (Panels H–O of Figure 12) of the MAT1-2-1 proteins under the 8 AlphaFold codes summarized in Table S7. The mutant HMG-box_ROX1-like domains clustered into Branch b1α in the Bayesian clustering tree (*cf*. Figure 2, Table S7).

Figure 13 compares the hydrophobicity and structure of the HMG-box_ROX1-like domain of the MAT1-2-1 protein ACV60399 (under the AlphaFold code D7F2H9) derived from the wild-type *C. sinensis* isolate SC-3 (*cf*. Table S2) [Zhang *et al*. 2009] with those of the HMG-box_ROX1-like domain of the reference protein AEH27625 (under the AlphaFold code D7F2E9) derived from the *H. sinensis* strain CS2 [Zhang *et al*. 2009]. Panel A shows substitutions of Y-to-H (aromatic tyrosine to basic histidine; hydropathy

759 indices changed from -1.3 to -3.2 [Kyte & Doolittle 1982]) and Q-to-R (glutamine, which possesses polar
760 neutral side chains, to basic arginine; hydropathy indices changed from -3.5 to -4.5); both of these
761 substitutions caused reduced hydrophobicity, as illustrated by the changes in topology and waveform shown
762 in the hydropathy plot in Panel B. These changes resulted in alteration of the secondary structure
763 surrounding the mutation sites in the HMG-box_ROX1-like domain of the mutant MAT1-2-1 protein
764 ACV60399, as illustrated by the changes in topology and waveform seen in the ExPASy ProtScale plots for
765 α-helices, β-sheets, β-turns, and coils presented in Panels C–F. As shown in the representations of 3D
766 structures in Panels G–H, the 2 replaced residues with reduced hydrophobicity are located inside and outside
767 the hydrophobic core structure of the 3 α-helices, and they destabilize and alter the core stereostructure of
768 the domain [Baxevanis *et al*. 1995; Thapar 2015]. The HMG-box_ROX1-like domain of the mutant protein
769 ACV60399 under the AlphaFold code D7F2H9 clustered into Branch b1β in the Bayesian clustering tree
770 (*cf*. Figure 2, Table S7).

Panel A: Amino acid sequence alignment

```
AEH27625 118 APPSPKDIKIPRPPNAYILYRKERHHYVKDANPGITNNEISQILGKAWNMESNDVRQKYK 177
ACV60399 118 --------------------------H--------------------------------- 177

AEH27625 178 DMSQQVKQALLEKHPDYQYKPRRPCERRR                                206
ACV60399 178 -----------------R-----------                                206
```

771

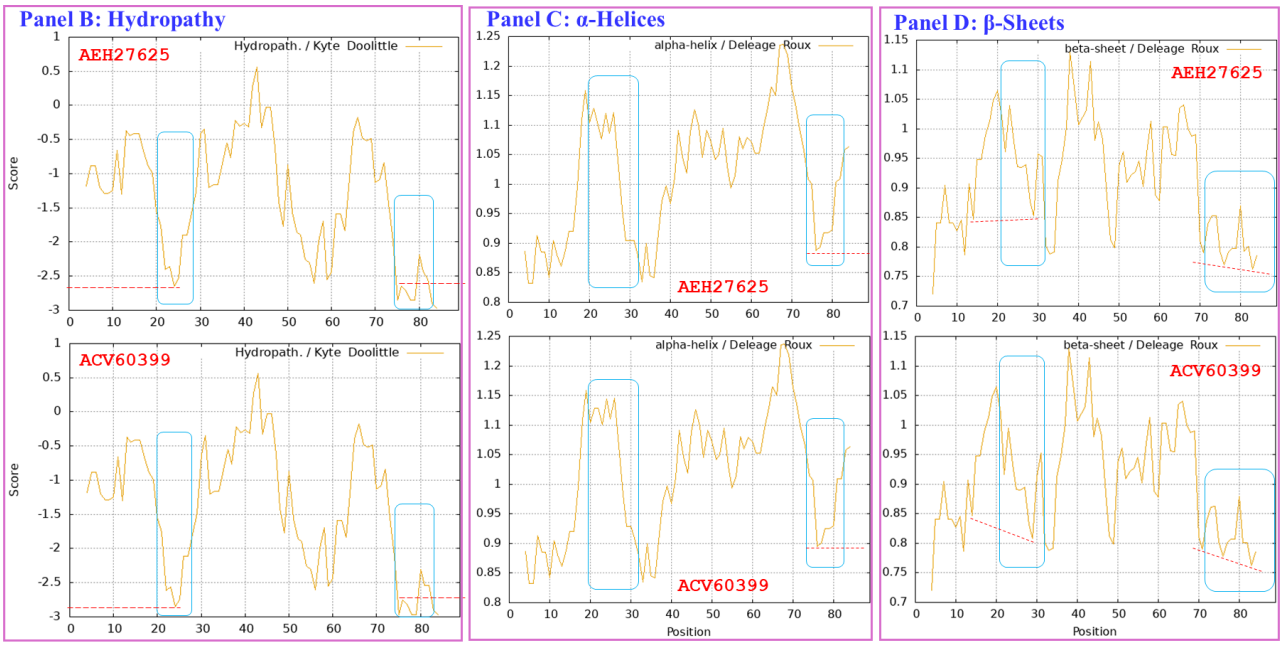

772

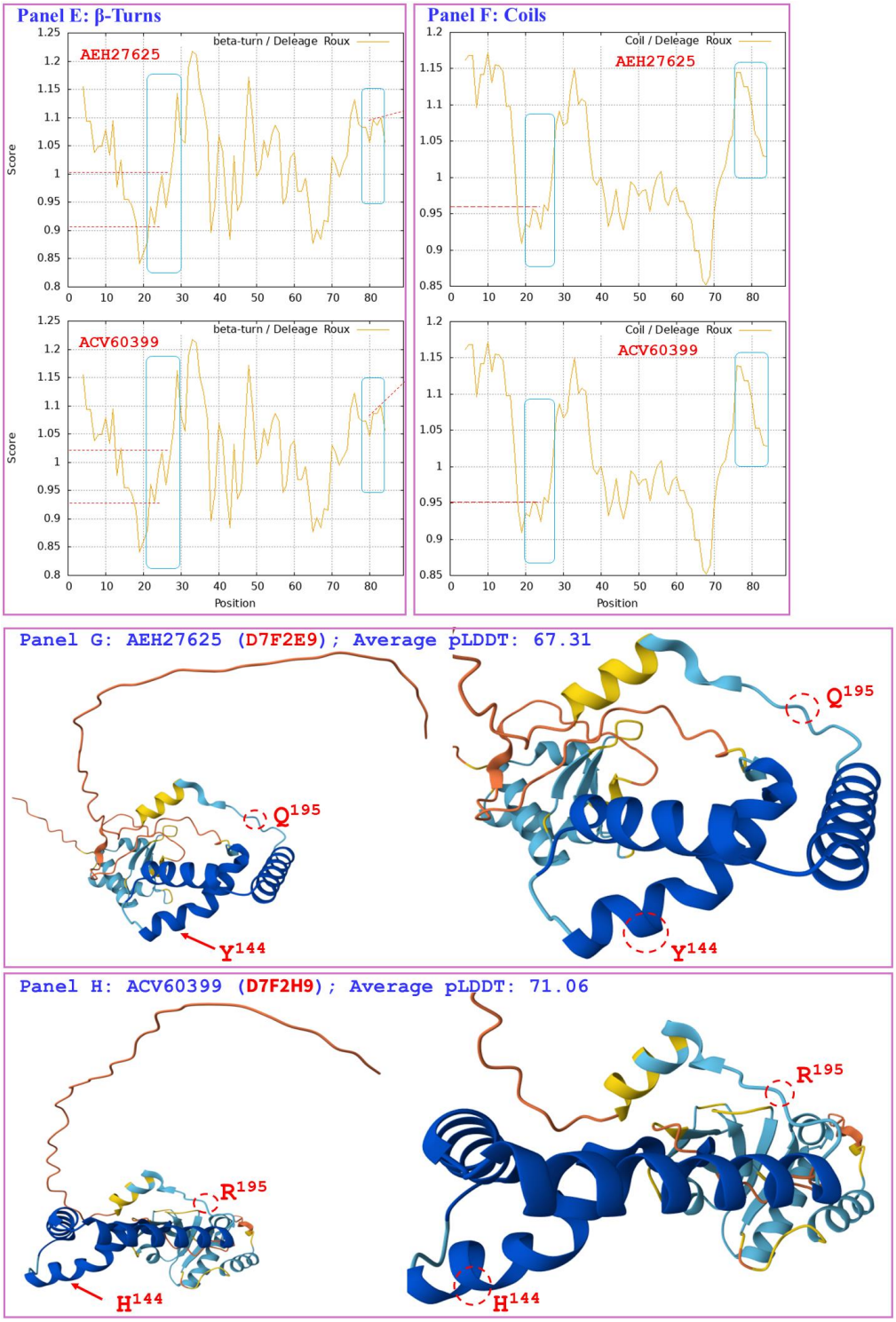

Figure 13. Correlation of the changes in the primary, secondary, and tertiary structures of the HMG-box_ROX1-like domains of MAT1-2-1 proteins: the reference protein AEH27625 (under the AlphaFold code D7F2E9) is derived from the *H. sinensis* strain CS2, and the mutant MAT1-2-1 protein ACV60399 (under the AlphaFold code D7F2H9) is derived from the wild-type *C. sinensis* isolate SC-3. Panel A shows an alignment of the amino acid sequences of the HMG-box_ROX1-like domains of the MAT1-2-1 proteins; amino acid substitutions are shown in red, whereas the hyphens indicate identical amino acid residues. The ExPASy ProtScale plots show the changes in hydrophobicity (Panel B) and in the 2D structure (Panels C–F for α-helices, β-sheets, β-turns, and coils) of the protein; the open rectangles in blue outline the changes in topology and waveform of the plots. Panels G–H show the 3D structures of the full-length proteins on the left and the locally amplified structures at the sites of substitutions on the right. The model confidence for the AlphaFold-predicted 3D structures is indicated as follows: ■ very high (pLDDT>90); □

high (90>pLDDT>70); low (70>pLDDT>50); very low (pLDDT<50).

Aggregating the data presented in Section III-7, Panels A in Figures 10–13 demonstrate the 1–3 amino acid substitutions detected in the HMG-box_ROX1-like domains that caused changes in the topologies and waveforms shown in the ExPASy ProtScale plots presented in Panels B–F of the figures. These changes indicate the presence of altered hydrophobicity and secondary structures (α-helices, β-sheets, β-turns, and coils) of the HMG-box_ROX1-like domains of the mutant MAT1-2-1 proteins. These changes resulted in alterations in the stereostructures of the domains of the mutant proteins under different AlphaFold codes, as illustrated in Panel H of Figures 10–13, Panel I of Figure 11, Panels I–O of Figures 12 and summarized in Table S7. The mutant HMG-box_ROX1-like domains clustered into various clades in the Bayesian clustering tree (*cf*. Figure 2; Table S7) and ultimately change the DNA-binding specificities and affinities and the functionalities of gene transcriptional regulation, factors that play key roles in the sexual reproduction of *O. sinensis*.

III-8 Diverse primary and secondary structures of the HMG-box_ROX1-like domains of MAT1-2-1 proteins encoded by the genome and transcriptome assemblies of *H. sinensis* and the metatranscriptome assembly of the *C. sinensis* insect–fungal complex

Figure 14 shows a comparison of the hydrophobicity and structure of the HMG-box_ROX1-like domain of the MAT1-2-1 protein encoded by the genome assembly ANOV01000063 (9759→9851 & 9907→10,026) derived from *H. sinensis* strain Co18 [Hu *et al*. 2013] with the hydrophobicity and structure of the reference MAT1-2-1 protein AEH27625 derived from *H. sinensis* strain CS2 (under the AlphaFold code D7F2E9) [Zhang *et al*. 2009]. Panel A shows an S-to-A substitution (serine with polar neutral side chains to aliphatic alanine; hydropathy indices changed from -0.8 to 1.8 [Kyte & Doolittle 1982]). This substitution caused increased hydrophobicity surrounding the mutation site in the domain of the MAT1-2-1 protein encoded by the genome assembly ANOV01000063, as illustrated by the changes in topology and waveform changes seen in the hydropathy plot in Panel B.

Panel A: Amino acid sequence alignment

```
AEH27625     118  APPSPKDIKIPRPPNAYILYRKERHHYVKDANPGITNNEISQILGKAWNMESNDVRQKYK 177
ANOV01000063 9732 ----------------------------------------A------------------- 9967

AEH27625     178  DMSQQVKQALLEKHPDYQYKPRRPCERRR                               206
ANOV01000063 9968 ----------------------------                                 10,164
```

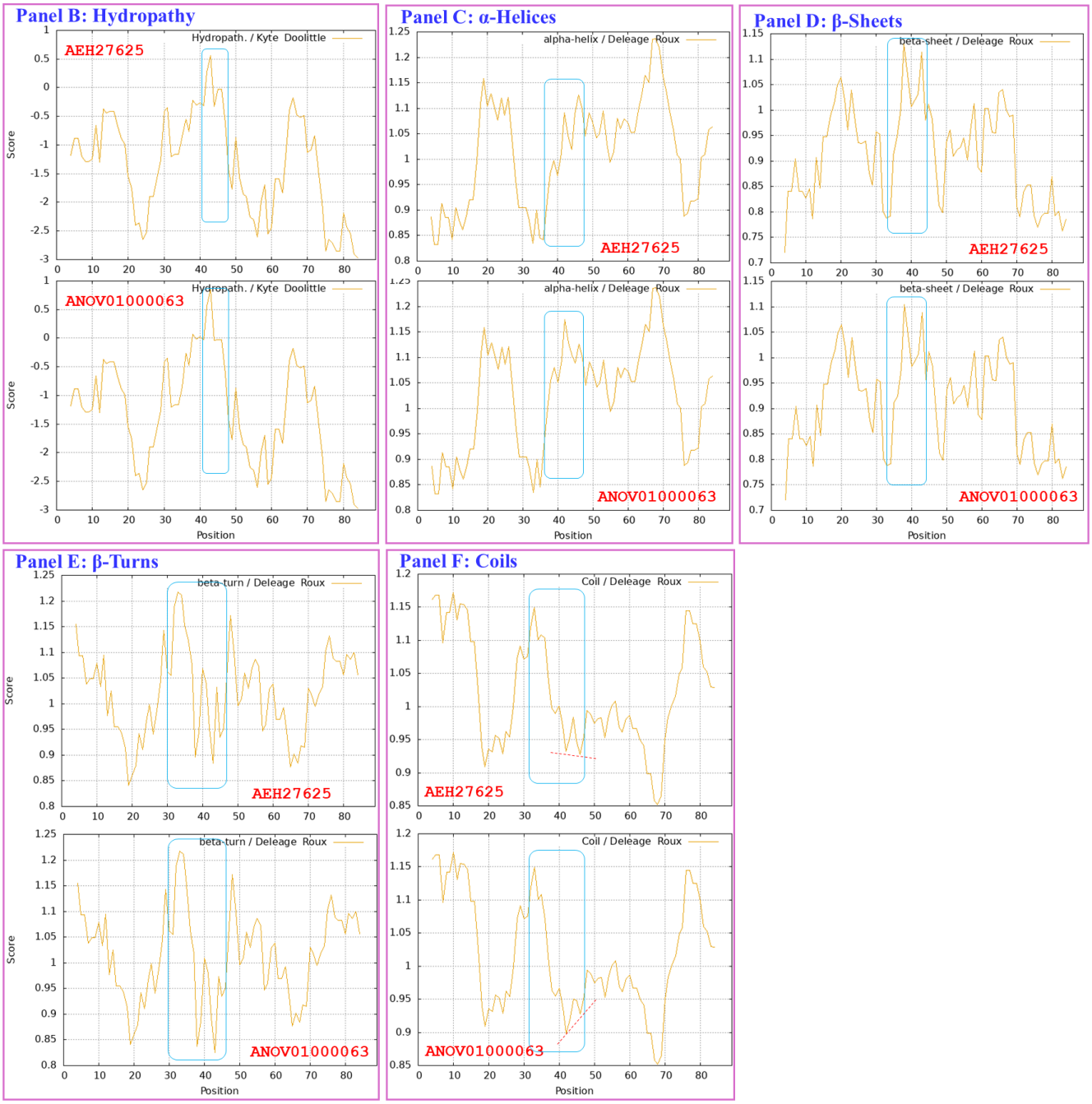

Figure 14. Correlation of the changes in the primary and secondary structures of the HMG-box_ROX1-like domains of the reference MAT1-2-1 protein AEH27625 (under the AlphaFold code D7F2E9) derived from the *H. sinensis* strain CS2 and the mutant MAT1-2-1 protein encoded by the genome assembly ANOV01000063 derived from the *H. sinensis* strain Co18. Panel A shows an alignment of the amino acid sequences of the HMG-box_ROX1-like domains of the MAT1-2-1 proteins; amino acid substitutions are shown in red, whereas the hyphens indicate identical amino acid residues. The ExPASy ProtScale plots show the changes in hydrophobicity (Panel B) and in the 2D structure (Panels C–F for α-helices, β-sheets, β-turns, and coils, respectively) of the protein; the open rectangles in blue outline the changes in topology and waveform of the plots.

These changes in the amino acid sequence and hydrophobicity resulted in altered secondary structure (α-helices, β-sheets, β-turns, and coils) within the HMG-box_ROX1-like domain of the mutant MAT1-2-1 protein encoded by the genome assembly ANOV01000063, as illustrated in the ExPASy ProtScale plots for α-helices, β-sheets, β-turns, and coils shown in Panels C–F, respectively, in Figure 14 [Baxevanis *et al.*

1995; Thapar 2015]. These changes in the sequences and hydrophobicity may have altered the tertiary structure of the HMG-box_ROX1-like domain of the genome-encoded protein. The altered HMG-box_ROX1-like domain clustered into Branch a2 in the Bayesian clustering tree (*cf*. Figure 2; Table S8).

Figure 15 compares the hydrophobicities and structures of the HMG-box_ROX1-like domains of the MAT1-2-1 proteins encoded by the genome assemblies LKHE01001605 (14,016←14,135 & 14,191←14,283), LWBQ01000021 (14,016←14,135 & 14,191←14,283), and NGJJ01000619 (23,186←23,305 & 23,361←23,453) of the *H. sinensis* strains 1229, ZJB12195, and CC1406-20395, respectively [Li *et al*. 2016a; Jin *et al*. 2020; Liu *et al*. 2020], with the hydrophobicity and structure of the reference protein AEH27625 (under the AlphaFold code D7F2E9) derived from the *H. sinensis* strain CS2 [Zhang *et al*. 2009]. Panel A shows Y-to-H (aromatic tyrosine to basic histidine; hydropathy indices changed from -1.3 to -3.2 [Kyte & Doolittle 1982]) and S-to-A substitutions (serine, which has polar neutral side chains, to aliphatic alanine; hydropathy indices changed from -0.8 to 1.8), which resulted in altered hydrophobicity, as illustrated in the hydropathy plot in Panel B. These changes altered the secondary structures surrounding the mutation sites in the HMG-box_ROX1-like domains of the mutant MAT1-2-1 proteins encoded by the genome assemblies LKHE01001605, LWBQ01000021, and NGJJ01000619, as illustrated in the ExPASy ProtScale plots for α-helices, β-sheets, β-turns, and coils shown in Panels C–F, respectively [Baxevanis *et al*. 1995; Thapar 2015], and subsequently altered the tertiary structures of the core stereostructures of the domains. The mutant HMG-box_ROX1-like domains of the genome-encoded proteins clustered into Branch b3 in the Bayesian clustering tree (*cf*. Figure 2, Table S8).

Panel A: Amino acid sequence alignment

```
AEH27625     118     APPSPKDIKIPRPPNAYILYRKERHHYVKDANPGITNNEISQILGKAWNMESNDVRQKYK 177
LKHE01001605 14,310  ----------------H-----------------------A------------------- 14,076
LWBQ01000021 239,323 ----------------H-----------------------A------------------- 239,089
NGJJ01000619 23,480  ----------------H-----------------------A------------------- 23,246

AEH27625     178     DMSQQVKQALLEKHPDYQYKPRRPCERRR                                206
LKHE01001605 14,075  ----------------------------                                  13,989
LWBQ01000021 239,088 ----------------------------                                  239,002
NGJJ01000619 23,245  ----------------------------                                  23,159
```

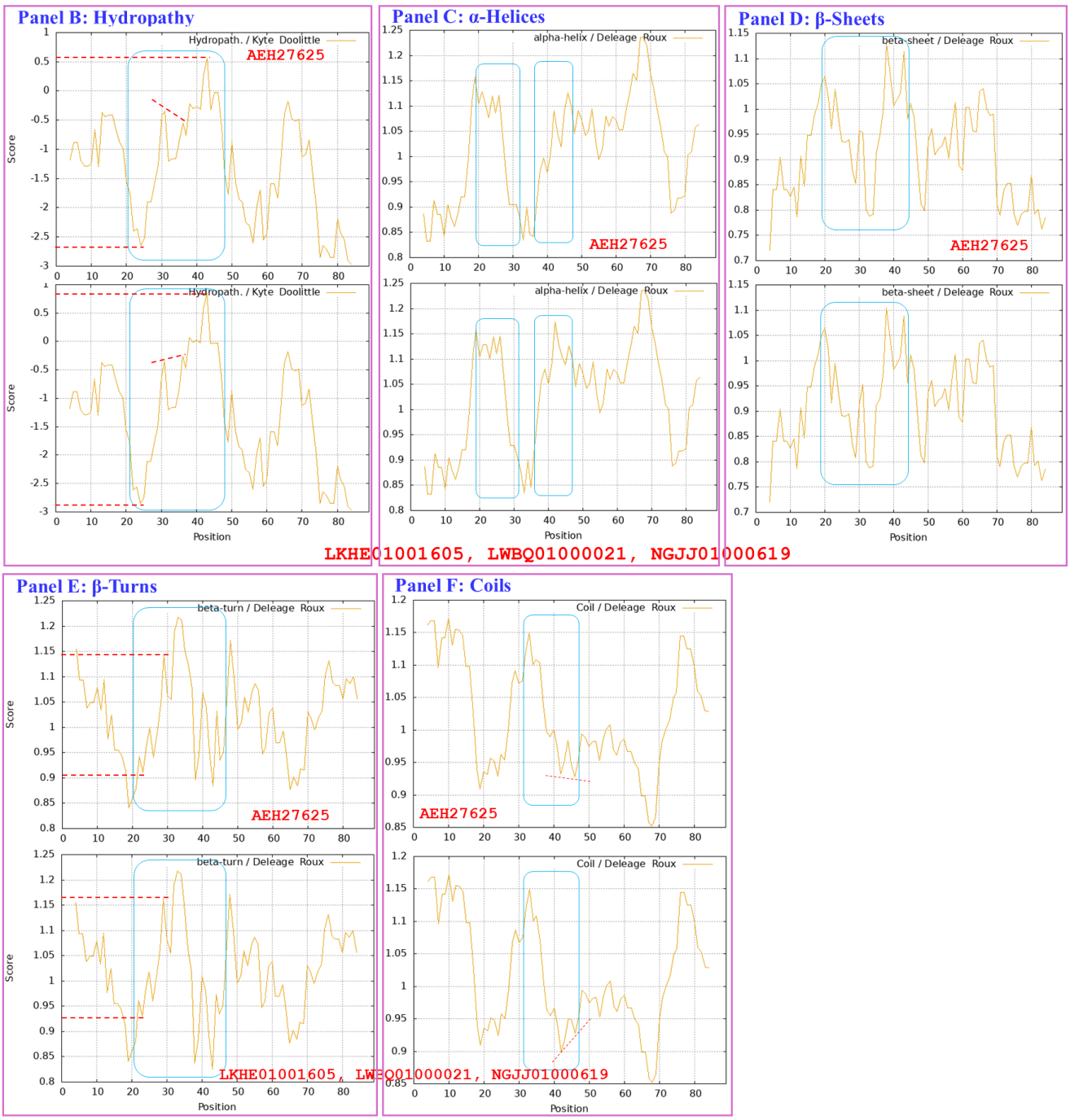

Figure 15. Correlation of the changes in the primary and secondary structure of the HMG-box_ROX1-like domain of the reference MAT1-2-1 protein AEH27625 (under the AlphaFold code D7F2E9) derived from the *H. sinensis* strain CS2 in and the mutant MAT1-2-1 proteins encoded by the genome assemblies LKHE01001605, LWBQ01000021, and NGJJ01000619 derived from *H. sinensis* strains 1229, ZJB12195, and CC1406-20395, respectively. Panel A shows an alignment of the amino acid sequences of the HMG-box_ROX1-like domains of the MAT1-2-1 proteins; amino acid substitutions are shown in red, whereas the hyphens indicate identical amino acid residues. The ExPASy ProtScale plots show the changes in hydrophobicity (Panel B) and in the 2D structures (Panels C–F for α-helices, β-sheets, β-turns, and coils, respectively) of the proteins; the open rectangles in blue outline the changes in topology and waveform seen in the plots.

The genome assembly JAAVMX000000000 of the *H. sinensis* strain IOZ07 does not contain a gene encoding the MAT1-2-1 protein [Shu *et al*. 2020].

Figure 16 compares the hydrophobicity and structure of the HMG-box_ROX1-like domain of the

MAT1-2-1 proteins encoded by the transcriptome assembly GCQL01020543 (553←765) of the *H. sinensis* strain L0106 and by the metatranscriptome assembly OSIN7649 (379→591) of the mature *C. sinensis* insect–fungal complex [Liu *et al*. 2015; Xia *et al*. 2017] with the hydrophobicity and structure of the reference protein AEH27625 (under the AlphaFold code D7F2E9) derived from the *H. sinensis* strain CS2 [Zhang *et al*. 2009]. Panel A shows Y-to-H substitutions (aromatic tyrosine to basic histidine; hydropathy indices changed from -1.3 to -3.2 [Kyte & Doolittle 1982]). The substitutions caused decreased hydrophobicity, as illustrated by the changes in topology and waveform seen in the hydropathy plot in Panel B. These changes resulted in alterations of the secondary structure surrounding the mutation sites in the HMG-box_ROX1-like domains of the MAT1-2-1 proteins encoded by the transcriptome assembly GCQL01020543 and the metatranscriptome assembly OSIN7649, as illustrated by the changes in topology and waveform shown in the ExPASy ProtScale plots for α-helices, β-sheets, β-turns, and coils in Panels C–F.

Panel A: Amino acid sequence alignment

```
AEH27625     118 APPSPKDIKIPRPPNAYILYRKERHHYVKDANPGITNNEISQILGKAWNMESNDVRQKYK 177
GCQL01020543 792 ----------------H------------------------------------------ 613
OSIN7649     352 ----------------H------------------------------------------ 531

AEH27625     178 DMSQQVKQALLEKHPDYQYKPRRPCERRR                                206
GCQL01020543 612 ------------------------------                               526
OSIN7649     532 ------------------------------                               618
```

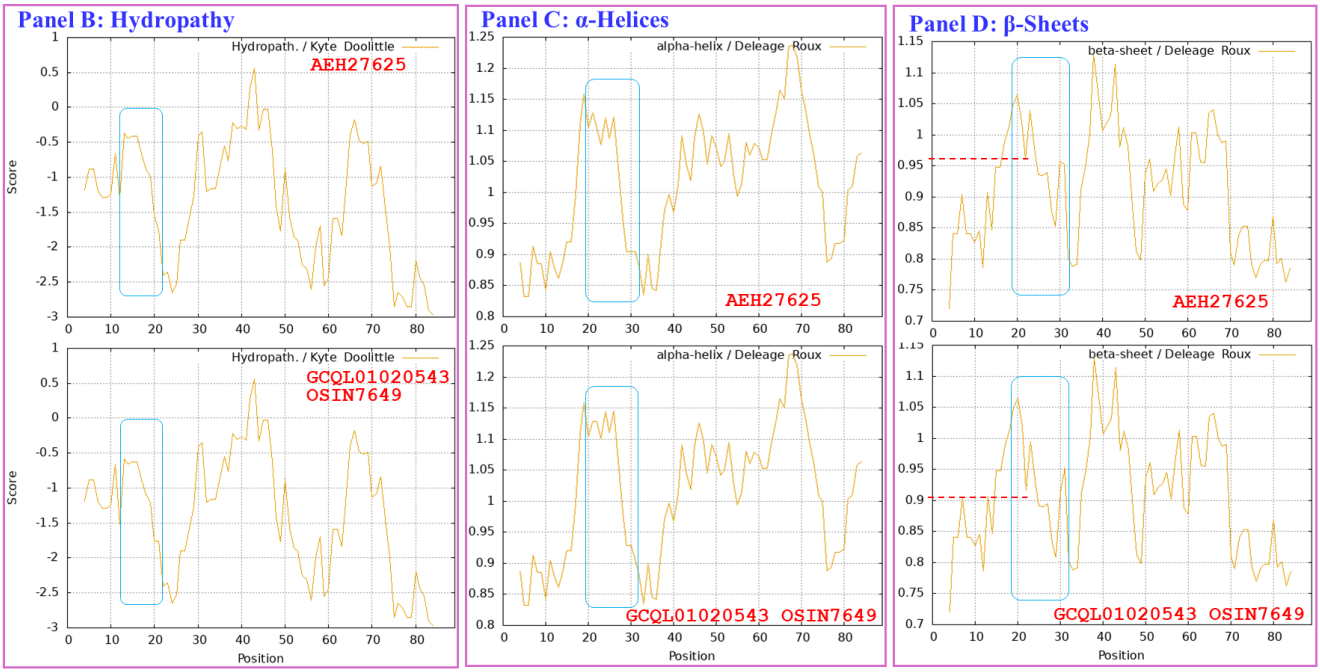

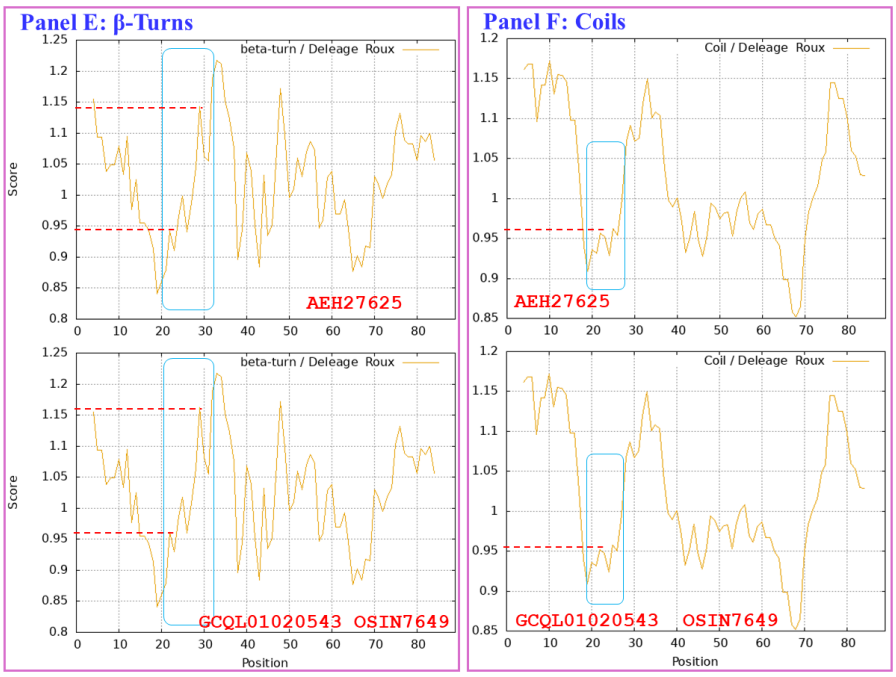

Figure 16. Correlation of the primary and secondary structure of the HMG-box_ROX1-like domain of the reference MAT1-2-1 protein AEH27625 (under the AlphaFold code D7F2E9) derived from the *H. sinensis* strain CS2 with the primary and secondary structures of the mutant MAT1-2-1 proteins encoded by the transcriptome assembly GCQL01020543 derived from the *H. sinensis* strain L0106 and the metatranscriptome assembly OSIN7649 (379→591) of the mature C. sinensis insect–fungal complex. Panel A shows an alignment of the amino acid sequences of the HMG-box_ROX1-like domains of the MAT1-2-1 proteins; amino acid substitutions are shown in red, whereas the hyphens indicate identical amino acid residues. The ExPASy ProtScale plots show the changes in hydrophobicity (Panel B) and in the 2D structures (Panels C–F for α-helices, β-sheets, β-turns, and coils, respectively) of the proteins; the open rectangles in blue outline the changes in topology and waveform seen in the plots.

Similar to the Y-to-H substitutions in the HMG-box_ROX1-like domains of the mutant MAT1-2-1 proteins under various AlphaFold 3D structural models (such as V9LWC9, V9LVS8, D7F2E3, V9LVU8, D7F2G5, V9LW71, V9LWG5, and U3N6V5) shown in Figure 12, the changes in hydrophobicities and primary and secondary structures shown in Figure 16 may subsequently alter the tertiary structures of the HMG-box_ROX1-like domains of the transcriptome-encoded and metatranscriptome-encoded mutant proteins. The mutant HMG-box_ROX1-like domains of the transcriptome- and metatranscriptome-encoded proteins clustered into Branch b1α in the Bayesian clustering tree (*cf.* Figure 2, Table S8).

III-9 Heterogenous fungal sources of the MAT1-1-1 and MAT1-2-1 proteins

Although wild-type *C. sinensis* isolates are often considered impure as *H. sinensis*, analysis of mutant full-length mating proteins revealed their heterogeneous fungal sources, as shown in Table S3. Of the wild-type *C. sinensis* isolates whose full-length MAT1-1-1 and MAT1-2-1 proteins were analyzed (*cf.* Figures 3–8 and 10–13), 34 had ITS genotyping information in the GenBank database and belonged to GC-biased Genotypes #1 and #3 of genome-independent *O. sinensis* fungi (Table S3) [Zhu & Li 2017; Li *et al.* 2022]. Although the ITS sequences of 29 of the 34 wild-type *C. sinensis* isolates appeared to show high homology (≥97%) to the ITS sequences of GC-biased Genotype #1 *H. sinensis*, the mutant MAT1-1-1 and MAT1-2-1

895 proteins might not necessarily be derived from GC-biased Genotype #1 *H. sinensis* within the impure fungal
896 complex containing more than one fungal species [Li *et al*. 2016b], while the *H. sinensis* ITS sequences
897 were most easily amplified during regular simple-step PCR under the experimental settings, unless the PCR
898 experiments using multiple pairs of primers and combining with amplicon cloning techniques with selection
899 and sequencing of sufficient (usually 30–50) white colonies. In other words, because of the impure nature
900 of the wild-type *C. sinensis* isolates [Li *et al*. 2016b, 2022; Zhu & Li 2017], the mutant proteins may be
901 derived from cooccurring unvalidated heterospecific or genotypic fungi.

902 IV. Discussion

903 IV-1 Correlation of the hydrophobicity and the primary, secondary, and tertiary 904 structures of the DNA-binding domains of the MAT1-1-1 and MAT1-2-1 proteins

905 The MATα_HMGbox domain of the MAT1-1-1 protein and the HMG-box_ROX1-like domain of the
906 MAT1-2-1 protein are distinct DNA-binding domains that are critical for fungal mating-type regulation but
907 differ in their evolutionary lineage, structural architecture, and functional roles [Jackson *et al*. 2013; Zheng
908 *et al*. 2013; Kim *et al*. 2015]. The HMGbox domains in mating proteins are multifunctional motifs central
909 to the transcriptional regulation of mating-related genes, *O. sinensis* sexual reproduction, and host
910 adaptation in the *C. sinensis* insect–fungal complex. Our study demonstrates that various 1–3 amino acid
911 substitutions within the MATα_HMGbox and HMG-box_ROX1-like domains of the MAT1-1-1 and MAT1-
912 2-1 proteins, respectively, of the wild-type *C. sinensis* isolates and *C. sinensis* insect–fungal complexes
913 result in changes in the hydrophobic properties and in the secondary and tertiary structures of the DNA-
914 binding domains of the proteins (*cf*. Figures 3–16). The variable sequences of the DNA-binding domains
915 clustered into different clades in the Bayesian clustering trees (*cf*. Figures 1–2; Tables S5–S8).

916 The MATα_HMGbox domain of the MAT1-1-1 protein contains a core structure of 3 α-helices that
917 ensures high-affinity, sequence-dependent binding to AT-rich DNA motifs [Ramšak *et al*. 2020, 2021;
918 Ramšak & Kück 2022]. This binding facilitates the assembly of transcriptional machinery in a way that
919 involves mating-type-specific genes and activates gene transcription by inducing DNA conformational
920 changes through physical bending or twisting of the target DNA segments [Martin *et al*. 2010; Ait Benkhali
921 *et al*. 2013; Ramšak & Kück 2022]. The domain participates directly in promoter recognition of specific
922 genes related to the heterothallic reproductive process [Yamamoto *et al*. 1997].

923 Table S4 shows the hydropathy values for amino acids that are defined by their side chains according
924 to Kyte & Doolittle [1982] (provided by https://web.expasy.org/protscale/). Larger hydropathy values
925 indicate stronger hydrophobicity, while negative values indicate hydrophilicity [Kyte & Doolittle 1982;
926 Baxevanis *et al*. 1995; Thapar 2015]. The core α-helical stereostructures of the MATα_HMGbox domains

927 are stabilized through a hydrophobic core that is composed of nonpolar amino acids such as isoleucine (Ile,
928 I), valine (Val, V), leucine (Leu, L), phenylalanine (Phe, F), cysteine (Cys, C), methionine (Met, M), and
929 alanine (Ala, A); these amino acids have hydropathy indices of 4.5, 4.2, 3.8, 2.8, 2.5, 1.9, and 1.8,
930 respectively (*cf*. Table S4) [Kyte & Doolittle 1982].

931 The HMG-box_ROX1-like domain of the MAT1-2-1 protein also consists of 3 asymmetrically arranged
932 α-helices that are connected by flexible loops, forming a key hydrophobic core that is stabilized through the
933 presence of the aforementioned nonpolar amino acids (*cf*. Table S4). The HMG-box_ROX1-like domain of
934 the MAT1-2-1 protein regulates gene expression in a sequence-specific manner by binding to ATTAAT or
935 ATTGTT motifs [Jackson *et al*. 2013; Zheng *et al*. 2013; Kim *et al*. 2015]. This domain has been implicated
936 in chromatin remodeling and transcriptional repression through its interaction with other corepressors,
937 similar to the repressor of oxygen-regulated genes 1 (ROX1) domain in yeast, through opposing pathways
938 to the MATα_HMGbox domain of the MAT1-1-1 protein [Balasubramanian *et al*. 1993; Zitomer *et al*. 1997;
939 Zheng *et al*. 2013]. ROX1 represses its own promoter, creating a feedback loop for hypoxic response
940 regulation as a central hypoxia-responsive regulator that plays roles in chromatin remodeling following
941 DNA binding and in the integration of metabolic signals [Kastaniotis & Zitomer 2000].

942 To date, no studies have directly addressed heterodimerization between the MAT1-1-1 and MAT1-2-1
943 proteins of *O. sinensis*, although formation of heterodimers between the MATα_HMGbox domain of the
944 MAT1-1-1 protein and the HMG-box_ROX1-like domain of the MAT1-2-1 protein is believed to be a
945 critical mechanism in the regulation of fungal mating, particularly in heterothallic ascomycetes [Kües &
946 Casselton 1993; Asante-Owusu *et al*. 1996; Jacobsen *et al*. 2002]. However, the MATα_HMGbox and
947 HMG-box_ROX1-like domains likely interact with each other, enabling them to cooperate synergistically
948 in DNA binding through their complementary electrostatic surfaces [Hancock *et al*. 2019]. The
949 heteromorphic stereostructures of the HMGbox domains of the mutant mating proteins derived from wild-
950 type *C. sinensis* isolates presented in this study likely alter the complementary cooperation of the mating
951 proteins of the self-sterile *O. sinensis* under heterothallic or hybrid outcrossing and affect the subsequent
952 functionalities of activation or repression of mating-related gene transcription [Li *et al*. 2023c, 2024b,
953 2025].

954 **IV-2 Heterogenous fungal sources of the MAT1-1-1 and MAT1-2-1 proteins**

955 The analysis of mutant full-length mating proteins derived from wild-type *C. sinensis* isolates (Figures
956 3–8 and 10–13) revealed their heterogeneous fungal sources (Table S3) [Zhang *et al*. 2009, 2011, 2012,
957 2013, 2014; Zhang & Zhang 2015]. A total of 34 wild-type *C. sinensis* isolates were examined for molecular
958 taxonomy ITS sequences that are available in GenBank and were found to belong to genomically
959 independent GC-biased Genotypes #1 and #3 of *O. sinensis* fungi. However, whether the impure wild-type

960 *C. sinensis* isolates cooccur with other heterospecific fungi remains unclear, which remains to be determined
961 through the use of culture-dependent techniques or culture-independent PCR protocols involving the use of
962 amplicon cloning techniques with the selection and sequencing of sufficient amounts (usually ≥30) of white
963 colonies.

964 Li et al. [2016b] conducted a similar *C. sinensis* isolate study and reported 2 other wild-type *C. sinensis*
965 isolates, CH1 and CH2. With using multiple pairs of PCR and rigorous amplicon cloning techniques, these
966 isolates were proven to coexist GC-biased Genotype #1 and AT-biased Genotypes #4–5 of *O. sinensis*, and
967 heterospecific *Paecilomyces hepiali*. Li et al. [2022. 2023c, 2023d, 2024b] further proved that the ITS
968 sequences of Genotypes #2–17 of *O. sinensis* with multiple transition and transversion point mutations are
969 not the repetitive copies in the genome of GC-biased Genotype #1 *H. sinensis* but belong to independent *O.*
970 *sinensis* fungi, regardless of whether they are GC- or AT-biased. Although displaying the key genetic
971 features of fungal complexes, these wild-type isolates phenotypically exhibited *in vitro* growth and
972 microscopic morphological characteristics of psychrophilic *H. sinensis* in phenotype. Functionally, in the
973 inoculation experiments on larvae of *Hepialus armoricanus* (n=100 larvae each study group), the infection
974 rate was significantly increased 15- to 39-fold to 55.2% for the wild-type isolates CH1 and CH2 from nearly
975 non-infectious 1–3% for *H. sinensis* ($P<0.001$) and the larval death latency was largely shortened to 5–8
976 days for the CH1 and CH2 from 35–50 days for *H. sinensis*.

977 IV-3 The MAT1-1-1 and MAT1-2-1 proteins are involved in the sexual reproduction 978 of *O. sinensis*

979 The MAT1-1-1 and MAT1-2-1 proteins coregulate mating compatibility and sexual development
980 during the sexual reproduction of *O. sinensis*, a process in which the MATα_HMGbox and HMG-
981 box_ROX1-like domains play key roles. The hypothesis of self-fertilization via a homothallism or
982 psuedohomothalism strategy has been proposed for *O. sinensis* [Bushley *et al*. 2013; Hu *et al*. 2013] on the
983 basis of genetic research. However, Zhang and Zhang [2015] argued against this hypothesis and suggested
984 that *O. sinensis* uses facultative hybridization in its sexual reproduction on the basis of findings of
985 differential occurrence of the *MAT1-1-1* and *MAT1-2-1* genes in more than 170 wild-type *C. sinensis*
986 isolates derived from natural *C. sinensis* insect–fungal complex specimens collected from different
987 production areas on the Qinghai–Tibet Plateau. Furthermore, Li *et al*. [2023c, 2024b, 2025] reported
988 differential occurrence, differential translation, and alternative splicing of the *MAT1-1-1* and *MAT1-2-1*
989 genes and heteromorphic stereostructures of the MAT1-1-1 and MAT1-2-1 proteins of wild-type *C. sinensis*
990 isolates. In addition, the analysis of DNA-binding domains presented in this study further revealed diverse
991 stereostructures of the MATα_HMGbox domain of the MAT1-1-1 protein and the HMG-box_ROX1-like
992 domain of the MAT1-2-1 protein. Apperantly, *O. sinensis* experiences self-sterility and uses a heterothallic

993 or hybrid strategy, even parasexuality, to accomplish sexual reproduction during the lifecycle of the *C.*
994 *sinensis* insect–fungal complex [Kück 1993; Bennett & Johnson 2003; Sherwood & Bennett 2009; Seervai
995 *et al*. 2013; Zhu & Li 2017; Nakamura *et al*. 2019; Samarasinghe *et al*. 2020; Steensels *et al*. 2021; Mishra
996 *et al*. 2021; Kück *et al*. 2021; Li *et al*. 2023c, 2023e, 2024b, 2025].

997 Unlike homothallic reproduction, heterothallic or hybrid reproduction of *O. sinensis* requires mating
998 partners. Among the 17 genotypes of *O. sinensis* [Kinjo & Zang 2001; Chen *et al*. 2004, 2011; Stensrud *et*
999 *al*. 2005, 2007; Xiao *et al*. 2008; Zhu *et al*. 2010; Barseghyan *et al*. 2011; Li *et al*. 2013, 2022; Mao *et al*.
1000 2013; Zhu & Li 2017; Du *et al*. 2020; Hėnault *et al*. 2020], GC-biased Genotype #1 *H. sinensis* has been
1001 proposed as the sole anamorph of *O. sinensis* [Wei *et al*. 2006]. Wei *et al*. [2016] reported successful
1002 industrial cultivation of *C. sinensis* insect–fungal complexes; the cultivated complexes, however, exhibited
1003 a species contradiction between the anamorphic inoculants of 3 *H. sinensis* strains and the sole teleomorph
1004 of AT-biased Genotype #4 that was detected in the fruiting body of the cultivated *C. sinensis* insect–fungal
1005 complexes. The sequences of AT-biased Genotypes #4–6 and #15–17, as well as the sequences of GC-
1006 biased Genotypes #2–3 and #7–14 of *O. sinensis*, do not reside in the genome assemblies ANOV00000000,
1007 JAAVMX000000000, LKHE00000000, LWBQ00000000, or NGJJ00000000 of the *H. sinensis* strains
1008 Co18, IOZ07, 1229, ZJB12195, and CC1406-20395, respectively [Stensrud *et al*. 2007; Xiao *et al*. 2008;
1009 Gao *et al*. 2012; Hu *et al*. 2013; Li *et al*. 2013, 2016a, 2020b, 2022, 2023d, 2023e; 2024a; Mao *et al*. 2013;
1010 Zhu & Li 2017; Jin *et al*. 2020; Liu *et al*. 2020; Shu *et al*. 2020]. Li *et al*. [2024a] further demonstrated that
1011 the sequences of Genotypes #2–17 of *O. sinensis* did not appear as repetitive copies in the genome of
1012 Genotype #1 *H. sinensis*, invalidating the hypothesis proposed by Li *et al*. [2013, 2017, 2020c] that "RIP
1013 mutation" induces or generates "ITS pseudogenes" and "rRNA pseudogenes" in the genome of *H. sinensis*.
1014 These data indicate that the 17 genotypes of *O. sinensis* are genome-independent and that they belong to
1015 different fungi. In addition, the data demonstrate that the sole anamorph hypothesis for *H. sinensis* proposed
1016 by Wei *et al*. [2006] fails to pass examination via Koch's postulates.

1017 Li *et al*. [2020a, 2023b] revised the inoculant information for the industrial cultivation project and
1018 reported that the cultivation project used cultures of *C. sinensis* ascospores rather than pure *H. sinensis*
1019 strains as inoculants, as previously reported by Wei *et al*. [2016]. However, Li *et al*. [2023d, 2023e] reported
1020 the detection of GC-biased Genotypes #1 and #14 and AT-biased Genotypes #5–6 and #16, as well as *P.*
1021 *hepiali,* in ascospores of natural *C. sinensis* insect–fungal complexes through a culture–independent
1022 approach using a PCR amplicon cloning technique with the selection and sequencing of ≥30 white colonies.
1023 In addition, Li *et al*. [2013] used a culture-dependent protocol and reported the detection of GC-biased
1024 Genotype #1 and AT-biased Genotype #5 in 8 cultures of mono-ascospores. Li *et al*. [2016b] demonstrated
1025 the nearly non-infectious feature of *H. sinensis* conidia and mycelia on 200 larvae of *H. armoricanus* in the

1026 inoculation experiments. Furthermore, Li *et al*. [2020b, 2022, 2023d, 2023e] and Gao *et al*. [2012] reported
1027 that AT-biased Genotype #4 of *O. sinensis* occurred in the stromata throughout the entire course of *C.*
1028 *sinensis* maturation and that the stromal fertile portion (SFP) contained numerous ascocarps of the *C.*
1029 *sinensis* insect–fungal complex; the abundance of Genotype #4 was high in immature stromata, which are
1030 in asexual growth stages, and largely declined in mature stromata and SFP, which are in sexual production
1031 stages or in the transitional stages from asexual growth to sexual reproduction. Unfortunately, Genotype #4
1032 of *O. sinensis* was absent from the *C. sinensis* ascospores. Thus, although Wei *et al*. [2016] reported the
1033 detection of the sole teleomorphic AT-biased Genotype #4 in the cultivated *C. sinensis* insect–fungal
1034 complex and Li *et al*. [2020a, 2023b] reviewed the inoculant information, the fungal source of the sole
1035 teleomorphic, AT-biased Genotype #4 of *O. sinensis* remains scientifically uncertain in the artificial
1036 cultivation of the *C. sinensis* insect–fungal complex.

1037 In addition to the formal reports of unsuccessful attempts at artificial cultivation of the fruiting bodies
1038 of *C. sinensis* [Holliday *et al*. 2008; Stone 2010; Hu *et al*. 2013], Zhang *et al*. [2013] summarized the 40-
1039 year history of cultivation failures of insect–fungal complexes using a "pure" mycological strategy in
1040 academic research-oriented settings and Qin *et al*. [2018] summarized the obstacles to the cultivation of *O.*
1041 *sinensis* fruiting bodies and ascospores. In contrast, Wei *et al*. [2016] reported success in such a cultivation
1042 effort in industrial product-oriented settings. This industrial success might be attributed to the application
1043 of a "mycologically impure" cultivation strategy on the basis of two facts:

1044 (1) Cultures of mycologically impure ascospores of natural *C. sinensis* are used as inoculants [Li *et al*.
1045 2020a, 2023b]; these are most likely combined with cocultures of *C. sinensis* stroma and/or a stromal fertile
1046 portion (SFP) containing numerous ascocarps that, most importantly, contain AT-biased Genotype #4 of *O.*
1047 *sinensis*, consistent with the discovery of the sole teleomorphic *O. sinensis* genotype [Wei *et al*. 2016];

1048 (2) Soil collected from the natural *C. sinensis* production areas on the Qinghai–Tibet Plateau was added to
1049 the industrial cultivation system as described by Wei *et al*. [2016].

1050 Unfortunately, purification and genomic sequencing of GC- and AT-biased Genotypes #2–17 of *O. sinensis*
1051 have not been reported to date. Thus, genomic and transcriptomic information regarding mutations in the
1052 *MAT1-1-1* and *MAT1-2-1* genes in the genome-independent *O. sinensis* fungi of Genotypes #2–17,
1053 especially the DNA-binding domains of the MAT1-1-1 and MAT1-2-1 proteins, is lacking. Table S3 shows
1054 that MAT1-1-1 proteins ALH25057, ALH25005, and ALH25006 and MAT1-2-1 proteins AIV43040,
1055 AFX66443, ACV60417, AFH35020, and ACV60418 were most likely produced by Genotype #3 of *O.*
1056 *sinensis*, if GC-biased Genotype #3 of *O. sinensis* does not coexist with other fungi in the wild-type *C.*
1057 *sinensis* isolates XZ12_16, XZ05_8, XZ-LZ07-H1, XZ06-124, and XZ-LZ07-H2.

1058 Regardless of whether the MAT1-1-1 and MAT1-2-1 proteins form heterodimers or interact via

complementary electrostatic surfaces and thereby enable cooperative DNA binding, the synergy of the mating proteins of *O. sinensis* constitutes the core mechanism that regulates mating type recognition, triggering downstream nuclear fusion signaling pathways and fruiting body development [Debuchy *et al*. 2006; Jones & Bennett 2011; Zheng & Wang 2013; Wilson *et al*. 2015; Sun *et al*. 2019]. The differential occurrence, differential transcription, and alternative splicing of mating-type and pheromone receptor genes in *H. sinensis* and *C. sinensis* isolates invalidates the self-fertilization hypothesis at the genomic and transcriptomic levels but suggests self-sterility of *O. sinensis* under heterothallic or hybrid reproduction [Hu *et al*. 2013; Bushley *et al*. 2013; Zhou *et al*. 2013; Wei *et al*. 2006; Li *et al*. 2019, 2023c, 2024b, 2025]. Furthermore, at the protein level, the discovery of many mutant MAT1-1-1 and MAT1-2-1 proteins reported by Li *et al*. [2025] that contain mutant MATα_HMGbox domains and HMG-box_ROX1-like domains, respectively, and have been detected in wild-type *C. sinensis* isolates, and the insect–fungal complex demonstrated in this study, may indicate that mating proteins from heterogeneous fungal sources may accomplish coordinated heterothallic or hybrid reproduction of *O. sinensis* during the lifecycle of *C. sinensis* insect–fungal complexes.

Conclusions

Analysis of the DNA-binding domains of mating proteins revealed heteromorphic stereostructures of the MATα_HMGbox and HMG-box_ROX1-like domains of the MAT1-1-1 and MAT1-2-1 proteins, respectively. A few amino acid substitutions at various sites in the DNA-binding domains were demonstrated to be present in numerous mutant mating proteins derived from wild-type *C. sinensis* isolates. These substitutions correlated with changes in the hydrophobic properties and secondary and tertiary structures of the proteins under different AlphaFold 3D structural cords clustered into various Bayesian clustering clades. The diversity of heteromorphic MATα_HMGbox and HMG-box_ROX1-like domains of the mating proteins present in wild-type *C. sinensis* isolates may lead to stereostructure-related functional alterations in the mating process. The observed variation in the stereostructures of the DNA-binding domains of the mutant MAT1-1-1 and MAT1-2-1 proteins suggest that the mating proteins arise from diverse fungal sources and that they are produced by cooccurring *O. sinensis* genotypes or heterospecific fungi coexisting in wild-type *C. sinensis* isolates and natural *C. sinensis* insect-fungal complexes that have been identified in mycobiota, molecular, metagenomic, and metatranscriptomic studies, regardless of whether culture-dependent or culture-independent research strategies were used.

Acknowledgments

The authors are grateful to Prof. Mu Zang, Prof. Ru-Qin Dai, Prof. Ping Zhu, Prof. Wei Liu, Prof. Zong-Qi Liang and Prof. Yong-Jie Zhang for their consultation.

1091 **Supplementary Materials:** The following supporting information can be downloaded at www.xxxxxx.
1092 **Figure S1**. Alignment of the MAT1-1-1 protein sequences with various animo acid residue substitutions
1093 derived from wild-type *C. sinensis* isolates and from the genome and metatranscriptome assemblies of *H.*
1094 *sinensis* strains or the *C. sinensis* insect–fungi complexes. The underlined segment in blue refer to the
1095 MATα_HMGbox domain (amino acids 51→225) of the reference MAT1-1-1 protein AGW27560, and the
1096 9 external amino acid residues upstream and downstream of the domain are shown blue but not underlined.
1097 The amino acid substitution is shown in red, whereas the hyphens indicate identical amino acid residues
1098 and the spaces denote unmatched protein sequence gaps.
1099 **Figure S2**. Alignment of the MAT1-2-1 protein sequences with various animo acid residue substitutions
1100 derived from wild-type *C. sinensis* isolates and from the genome and metatranscriptome assemblies of *H.*
1101 *sinensis* strains or the *C. sinensis* insect–fungi complexes. The underlined segment in blue refer to the
1102 HMG-box_ROX1-like domain (127→197 of the reference sequence AEH27625, and the 9 external amino
1103 acid residues upstream and downstream of the domain are shown blue but not underlined. The amino acid
1104 substitution is shown in red, whereas the hyphens indicate identical amino acid residues and the spaces
1105 denote unmatched protein sequence gaps.
1106 **Figure S3**. Correlation of the changes in the primary and secondary structures of the MATalpha_HMGbox
1107 domains of MAT1-1-1 proteins: the reference protein AGW27560 derived from the *H. sinensis* strain CS68-
1108 2-1229 and the truncated protein encoded by the metatranscriptome assembly GAGW01008880 derived
1109 from the *C. sinensis* insect–fungi complex. Panel A shows alignment of amino acid sequences of the
1110 MATalpha_HMGbox domain sequences of the MAT1-1-1 proteins; the hyphens indicate identical amino
1111 acid residues. The ExPASy ProtScale plots show below the changes in hydrophobicity (Panel B) and in the
1112 2D structure (Panels C–F for α-helices, β-sheets, β-turns, and coils) with open rectangles in blue outlining
1113 the truncation region in the plots.
1114 **Table S1**. GenBank accession numbers (in red in parentheses) for the full-length MAT1-1-1 proteins in the
1115 AlphaFold database under the corresponding AlphaFold UniProt codes **[Li *et al*. 2025]**.
1116 **Table S2**. GenBank accession numbers (in red) for the full-length MAT1-2-1 proteins of 69 *H. sinensis*
1117 strains or *C. sinensis* isolates under the corresponding AlphaFold UniProt codes **[Li *et al*. 2025]**.
1118 **Table S3**. Wild-type *C. sinensis* isolates, GenBank accession numbers for the ITS nucleic acid sequences
1119 and mating protein sequences, and percentage similarities *vs*. GC-biased *O. sinensis* Genotypes #1–3 and
1120 #7–9.
1121 **Table S4**. Amino acid scales based on the general chemical characteristics of their side chains for ProtScale
1122 analysis (https://web.expasy.org/protscale/) to predict hydrophobicity and secondary structures (α-helices,
1123 β-sheets, β-turns, and coils) of proteins.

1124 **Table S5**. Summary of the Bayesian clustering results in Figure S1 with the amino acid substitutions in the
1125 MATα_HMGbox domains of the 19 full-length MAT1-1-1 proteins of wild-type *C. sinensis* isolates under
1126 the AlphaFold UniProt codes and GenBank accession numbers.
1127 **Table S6**. Summary of the Bayesian clustering results in Figure S1 with the amino acid substitutions in the
1128 MATα_HMGbox domains of the MAT1-1-1 proteins encoded by the genome assemblies of *H. sinensis*
1129 strains and the metatranscriptome assemblies of natural *C. sinensis* under the GenBank accession numbers.
1130 **Table S7**. Summary of the Bayesian clustering results in Figure 4 with the amino acid substitutions in the
1131 HMG-box_ROX1-like domains of the 25 full-length MAT1-2-1 proteins of wild-type *C. sinensis* isolates
1132 under the AlphaFold UniProt codes and GenBank accession numbers.
1133 **Table S8**. Summary of the Bayesian clustering results in Figure 4 with the amino acid substitutions and
1134 deletions in the HMG-box_ROX1-like domains of the MAT1-2-1 proteins encoded by the genome and
1135 transcriptome assemblies of *H. sinensis* strains and metatranscriptome assembly of natural *C. sinensis*
1136 insect–fungi complexes under the GenBank accession numbers.
1137 **Author Contributions:** Conceptualization, XZL, YLL, and JSZ; methodology, JSZ; formal analysis, JSZ;
1138 investigation, XZL and JSZ; data curation, XZL and JSZ; writing–original draft preparation, JSZ; writing—
1139 review and editing, XZL, YLL, and JSZ; project administration, YLL; funding acquisition, YLL. All authors
1140 have read and agreed to the published version of the manuscript.
1141 **Funding:** This research was supported by (1) the Major Science and Technology Projects of Qinghai
1142 Province, China (#2021-SF-A4); (2) the Joint Science Project of the Chinese Academy of Sciences, Qinghai
1143 Provincial Government, and Sanjiangyuan National Park (#LHZX-2022-01); (3) the grant "The protective
1144 harvesting and utilization project for *Ophiocordyceps sinensis* in Qinghai Province" (#QHCY-2023-057)
1145 awarded by Qinghai Province of China; and (4) Qinghai Province Science and Technology Commissioner
1146 Special Project (#2024-NK-P67).
1147 **Institutional Review Board Statement:** Not applicable because this paper is an *in silico* reanalysis of
1148 public data.
1149 **Informed Consent Statement:** Not applicable because this paper is a public bioinformatic data reanalysis.
1150 **Data Availability Statement:** All sequence and 3D structure data are available in the GenBank and
1151 AlphaFold databases, except for one set of metatranscriptome sequences from natural *C. sinensis* that was
1152 uploaded to the repository database
1153 www.plantkingdomgdb.com/Ophiocordyceps_sinensis/data/cds/Ophiocordyceps_sinensis_CDS.fas
1154 (accessed from 18 May 2017 to 18 January 2018) by Xia *et al*. [2017], which is currently inaccessible, but
1155 a previously downloaded cDNA file (accessed on 18 January 2018) was used for the mating protein
1156 analysis.

Conflicts of Interest: The authors declare no conflicts of interest.

[REFERENCES]

1. Abramson J, Adler J, Dunger J, Evans R, Green T, Pritzel A, Ronneberger O, Willmore L, Ballard AJ, Bambrick J, Bodenstein SW, Evans DA, Hung CC, O'Neill M, Reiman D, Tunyasuvunakool K, Wu Z, Žemgulytė A, Arvaniti E, Beattie C, Bertolli O, Bridgland A, Cherepanov A, Congreve M, Cowen-Rivers AI, Cowie A, Figurnov M, Fuchs FB, Gladman H, Jain R, Khan YA, Low CMR, Perlin K, Potapenko A, Savy P, Singh S, Stecula A, Thillaisundaram A, Tong C, Yakneen S, Zhong ED, Zielinski M, Žídek A, Bapst V, Kohli P, Jaderberg M, Hassabis D, Jumper JM. Accurate structure prediction of biomolecular interactions with AlphaFold 3. Nature. 2024; 630(8016): 493−500. doi: 10.1038/s41586-024-07487-w
2. Asante-Owusu RN, Banham AH, Böhnert HU, Mellor EJC, Casselton LA. Heterodimerization between two classes of homeodomain proteins in the mushroom *Coprinus cinereus* brings together potential DNA-binding and activation domains. Gene 1996; 172(1): 25−31. https://doi.org/10.1016/0378-1119(96)00177-1
3. Balasubramanian B, Lowry CV, Zitomer RS. The Rox1 repressor of the *Saccharomyces cerevisiae* hypoxic genes is a specific DNA-binding protein with a high-mobility-group motif. Mol Cell Biol. 1993; 13(10): 6071−6078. doi: 10.1128/mcb.13.10.6071-6078.1993
4. Barseghyan GS, Holliday JC, Price TC, Madison LM, Wasser SP. Growth and cultural-morphological characteristics of vegetative mycelia of medicinal caterpillar fungus *Ophiocordyceps sinensis* G.H. Sung *et al*. (Ascomycetes) Isolates from Tibetan Plateau (P. R. China). Intl. J. Med. Mushrooms. 2011; 13(6): 565−581. DOI: 10.1615/intjmedmushr.v13.i6.90
5. Baxevanis AD, Bryant SH, Landsman D. Homology model building of the HMG-1 box structural domain. Nucleic Acids Research 1995; 23(6): 1019−1029. DOI: 10.1093/nar/23.6.1019
6. Ait Benkhali J, Coppin E, Brun S, Peraza-Reyes L, Martin T, Dixelius C, Lazar N, van Tilbeurgh H, Debuchy R. A Network of HMG-box Transcription Factors Regulates Sexual Cycle in the Fungus Podospora anserina. PLoS Genet 2013; 9(7): e1003642. doi:10.1371/journal.pgen.1003642
7. Bennett RJ, Johnson AD. Completion of a parasexual cycle in *Candida albicans* by induced chromosome loss in tetraploid strains. EMBO J. 2003; 22(10): 2505−2515. DOI: 10.1093/emboj/cdg235
8. Bushley KE, Li Y, Wang W-J, Wang X-L, Jiao L, Spatafora JW, Yao Y-J. Isolation of the MAT1-1 mating type idiomorph and evidence for selfing in the Chinese medicinal fungus *Ophiocordyceps sinensis*. Fungal Biol. 2013; 117(9): 599−610. DOI: 10.1016/j.funbio.2013.06.001
9. Chen C-S, Hseu R-S, Huang C-T. Quality control of *Cordyceps sinensis* teleomorph, anamorph, and Its products. Chapter 12, in (Shoyama, Y., Ed.) Quality Control of Herbal Medicines and Related Areas. InTech, Rijeka, Croatia (2011). pp. 223–238. www.intechopen.com
10. Chen Y-Q, Hu B, Xu F, Zhang W, Zhou H, Qu L-H. Genetic variation of *Cordyceps sinensis*, a fruit-body-producing entomopathogenic species from different geographical regions in China. FEMS Microbiol Lett. 2004; 230: 153–158. Doi: 10.1016/S0378-1097(03)00889-9 (accessed on 30 January 2025).
11. China Ministry of Agriculture and Rural Affairs. Announcement (No. 15 of 2021) of National Forestry and Grassland Administration: List of National Key Protected Wild Plants. September 7, 2021. Available online: https://m.163.com/dy/article/HHCVOJPU055360T7.html (accessed on 3 May 2025).
12. Dai R-Q, Lan J-L, Chen W-H, Li X-M, Chen Q-T, Shen C-Y. Discovery of a new fungus *Paecilomyces hepiali* Chen & Dai. Acta Agricult. Univ. Pekin. 1989; 15(2): 221−224.
13. David A, Islam S, Tankhilevich E, Sternberg MJE. The AlphaFold Database of Protein Structures: A Biologist's Guide. J Mol Biol. 2022; 434(2): 167336. https://doi.org/10.1016/j.jmb.2021.167336
14. Debuchy R, Turgeo BG. Mating-Type Structure, Evolution, and Function in Euascomycetes. In (eds. Kües U. &

Fischer, R.) Growth, Differentiation and Sexuality. Springer (2006). pp. 293–323.

15. Deleage G, Roux B. An algorithm for protein secondary structure prediction based on class prediction. Protein Engineering, Design and Selection 1987; 1: 289–294. https://doi.org/10.1093/protein/1.4.289
16. Du X-H, Wu D-M, Kang H, Wang H-C, Xu N, Li T-T, Chen K-L. Heterothallism and potential hybridization events inferred for twenty-two yellow morel species. IMA Fungus. 2020; 11: 4. https://doi.org/10.1186/s43008-020-0027-1
17. Gao L, Li X-H, Zhao J-Q, Lu J-H, Zhao J-G, Zhu J-S. Maturation of *Cordyceps sinensis* associates with alterations of fungal expressions of multiple *Ophiocordyceps sinensis* mutants with transition and transversion point mutations in stroma of *Cordyceps sinensis*. Beijing Da Xue Xue Bao. 2012; 44(3): 454–463. doi: 10.3969/j.issn.1671-167X.2012.03.025
18. Gasteiger E, Hoogland C, Gattiker A, Duvaud S, Wilkins MR, Appel RD, Bairoch A. Protein Identification and Analysis Tools on the ExPASy Server. Chapter 52 (In) John M. Walker (ed): The Proteomics Protocols Handbook, Humana Press (2005). pp. 571–607.
19. Guo M-Y, Liu Y, Gao Y-H, Jin T, Zhang H-B, Zhou X-W. Identification and bioactive potential of endogenetic fungi isolated from medicinal caterpillar fungus *Ophiocordyceps sinensis* from Tibetan Plateau. Int J Agric Biol. 2017; 19: 307–313. DOI: 10.17957/IJAB/15.0281
20. Hancock SP, Cascio D, Johnson RC. Cooperative DNA binding by proteins through DNA shape complementarity. Nucleic Acids Res. 2019; 47(16):8874–8887. doi: 10.1093/nar/gkz642
21. Hawksworth DL, Crous PW, Redhead SA, Reynolds DR, Samson RA, Seifert KA, and 82 other authors. The Amsterdam declaration on fungal nomenclature. IMA Fungus. 2011; 2: 105−112. DOI: 10.5598/imafungus.2011.02.01.14
22. Hénault M, Marsit S, Charron G, Landry CR. The effect of hybridization on transposable element accumulation in an undomesticated fungal species. eLife. 2020; 9: e60474. DOI: https://doi.org/10.7554/eLife.60474
23. Holliday J, Cleaver M. Medicinal value of the caterpillar fungi species of the genus Cordyceps (Fr.) Link (Ascomycetes). A review. Int. J. Med. Mushrooms. 2008; 10: 219–234. DOI: 10.1615/IntJMedMushr.v10.i3.30
24. Hu X, Zhang Y-J, Xiao G-H, Zheng P, Xia Y-L, Zhang X-Y, St Leger RJ, Liu X-Z, Wang C-S. Genome survey uncovers the secrets of sex and lifestyle in caterpillar fungus. Chin. Sci. Bull. 2013; 58: 2846–2854. doi: 10.1007/s11434-013-5929-5
25. Huelsenbeck JP, Ronquist F. MRBAYES: Bayesian inference of phylogeny. Bioinformat. 2001; 17: 754−755. DOI: 10.1093/bioinformatics/17.8.754
26. Jackson D, Lawson T, Villafane R, Gary L. Modeling the structure of yeast MATα1: An HMG-Box motif with a C-terminal helical extension. Open J Biophysics, 2013, 3: 1−12. http://dx.doi.org/10.4236/ojbiphy.2013.31001
27. Jacobsen S, Wittig M, Pöggeler S. Interaction Between Mating-Type Proteins From the Homothallic Fungus Sordaria macrospora. Curr. Genet. 2002; 41: 150–158. doi: 10.1007/s00294-002-0276-0
28. Jiang Y, Yao Y-J. A review for the debating studies on the anamorph of *Cordyceps sinensis*. Mycosistema. 2003; 22(1): 161–176.
29. Jin L-Q, Xu Z-W, Zhang B, Yi M, Weng C-Y, Lin S, Wu H, Qin X-T, Xu F, Teng Y, Yuan S-J, Liu Z-Q, Zheng Y-G. Genome sequencing and analysis of fungus *Hirsutella sinensis* isolated from *Ophiocordyceps sinensis*. AMB Expr. 2020; 10: 105. https://doi.org/10.1186/s13568-020-01039-x
30. Jones SK, Bennett RJ. Fungal mating pheromones: choreographing the dating game. Fungal Genet. Biol. 2011; 48(7): 668–676. doi: 10.1016/j.fgb.2011.04.001
31. Jumper J, Evans R, Pritzel A, Green T, Figurnov M, Ronneberger O, Tunyasuvunakool K, Bates R, Žídek A, Potapenko A, Bridgland A, Meyer C, Kohl SAA, Ballard AJ, Cowie A, Romera-Paredes B, Nikolov S, Jain R, Adler J, Back T, Petersen S, Reiman D, Clancy E, Zielinski M, Steinegger M, Pacholska M, Berghammer T,

1244 Bodenstein S, Silver D, Vinyals O, Senior AW, Kavukcuoglu K, Kohli P, Hassabis D. Highly accurate protein
1245 structure prediction with AlphaFold. Nature 2021; 596: 583–589. https://doi.org/10.1038/s41586-021-03819-2
1246 32. Kang Q, Zhang J, Chen F, Dong C, Qin Q, Li X, Wang H, Zhang H and Meng Q. Unveiling mycoviral diversity
1247 in *Ophiocordyceps sinensis* through transcriptome analyses. Front. Microbiol. 2024; 15: 1493365. doi:
1248 10.3389/fmicb.2024.1493365
1249 33. Kastaniotis AJ, Zitomer RS. Rox1 mediated repression. Oxygen dependent repression in yeast. Adv Exp Med
1250 Biol. 2000; 475: 185–195. https://pubmed.ncbi.nlm.nih.gov/10849660/
1251 34. Kim H-K, Jo S-M, Kim G-Y, Kim D-W, Kim Y-K, Yun S-H. A large-scale functional analysis of putative target
1252 genes of mating-type loci provides insight into the regulation of sexual development of the cereal pathogen
1253 *Fusarium graminearum*. PLoS Genet 2015; 11(9): e1005486. doi:10.1371/journal.pgen.1005486
1254 35. Kinjo N, Zang M. Morphological and phylogenetic studies on *Cordyceps sinensis* distributed in southwestern
1255 China. Mycoscience. 2001; 42: 567–574. DOI: 10.1007/BF02460956
1256 36. Kück U, Bennett RJ, Wang L and Dyer PS. Editorial: Sexual and Parasexual Reproduction of Human Fungal
1257 Pathogens. Front. Cell. Infect. Microbiol. 2022; 12: 934267. doi: 10.3389/fcimb.2022.934267
1258 37. Kües U, Casselton LA. The origin of multiple mating types in mushrooms. J Cell Sci 1993; 104 (2): 227–230.
1259 https://doi.org/10.1242/jcs.104.2.227
1260 38. Kyte J, Doolittle RF. A simple method for displaying the hydropathic character of a protein. J Mol Biol 1982;
1261 157(1): 105−132. https://doi.org/10.1016/0022-2836(82)90515-0
1262 39. Leung P-H, Zhang Q-X, Wu J-Y. Mycelium cultivation, chemical composition and antitumour activity of a
1263 *Tolypocladium* sp. fungus isolated from wild *Cordyceps sinensis*. J. Appl. Microbiol. 2006; 101: 275−283. DOI:
1264 10.1111/j.1365-2672.2006.02930.x
1265 40. Li C-L. A study of *Tolypocladium sinense* C.L. Li. sp. nov. and cyclosporin production. Acta Mycol. Sinica.
1266 1988; 7: 93−98.
1267 41. Li M-M, Zhang J-H, Qin Q-L, Zhang H, Li X, Wang H-T, Meng Q. Transcriptome and Metabolome Analyses
1268 of Thitarodes xiaojinensis in Response to *Ophiocordyceps sinensis* Infection. Microorganisms 2023a; 11: 2361.
1269 https://doi.org/10.3390/microorganisms11092361
1270 42. Li W-J, Xia J-M, Li Q-P, Zhang Z-Y, Zhang W-W, Dong C-H, Wei J-C, Liu X-Z. Developmental recording of
1271 the ghost-moth larvae after ex situ infection by *Ophiocordyceps sinensis*. Sci China Life Sci 2020a; 63, 1093–
1272 1095. https://doi.org/10.1007/s11427-020-1686-7
1273 43. Li W-J, Xia J-M, Li Q-P, Zhang Z-Y, Zhang W-W, Dong C-H, Wei J-C, Liu X-Z. Erratum to: Developmental
1274 recording of the ghost-moth larvae after *ex situ* infection by *Ophiocordyceps sinensis*. Sci China Life Sci 2023b;
1275 66, 892. https://doi.org/10.1007/s11427-022-2232-5
1276 44. Li X, Wang F, Liu Q, Li Q-P, Qian Z-M, Zhang X-L, Li K, Li W-J, Dong C-H. Developmental transcriptomics
1277 of Chinese cordyceps reveals gene regulatory network and expression profiles of sexual development-related
1278 genes. BMC Genomics. 2019; 20: 337. https://doi.org/10.1186/s12864-019-5708-z
1279 45. Li X-Z, Li Y-L, Wang Y-N, Zhu J-S. Translations of mutant repetitive genomic sequences in *Hirsutella sinensis*
1280 and changes in secondary structures and functional specifications of the encoded proteins. International J Mol
1281 Sci 2024a; 25(20), 11178; https://doi.org/10.3390/ijms252011178
1282 46. Li X-Z, Li Y-L, Yao Y-S, Xie W-D, Zhu J-S. Further discussion with Li *et al*. (2013, 2019) regarding the "ITS
1283 pseudogene hypothesis" for *Ophiocordyceps sinensis*. Mol. Phylogenet. Evol. 2020b; 146: 106728.
1284 https://doi.org/10.1016/j.ympev.2019.106728
1285 47. Li X-Z, Li Y-L, Zhu J-S. Differential transcription of mating-type genes during sexual reproduction of natural
1286 *Cordyceps sinensis*. Chin. J. Chin. Materia Medica. 2023c; 48(10): 2829–2840. DOI:
1287 10.19540/j.cnki.cjcmm.20230213.102

1288 48. Li X-Z, Li Y-L, Zhu J-S. Three-dimensional structural heteromorphs of mating-type proteins in *Hirsutella*
1289 *sinensis* and the natural *Cordyceps sinensis* insect–fungal complex. J Fungi. 2025; 11(4): 244.
1290 https://doi.org/10.3390/ jof11040244
1291 49. Li X-Z, Xiao M-J, Li Y-L, Gao L, Zhu J-S. Mutations and differential transcription of mating-type and
1292 pheromone receptor genes in *Hirsutella sinensis* and the natural *Cordyceps sinensis* insect–fungi complex. Biol.
1293 (Basel) 2024b; 13(8): 632. https://doi.org/10.3390/biology13080632
1294 50. Li Y, Hsiang T, Yang R-H, Hu X-D, Wang K, Wang W-J, Wang X-L, Jiao L, Yao Y-J. Comparison of different
1295 sequencing and assembly strategies for a repeat-rich fungal genome, *Ophiocordyceps sinensis*. J. Microbiol.
1296 Methods. 2016a; 128: 1−6. DOI: 10.1016/j.mimet.2016.06.025
1297 51. Li Y, Jiang L, Wang K, Wu H-J, Yang R-H, Yan Y-J, Bushley KE, Hawksworth DL, Wu Z-J, Yao Y-J. RIP mutated
1298 ITS genes in populations of *Ophiocordyceps sinensis* and their implications for molecular systematics. IMA
1299 Fungus. 2020c; 11: 18. DOI:10.1016/j.mimet.2016.06.025
1300 52. Li Y, Jiao L, Yao Y-J. Non-concerted ITS evolution in fungi, as revealed from the important medicinal fungus
1301 *Ophiocordyceps sinensis*. Mol. Phylogenet. Evol. 2013; 68: 373−379. doi: 10.1016/j.ympev.2013.04.010
1302 53. Li Y, Yang R-H, Jiang L, Hu X-D, Wu Z-J, Yao Y-J. rRNA Pseudogenes in Filamentous Ascomycetes as Revealed
1303 by Genome Data. G3-Genes│Genomics│Genetics. 2017; 7(8): 2695−2703. doi: 10.1534/g3.117.044016
1304 54. Li Y-L, Gao L, Yao Y-S, Wu Z-M, Lou Z-Q, Xie W-D, Wu J-Y, Zhu J-S. Altered GC- and AT-biased genotypes
1305 of *Ophiocordyceps sinensis* in the stromal fertile portions and ascospores of natural *Cordyceps sinensis*. PLoS
1306 ONE. 2023d; 18(6): e0286865. https://doi.org/10.1371/journal.pone.0286865
1307 55. Li Y-L, Li X-Z, Yao Y-S, Wu Z-M, Gao L, Tan N-Z, Lou Z-Q, Xie W-D, Wu J-Y, Zhu J-S. Differential
1308 cooccurrence of multiple genotypes of *Ophiocordyceps sinensis* in the stromata, stromal fertile portion
1309 (ascocarps) and ascospores of natural *Cordyceps sinensis*. PLoS ONE. 2023e; 18(3): e0270776. DOI:
1310 10.1371/journal.pone.0270776
1311 56. Li Y-L, Li X-Z, Yao Y-S, Xie W-D, Zhu J-S. Molecular identification of *Ophiocordyceps sinensis* genotypes and
1312 the indiscriminate use of the Latin name for the multiple genotypes and the natural insect–fungi complex. Am J
1313 BioMed Sci. 2022; 14(3): 115–135. doi: 10.5099/aj220300115
1314 57. Li Y-L, Yao Y-S, Zhang Z-H, Xu H-F, Liu X, Ma S-L, Wu Z-M, Zhu J-S. Synergy of fungal complexes isolated
1315 from the intestines of *Hepialus lagii* larvae in increasing infection potency. J. Fungal Res. 2016b; 14: 96−112.
1316 58. Liu J, Guo L-N, Li Z-W, Zhou Z, Li Z, Li Q, Bo X-C, Wang S-Q, Wang J-L, Ma S-C, Zheng J, Yang Y. Genomic
1317 analyses reveal evolutionary and geologic context for the plateau fungus *Ophiocordyceps sinensis*. Clin. Med.
1318 2020; 15: 107–119. https://doi.org/10.1186/s13020-020-00365-3
1319 59. Liu Z-Q, Lin S, Baker PJ, Wu L-F, Wang X-R, Wu H, Xu F, Wang H-Y, Brathwaite ME, Zheng Y-G.
1320 Transcriptome sequencing and analysis of the entomopathogenic fungus *Hirsutella sinensis* isolated from
1321 *Ophiocordyceps sinensis*. BMC Genomics. 2015; 16: 106–123. DOI: 10.1186/s12864-015-1269-y
1322 60. Lu H-L, St Leger RJ. Chapter Seven - Insect Immunity to Entomopathogenic Fungi, Editors: Lovett B, St. Leger
1323 RJ. Advanc Genet, Academic Press, 2016. Vol. 94; pp. 251–85.
1324 61. Mao X-M, Zhao S-M, Cao L, Yan X, Han R-C. The morphology observation of *Ophiocordyceps sinensis* from
1325 different origins. J. Environ. Entomol. 2013; 35(3): 343–353.
1326 62. Mariani V, Biasini M, Barbato A, Schwede T. lDDT: a local superposition-free score for comparing protein
1327 structures and models using distance difference tests. Bioinformatics. 2013; 29(21): 2722–2728.
1328 http://dx.doi.org/10.1093/bioinformatics/btt473
1329 63. Martin T, Lu S-W, van Tilbeurgh H, Ripoll DR, Dixelius C, Dixelius C, Turgeon BG, Debuchy R. Tracing the
1330 Origin of the Fungal a1 Domain Places Its Ancestor in the HMG-Box Superfamily: Implication for Fungal
1331 Mating-Type Evolution. PLoS ONE 2010; 5(12): e15199. doi:10.1371/journal.pone.0015199

64. Meng Q, Yu H-Y, Zhang H, Zhu W, Wang M-L, Zhang J-H, Zhou G-L, Li X, Qin Q-L, Hu S-N, Zou Z. Transcriptomic insight into the immune defenses in the ghost moth, Hepialus xiaojinensis, during an *Ophiocordyceps sinensis* fungal infection. Insect Biochem. Mol. Biol. 2015; 64: 1−15. DOI: 10.1016/j.ibmb.2015.06.014
65. Metin B, Findley K, Heitman J. The mating type locus (MAT) and sexual reproduction of *Cryptococcus heveanensis*: insights into the evolution of sex and sex-determining chromosomal regions in fungi. PLoS Genet 2010; 6(5): e1000961. doi:10.1371/journal.pgen.1000961
66. Mishra A, Forche A and Anderson MZ. Parasexuality of Candida Species. Front. Cell. Infect. Microbiol. 2021; 11: 796929. doi: 10.3389/fcimb.2021.796929
67. Monzon V, Haft DH, Bateman A. Folding the unfoldable: using AlphaFold to explore spurious proteins. Bioinformatics Advances, 2022; 1(2): vbab043. https://doi.org/10.1093/bioadv/vbab043
68. Nakamura N, Tanaka C, Takeuchi-Kaneko Y. Transmission of antibiotic-resistance markers by hyphal fusion suggests partial presence of parasexuality in the root endophytic fungus Glutinomyces brunneus. Mycol. Progress 2019; 18: 453–462. https://doi.org/10.1007/s11557-018-1455-9
69. Peters C, Elofsson A. Why is the biological hydrophobicity scale more accurate than earlier experimental hydrophobicity scales? Proteins. 2014; 82(9): 2190–2198. doi: 10.1002/prot.24582
70. Qin Q-L, Zhou G-L, Zhang H, Meng Q, Zhang J-H, Wang H-T, Miao L, Li X. Obstacles and approaches in artificial cultivation of Chinese cordyceps. Mycol. 2018; 9(1): 7–9. https://doi.org/10.1080/21501203.2018.1442132
71. Ramšak B, Markau J, Pazen T, Dahlmann TA, Krappmann S, Kűck U. The master regulator MAT1-1-1 of fungal mating binds to its targets via a conserved motif in the human pathogen *Aspergillus fumigatus*. G3-Genes│Genomics│Genetics. 2020; 11(2): jkaa012/6026963. DOI: 10.1093/g3journal/jkaa012
72. Ramšak B, Kűck U, Hofmann E. The mating type transcription factor MAT1-1-1 from the fungal human pathogen *Aspergillus fumigatus*: synthesis, purification, and crystallization of the DNA binding domain. BioRxiv preprint. doi: https://doi.org/10.1101/2021.12.13.472399
73. Ramšak B, Kück U. The *Penicillium chrysogenum* tom1 gene a major target of transcription factor MAT1-1-1 encodes a nuclear protein involved in sporulation. Front. Fungal Bio. 2022; 3: 937023. doi: 10.3389/ffunb.2022.937023
74. Ren Y, Wan D-G, Lu X-M, Guo J-L. The study of scientific name discussion for TCM Cordyceps. LisShenzhen Med. Material Medica Res. 2013; 24(9): 2211−2212.
75. Rettie SA, Campbell KV, Bera AK, Kang A, Kozlov S, De La Cruz J, Adebomi V, Zhou G, DiMaio F, Ovchinnikov S, Bhardwaj G. Cyclic peptide structure prediction and design using AlphaFold. bioRxiv [Preprint]. 2023; 26:2023.02.25.529956. doi: 10.1101/2023.02.25.529956
76. Ronquist F, Teslenko M, van der Mark P, Ayres DL, Darling A, Höhna S, Larget B, Liu L, Suchard MA, Huelsenbeck JP. MrBayes 3.2: Efficient Bayesian Phylogenetic Inference and Model Choice Across a Large Model Space, Systematic Biology, 2012; 61(3): 539–542. https://doi.org/10.1093/sysbio/sys029
77. Samarasinghe H, You M, Jenkinson TS, Xu J-P, James TY. Hybridization Facilitates Adaptive Evolution in Two Major Fungal Pathogens. Genes. 2020; 11: 101. doi:10.3390/genes11010101
78. Seervai RNH, Jones SK, Hirakawa MP, Porman AM, Bennett RJ. Parasexuality and ploidy change in *Candida tropicalis*. Eukaryotic Cell. 2013; 12(12): 1629–1640. DOI: 10.1128/EC.00128-13
79. Sherwood RK, Bennett RJ. Fungal meiosis and parasexual reproduction--lessons from pathogenic yeast. Current Opinion Microbiol. 2009; 12(6): 599–607. DOI: 10.1016/j.mib.2009.09.005
80. Shu R-H, Zhang J-H, Meng Q, Zhang H, Zhou G-L, Li M-M, Wu P-P, Zhao Y-N, Chen C, Qin Q-L. A new high-quality draft genome assembly of the Chinese cordyceps *Ophiocordyceps sinensis*. Genome Biol. Evol. 2020;

12(7): 1074−1079. DOI: 10.1093/gbe/evaa112

81. Simm S, Einloft J, Mirus O, Schleiff E. 50 years of amino acid hydrophobicity scales: revisiting the capacity for peptide classification. Biol. Res. 2016; 49(1): 31. doi: 10.1186/s40659-016-0092-5

82. Steensels J, Gallone B, Verstrepen KJ. Interspecific hybridization as a driver of fungal evolution and Adaptation. Nat. Rev. Microbiol. 2021; 19: 485–500.

83. Stensrud Ø, Hywel-Jones NL, Schumacher T. Towards a phylogenetic classification of Cordyceps: ITS nrDNA sequence data confirm divergent lineages and paraphyly. Mycol. Res. 2005; 109: 41−56. DOI: 10.1017/s095375620400139x

84. Stensrud Ø, Schumacher T, Shalchian-Tabrizi K, Svegardenib IB, Kauserud H. Accelerated nrDNA evolution and profound AT bias in the medicinal fungus *Cordyceps sinensis*. Mycol. Res. 2007; 111: 409–415. DOI: 10.1016/j.mycres.2007.01.015

85. Stone R. Improbable partners aim to bring biotechnology to a Himalayan kingdom. Sci. 2010; 327: 940–941. DOI: 10.1126/science.327.5968.940

86. Sun S, Coelho MA, David-Palma M, Priest SJ, Heitman J. The evolution of sexual reproduction and the mating-type locus: Links to pathogenesis of *Cryptococcus* human pathogenic fungi. Annu Rev Genet. 2019; 53:4 17-444. doi: 10.1146/annurev-genet-120116-024755

87. Sung G-H, Hywel-Jones NL, Sung J-M, Luangsa-ard JJ, Shrestha B, Spatafora JW. Phylogenetic classification of *Cordyceps* and the clavicipitaceous fungi. Stud. Mycol. 2007; 57: 5−59. DOI: 10.3114/sim.2007.57.01

88. Thapar R. Structure-specific nucleic acid recognition by L-motifs and their diverse roles in expression and regulation of the genome. Biochim Biophys Acta 2015; 1849(6): 677–687. doi: 10.1016/j.bbagrm.2015.02.006

89. Tunyasuvunakool, K., Adler, J., Wu, Z, Green T, Zielinski M, Žídek A, Bridgland A, Cowie A, Meyer C, Laydon A, Velankar S, Kleywegt GJ, Bateman A, Evans R, Pritzel A, Figurnov M, Ronneberger O, Bates R, Kohl SAA, Potapenko A, Ballard AJ, Romera-Paredes B, Nikolov S, Jain R, Clancy E, Reiman D, Petersen S, Senior AW, Kavukcuoglu K, Birney E, Kohli P, Jumper J, Hassabis D. Highly accurate protein structure prediction for the human proteome. Nature 2021; 596: 590–596. https://doi.org/10.1038/s41586-021-03828-1

90. Turgeon BG, Yoder OC. Proposed nomenclature for mating type genes of filamentous ascomycetes. Fungal Genet. Biol. 2000; 31: 1–5. DOI: 10.1006/fgbi.2000.1227

91. Varadi M, Bertoni D, Magana P, Paramval U, Pidruchna I, Radhakrishnan M, Tsenkov M, Nair S, Mirdita M, Yeo J, Kovalevskiy O, Tunyasuvunakool K, Laydon A, Žídek A, Tomlinson H, Hariharan D, Abrahamson J, Green T, Jumper J, Birney E, Steinegger M, Hassabis D, Velankar S. AlphaFold Protein Structure Database in 2024: providing structure coverage for over 214 million protein sequences. Nucleic Acids Res. 2024; 52(D1): D368–D375. doi: 10.1093/nar/gkad1011

92. Wang Y, Stata M, Wang W, Stajich JE, White MM, Moncalvo JM. Comparative genomics reveals the core gene toolbox for the fungus-insect symbiosis. mBio. 2018; 9: e00636-18. DOI: 10.1128/mBio.00636-18

93. Wei J-C, Wei X-L, Zheng W-F, Guo W, Liu R-D. Species identification and component detection of *Ophiocordyceps sinensis* cultivated by modern industry. Mycosystema. 2016; 35(4): 404–410.

94. Wei X-L, Yin X-C, Guo Y-L, Shen N-Y, Wei, J.-C. Analyses of molecular systematics on *Cordyceps sinensis* and its related taxa. Mycosystema. 2006; 25(2): 192–202.

95. Wilson AM, Wilken PM, van der Nest MA, Steenkamp ET, Wingfield MJ, Wingfield BD. Homothallism: an umbrella term for describing diverse sexual behaviours. IMA Fungus. 2015; 6(1): 207–214. DOI: 10.5598/imafungus.2015.06.01.13

96. Wroblewski K, Kmiecik S. Integrating AlphaFold pLDDT Scores into CABS-flex for enhanced protein flexibility simulations. Comput Struct Biotechnol J. 2024; 30(23): 4350–4356. doi: 10.1016/j.csbj.2024.11.047

97. Xia E-H, Yang D-R, Jiang J-J, Zhang Q-J, Liu Y, Liu Y-L, Zhang Y, Zhang H-B, Shi C, Tong Y, Kim C-H, Chen

1420 H, Peng Y-Q, Yu Y, Zhang W, Eichler EE, Gao L-Z. The caterpillar fungus, *Ophiocordyceps sinensis*, genome
1421 provides insights into highland adaptation of fungal pathogenicity. Sci. Rep. 2017; 7: 1806.
1422 DOI:10.1038/s41598-017-01869-z
1423 98. Xia F, Liu Y, Shen G-L, Guo L-X, Zhou X-W. Investigation and analysis of microbiological communities in
1424 natural *Ophiocordyceps sinensis*. Can. J. Microbiol. 2015; 61: 104–111. DOI: 10.1139/cjm-2014-0610
1425 99. Xiang L, Li Y, Zhu Y, Luo H, Li C, Xu X, Sun C, Song J-Y, Shi L-H, He L, Sun W, Chen S-L. Transcriptome
1426 analysis of the *Ophiocordyceps sinensis* fruiting body reveals putative genes involved in fruiting body
1427 development and cordycepin biosynthesis. Genomics. 2014; 103: 154−159.
1428 https://doi.org/10.1016/j.ygeno.2014.01.002
1429 100. Xiao W, Yang J-P, Zhu P, Cheng K-D, He H-X, Zhu H-X, Wang Q. Non-support of species complex hypothesis
1430 of *Cordyceps sinensis* by targeted rDNA-ITS sequence analysis. Mycosystema. 2009; 28(6): 724–730.
1431 101. Xu T, Xu Q, Li J-Y. Toward the appropriate interpretation of Alphafold2. Front Artif Intell. 2023; 6: 1149748.
1432 doi: 10.3389/frai.2023.1149748
1433 102. Yamamoto A, Ando Y, Yoshioka K, Saito K, Tanabe T, Shirakawa H, Yoshida M. Difference in affinity for DNA
1434 between HMG proteins 1 and 2 determined by surface plasmon resonance measurements. J Biochem.
1435 1997;122(3): 586–594. doi: 10.1093/oxfordjournals.jbchem.a021793. PMID: 9348088
1436 103. Yang J-L, Xiao W, He H-X, Zhu H-X, Wang S-F, Cheng -KD, Zhu P. Molecular phylogenetic analysis of
1437 *Paecilomyces hepiali* and *Cordyceps sinensis*. Acta Pharmaceut. Sinica 2008; 43(4): 421–426.
1438 104. Yang J-Y, Tong X-X, He C-Y, Bai J, Wang F, Guo J-L. Comparison of endogenetic microbial community
1439 diversity between wild *Cordyceps sinensis*, artificial *C. sinensis* and habitat soil. Chin. J. Chin. Materia Medica.
1440 2021; 46(12): 3106–3115.
1441 105. Yao Y-S, Zhu J-S. Indiscriminate use of the Latin name for natural *Cordyceps sinensis* and *Ophiocordyceps*
1442 *sinensis* fungi. Chin. J. Chin. Mater. Med. 2016; 41(7): 1316–1366.
1443 106. Zhang S; Zhang Y-J. Molecular evolution of three protein-coding genes in the Chinese caterpillar fungus
1444 *Ophiocordyceps sinensis*. Microbiol. China. 2015; 42(8): 1549−1560.
1445 107. Zhang S, Zhang Y-J, Liu X-Z, Wen H-A, Wang M, Liu D-S. Cloning and analysis of the MAT1-2-1 gene from
1446 the traditional Chinese medicinal fungus *Ophiocordyceps sinensis*. Fungal Biol. 2011; 115: 708−714.
1447 108. Zhang S, Zhang Y-J, Shrestha B, Xu J-P, Wang C-S, Liu X-Z. *Ophiocordyceps sinensis* and *Cordyceps militaris*:
1448 research advances, issues and perspectives. Mycosystema. 2013; 32: 577−597.
1449 109. Zhang S-W, Cen K, Liu Y, Zhou X-W, Wang C-S. Metatranscriptomics analysis of the fruiting caterpillar fungus
1450 collected from the Qinghai-Tibetan plateau. Sci. Sinica Vitae. 2018; 48(5): 562−570.
1451 110. Zhang Y-J, Li E-W, Wang C-S, Li Y-L, Liu X-Z. *Ophiocordyceps sinensis*, the flagship fungus of China:
1452 terminology, life strategy and ecology. Mycol. 2012; 3(1): 2–10.
1453 https://www.tandfonline.com/doi/full/10.1080/21501203.2011.654354
1454 111. Zhang Y-J, Sun B-D, Zhang S, Wàngmǔ, Liu X-Z, Gong W-F. Mycobiotal investigation of natural
1455 *Ophiocordyceps sinensis* based on culture-dependent investigation. Mycosistema. 2010; 29(4): 518–527.
1456 112. Zhang Y-J, Xu L-L, Zhang S, Liu X-Z, An Z-Q, Wàngmǔ, Guo Y-L. Genetic diversity of *Ophiocordyceps*
1457 *sinensis*, a medicinal fungus endemic to the Tibetan Plateau: implications for its evolution and conservation.
1458 BMC Evol. Biol. 2009; 9: 290. doi:10.1186/1471-2148-9-290
1459 113. Zhang Y-J, Zhang S, Li Y-L, Ma S-L, Wang C-S, Xiang M-C, Liu X, An Z-Q, Xu J-P, Liu X-Z. Phylogeography
1460 and evolution of a fungal–insect association on the Tibetan Plateau. Mol. Ecol. 2014; 23: 5337−5355. DOI:
1461 10.1111/mec.12940
1462 114. Zheng, P.; Wang, C.-S. Sexuality Control and Sex Evolution in Fungi. Sci. Sin. Vitae 2013, 43, 1090–1097.
1463 115. Zheng Q, Hou R, Zhang J-Y, Ma J, Ma J-W, Wu Z-S, Wang G-H, Wang C-F, Xu J-R. The MAT locus genes play

1464 different roles in sexual reproduction and pathogenesis in *Fusarium graminearum*. PLoS ONE 2013; 8(6):
1465 e66980. doi:10.1371/journal.pone.0066980
1466 116. Zhong X, Gu L, Wang H-Z, Lian D-H, Zheng Y-M, Zhou S, Zhou W, Gu J, Zhang G, Liu X. Profile of
1467 *Ophiocordyceps sinensis* transcriptome and differentially expressed genes in three different mycelia, sclerotium
1468 and fruiting body developmental stages. Fungal Biol. 2018; 122: 943–951. DOI: 10.1016/j.funbio.2018.05.011
1469 117. Zhou XW, Li LJ, Tian EW. Advances in research of the artificial cultivation of *Ophiocordyceps sinensis* in China.
1470 *Critical* Rev Biotechnol 2013; *34*(3), 233–243. https://doi.org/10.3109/07388551.2013.791245
1471 118. Zhu J-S, Gao L, Li X-H, Yao Y-S, Zhou Y-J, Zhao J-Q, Zhou Y-J. Maturational alterations of oppositely
1472 orientated rDNA and differential proliferations of CG:AT-biased genotypes of *Cordyceps sinensis* fungi and
1473 *Paecilomyces hepiali* in natural *C. sinensis*. Am. J. Biomed. Sci. 2010; 2(3): 217–238. doi: 10.5099/aj100300217
1474 119. Zhu J-S, Guo Y-L, Yao Y-S, Zhou Y-J, Lu J-H, Qi Y, Chen W, Zheng T-Y, Zhang L, Wu Z-M, Zhang L-J, Liu X-
1475 J, Yin W-T. Maturation of *Cordyceps sinensis* associates with co-existence of *Hirsutella sinensis* and
1476 *Paecilomyces hepiali* DNA and dynamic changes in fungal competitive proliferation predominance and chemical
1477 profiles. J. Fungal Res. 2007; 5(4): 214–224.
1478 120. Zhu J-S, Halpern GM, Jones K. The scientific rediscovery of a precious ancient Chinese herbal regimen:
1479 *Cordyceps sinensis*: Part I. J. Altern. Complem. Med. 1998a; 4(3): 289–303. DOI: 10.1089/acm.1998.4.3-289
1480 121. Zhu J-S, Halpern GM, Jones K. The scientific rediscovery of an ancient Chinese herbal medicine: *Cordyceps*
1481 *sinensis*: Part II. J. Altern. Complem. Med. 1998b; 4(4): 429–457. DOI: 10.1089/acm.1998.4.429
1482 122. Zhu J-S, Li C-L, Tan N-Z, Berger JL, Prolla TA. Combined use of whole-gene expression profiling technology
1483 and mouse lifespan test in anti-aging herbal product study. Proc. 2011 New TCM Products Innovation and
1484 Industrial Development Summit, Hangzhou, China (Nov 27, 2011). pp. 443–448. Available online:
1485 https://xueshu.baidu.com/usercenter/paper/show?paperid=08341c17fa58c8f85584b92572b90f75&site=xueshu
1486 _se (accessed on 30 Jannuary 2025)
1487 123. Zhu J-S, Li Y-L. A Precious Transitional Chinese Medicine, *Cordyceps sinensis*: Multiple heterogeneous
1488 *Ophiocordyceps sinensis* in the insect–fungi complex. Lambert Academic Publishing, Saarbrüchen. Germany,
1489 2017.
1490 124. Zitomer RS, Limbach MP, Rodriguez-Torres AM, Balasubramanian B, Deckert J, Snow PM. Approaches to the
1491 study of Rox1 repression of the hypoxic genes in the yeast Saccharomyces cerevisiae. Methods. 1997; 11(3):
1492 279–288. doi: 10.1006/meth.1996.0422